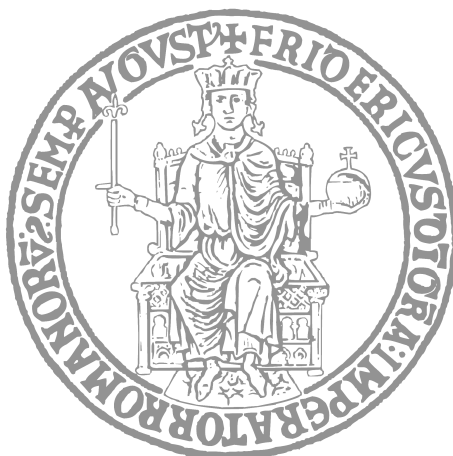


UNIVERSITÀ DEGLI STUDI DI NAPOLI FEDERICO II

Scuola Politecnica e delle Scienze di Base

Dipartimento di Ingegneria Elettrica e Tecnologie dell'Informazione



DOCTORAL THESIS

Modelling and Advanced Network Control of Future Smart Grids

Author:

Ricardo Cardona Rivera

Tutor:

Prof. Mario di Bernardo

Co-Tutor:

Prof. Francesco Lo Iudice

*Submitted in fulfilment of the requirements for the degree of
Doctor of Philosophy in Information Technology and Electrical
Engineering, XXXIV Ciclo. Coordinator: Prof. Daniele Riccio.*



31 January 2022

*A Pilar y Danilo,
que siempre están en mi corazón.*

Abstract

The power network is a key critical infrastructure for our everyday life. While there is a wide range of studies dealing with the modelling and control of power network components and their coordination for power generation, the links among different modelling approaches and control strategies are still not clear enough in the control theoretic literature. For this reason, in the first part of this Thesis we provide a review of the different dynamical models of the components of the power grid from a network perspective, the control specifications needed for their functioning and the control layers that fulfill them. As this detailed modelling of the power network can be cumbersome to handle for control design, we review the Swing Equation as a simplification of the frequency dynamics of the power network and provide a comprehensible framework to map each of the components of the power network into a set of parameters of the Swing Equation. This simpler model allows us to introduce additional control problems on the power network such as the secondary frequency control problem and the set-point scheduling problem and we frame these problems into a hierarchical description of the power network control. As the control architecture of the power network cannot always compensate the different disturbances it is subject to, we also discuss last resort strategies to contain failures. Specifically, we introduce the power network islanding problem and the Intentional Controlled Islanding (ICI) strategies found in literature. After this, we provide a novel self-organizing solution to the islanding problem based on the migration of nodes among islands defined by an initial partition of the network. This method uses a power balance estimator based on virtual consensus dynamics and a distributed migration strategy that uses this estimate to decide the migration. Our method finds, under some assumptions on the network structure and in a finite number of migration steps, a partition of the power network such that the average absolute power imbalance remains within a certain bound from the total power imbalance of the power network and we give an analytical expression for this bound. Finally, we also present work carried out on a different topic which we focused on because of the pandemic, related with the network modelling of the spread of COVID-19 in Italy and the development of possible decentralized containment strategies.

Acknowledgements

Describing my journey as a foreign Ph.D. student in a few words is, at least for me, impossible. Although I spent years understanding a problem, trying to summarize the big picture of it and finally connecting all its particularities, I feel like I still have to learn a lot about how to do research. Doing research is accompanied with a valuable self-growth path, that teaches you to be more aware of your capabilities and forces you to be true to yourself, but can be very demanding, competitive and rude, sometimes to the extent of being psychologically harmful.

For contributing to my personal growth as a researcher I wish to thank Prof. Mario di Bernardo, who also greatly contributed to this work with ingenious insights, accurate revisions and technical comments. I also thank him for his interesting lectures and for giving me the opportunity to come to Italy in the first place. I also wish to thank Francesco Lo Iudice for sharing his knowledge with me and for being supportive and patient when I needed it the most. I also thank him for the valuable collaborations and partnership we had on many of the matters in this Thesis. I would also like to thank Antonio Grotta and Marco Coraggio, with whom I had the pleasure to collaborate in some of the work discussed in this Thesis.

Although it has not been an easy task to complete this Ph.D., it has brought me a lot of joy, not only for being another finished step in my career, but also for the human kindness and loveliness it allowed me to witness after my arrival in Italy. I firstly have to thank the Scugnizzo Liberato and all the people that wander on its long corridors. Thanks to all of you for making me feel like if I was at home even if I was homesick. I also thank you for teaching me Italian and Napolitan, or as I would rather say, both at the same time in an indistinguishable way. I also have to express my immense gratitude to La Murga Los Espositos, for making me feel like one of them since the first time. For teaching me how to play the "Bombo" and the "Surdo" and, on the first place, for showing me a part of myself that I didn't know. I am also thankful to Peppe Treccia, for inspiring me in the most subtle ways, for teaching me all what he could and for being such a good friend. A special thanks to Lorenzo and Marilena, that made me feel so happy with their lovely dishes and never-ending lunches, to Gianluca, for being such a good roommate and friend and to Lily and Felipe for being a constant presence in my life, for their advises and friendship. A very special thanks to the city of Naples, although being difficult and noisy, you are a fountain of lovely people, experiences and food. Finally, but not less important, I

which to thank my parents, to whom I dedicated this Thesis, for their patience and support all over these years, for taking care of me and being part of each of my achievements in my life.

Contents

Abstract	iii
1 Introduction	1
1.1 Thesis structure and outline	4
1.2 List of Publications	5
2 Compositional modelling of the power grid and the primary control layer.	7
2.1 Preliminaries	8
2.1.1 Coordinate Transformations	8
2.1.2 Power Definition	10
2.1.3 Useful Identities	12
2.2 Generator models	12
2.2.1 The synchronous machine	12
2.2.2 The voltage source converter	16
2.2.3 Comparing the generator models	18
2.3 Load models	20
2.4 Transmission lines model	21
2.5 The electrical model of the power grid	23
2.6 Generator's control: a primary regulation layer	25
2.6.1 Steady state specifications	25
2.6.2 Perturbed steady state specifications	28
2.6.3 Transient specifications	30
2.6.4 Transient specifications for low inertia power systems	30
2.6.5 Primary control of synchronous machines	31
2.6.6 Primary control of voltage source converters	35
2.7 Summary	42
3 Network model of the power grid	43
3.1 The swing equation: a network model of the power grid	43
3.1.1 From the electrical power network model to the swing equation	45
3.1.2 Modelling power network components with the swing equation	49
3.1.3 Further simplifications	52

3.2	Summary	55
4	The control architecture of the power network	57
4.1	The hierarchical control architecture power grid	57
4.2	The secondary control layer: frequency regulation	59
4.2.1	Secondary control specifications	59
4.2.2	Secondary control problem statement	62
4.2.3	Secondary control design	64
4.3	The tertiary layer: set-point computation	69
4.3.1	Tertiary control specifications	70
4.3.2	Tertiary control problem statement	71
4.3.3	Tertiary control design	71
4.4	Summary	72
5	Self-organizing power network islanding	73
5.1	The power network islanding problem	73
5.2	Preliminaries	74
5.3	Islanding Specifications	74
5.4	Islanding Problem Formulation	75
5.5	Towards a distributed solution for the islanding problem	77
5.6	Distributed power imbalance estimation	78
5.7	A distributed migration strategy	81
5.8	Proof of Convergence	81
5.9	Migration Algorithm	84
5.10	Numerical Validation	86
5.10.1	IEEE 118 test system	87
5.10.2	IEEE 300 test system	88
5.11	Summary	92
6	Conclusions	93
A	A network model of Italy shows that intermittent regional strategies can alleviate the COVID-19 epidemic	95

1 Introduction

All of those who are privileged enough to have a steady flow of electrical power, can barely think of life without it. This high dependency on electrical power comes with a caveat as its demand grows with human development. In particular, there is not enough power generation capacity to satisfy the increasing power demand, leading to the need of constructing and increasing the capacity with new power plants of different types, including fossil fuel based generation [2]. This threatens the current steps towards an environmentally friendly power infrastructure as the expansion of renewable energy usage is not fast enough to cope with the demand [2, 3]. All of this also poses additional problems to the current infrastructure of the power network, as it has not been designed neither to transmit higher amounts of power nor to guarantee compliance with renewable generation.

In a nutshell, the power grid is mainly composed of power *generators*, power consuming devices or *loads* and a set of conductors that connect them, known as *transmission lines*, that allow the flow of electrical power. These components interact through three-phase AC signals that must have the same frequency, being 50 Hz in Europe and 60 Hz in the US, as keeping this frequency all over the network allows transmission of power [98]. Conventional power generation like hydroelectric and thermal plants are mainly interfaced with the network through *Synchronous Machines* (SM), which are devices that convert the mechanical power into AC electrical power [143]. Many modern power sources like wind and solar plants are instead mainly interfaced with the network through *Voltage Source Converters* (VSC), characterized by only using controlled electrical commutations to modulate the inputs electrical signal and convert it in appropriate three-phase AC signals [26, 178].

The functioning of the power network mainly depends on maintaining a balance between the total amount of power generation and consumption, known as *power balance*. The main consequence of the power imbalance is the loss of synchrony of generators that is then reflected in frequency drift from its nominal value all over the network, causing transmission problems, and frequency stability issues [58, 128]. The network is subject to a series of disturbances playing against it, that are originated, for example, from a change in the power generation/demand on a specific geographical zone or even a change in the infrastructure of the network due to equipment failures. For this reason, a hierarchical control architecture ensures the network operation by computing a series of compensation

actions that reject disturbances of different magnitudes and time-scales and keeps the power balance and the nominal frequency over time. The compensation is then applied directly to the SMs and VSCs, that can be considered as actuators of the power network. The hierarchical control architecture is composed of three main layers. The *Primary Layer* deals with the local control of SMs and VSCs such that they can provide the desired power generation and that power can be transmitted with proper three-phase AC signals. The *Secondary Layer* provides compensation actions that ensure zero frequency deviation from its nominal value, guaranteeing frequency stability and power balance. Finally, the *tertiary layer* provides power rescheduling after disturbances and provide technological constraints satisfaction related with generation limits and costs.

This classical view of the power network faces new challenges because new phenomena, devices and requirements, the network was not designed for, are coming into place. Among these, we have [85]

- the presence in the grid of aging equipment that makes the power conversion and transmission process inefficient.
- the increase of power demand as a consequence of the rampant power consumption increase in our households and daily life.
- the insertion of new power generation technologies like solar, wind, etc.

Over the last two decades, we have witnessed the increased need of a change of paradigm in the power generation, grounded on the need to cope with climate change and increasing demand. A transition from a fossil fuels based power generation to more ecological alternatives like solar and wind power based generation is happening, but penetration of this renewable generation has been found to cause new control issues throughout the hierarchical control architecture of the power network, e.g., [25, 62, 76, 115], leading to the more frequent occurrence of major power blackouts [38, 131, 134]. For this reason, a change of paradigm in the power generation must be accompanied by more sophisticated control strategies such that these new technologies can also work properly when connected to the preexisting infrastructure [56, 121].

Therefore, there has been a shift of focus in power network research aimed at solving the following open problems.

1. Design new primary control strategies for VSCs compatible with the power grid and able to work under the presence of SM [16, 140, 158].
2. The traditional power network has relied on the high inertia of the turbines and SMs as the first defence against large power imbalance disturbances [49]. Then the increase of renewable power sources, that are characterized by their low or lack of mechanical inertia, poses a threat to the power network's stability and new control tools must be developed [112, 115, 165].
3. Renewable power sources pose additional problems related to secondary frequency control and the power generation scheduling because of their uncontrollable and stochastic nature [22, 101]. Although energy storage and load demand management

[82, 92] technologies have been developed, a complete solution to this problem has not been given yet.

Even though these control problems are mainly solved at one of the three control layers, the links between these layers, the control problem they solve and the modelling approach they use are fuzzy and not well defined in the literature. This, indeed, poses a barrier for the proposal of new generation technologies and control strategies, as the power network cannot be studied properly and the compliance with the current infrastructure of the network becomes cumbersome. In this Thesis we provide a review of the different components of the power grid from a network perspective, with the aim of understanding the control specifications of the various layers and the role that each of them has in satisfying them; also we want to characterise how the control layers interact among themselves and the power network itself.

Addressing these questions is crucial for understanding the power network dynamics and for the proper definition of the control tasks needed, so that control and equipment designers account for the current infrastructure of the power network. To tackle these questions we propose a review of the primary layer, where the physics and the dynamics models of the main constituents of the power network is given. We also define the different control problems faced by each of the generator types and review the different control approaches that solve these problems (all of this from a micro-scale point of view). Then, after this, we introduce the secondary and tertiary layers and the different modelling approaches used. We explain the frequency control problem and the power scheduling task from a macro-scale point of view. We also show the control strategies that have been proposed to solve it.

As it is not always possible to guarantee that the power network hierarchical control architecture will provide proper compensation after a major disturbance (like transmission lines or generators tripping) last resort strategies have been devised to ensure frequency stability and power dispatch across sections of the grid. Among these, we find the *Intentional Controlled Islanding* (ICI) strategies in [?, 1, 70, 130, 155], i.e. algorithms to identify sections of the grid that can isolate and operate independently from it, guaranteeing a better degree of resilience to extreme events such as cascading failures by ensuring that power can be dispatched at least in some portions of the faulty grid. Also, the presence of storage devices in networks dominated by distributed energy generation makes it possible to isolate the power network into *multi-microgrids* or *networks of microgrids*, e.g., [13, 80, 172], allowing the mitigation of contingencies through ICI and giving further independence to each island.

In spite of the fact that many ICI strategies have been proposed to solve the islanding problem, all of them, to the best of our knowledge, depend on centralised computations, that may become a problem for large scale power networks and power networks dominated by distributed generation. For this reason, we propose a distributed power network partitioning algorithm that solves the islanding problem in a distributed manner through self-organized migration of nodes among islands of the power network such that the average absolute power imbalance of the network remains bounded.

The distributed solution to the islanding problem that we present can be of great interest for large-scale power grids management entities with many control areas and/ or large amounts of distributed generation, as it allows to decide a suitable power network partition in a distributed manner without sharing sensible information like generation costs and without the need of centralised computations, that can become impractical in the large scale setting.

As the pandemic struck during the course of this PhD, this Thesis also reports work carried out to model the epidemic by considering a regional network of Italy, with the aim of suggesting new possible mitigation strategies. The Appendix A contains a brief summary of this work. For further details, see [52].

1.1 Thesis structure and outline

The outline of the Thesis can be given as follows:

Chapter 2 presents an overview of the main components of the power network at a micro-scale, by explaining the physics behind their functioning and introducing a proper modelling approach of their nonlinear dynamics. Being the SMs and the VSCs the main actuation of the power network, we compare them from a control oriented perspective by highlighting their main inputs and outputs, and the role they play in the energy conversion process. We then introduce the electrical model of the power grid, which aims at modelling the interaction between all power network components with the aid of graph theoretical tools. After this modelling overview, we describe the primary control layer, in charge of controlling the power network at the generators level. We present the main control specifications that a generator must fulfill, its relation with the overall power network operation, the main control approaches that have been proposed in literature and how they fulfill these specifications.

Chapter 3 describes the power network as a complex system. First, we introduce the Swing Equation as a simplified model of the power network and then, through singular perturbation tools, we unveil the characteristic time-scale separation of the electrical model of the power grid, allowing us to show how this highly complex model can be simplified into the swing equation itself. We then explain how each of the components of the power network can be modelled using the swing equation, highlighting its simpler modelling capabilities.

Chapter 4 explains the control architecture of the power network as a whole, encompassing the control task of the primary layer, explaining the role of the secondary and the tertiary layer and the mechanisms that make them work together. Finally, a review of the secondary and tertiary control design is given.

Chapter 5 presents a novel distributed power network partitioning algorithm, for solving the power network islanding problem. Our proposal gives the ability to the nodes in the power network to migrate among the islands of a given initial partition of the power network, where the migration is decided in a distributed manner such that the *average absolute power imbalance* remains within a certain bound. In this manner, we formulate the islanding problem from a graph theoretical point of view and use the modelling approach of the Chapter 3 as a proxy for its formulation. Then, we give an overview of the *Intentional Controlled Islanding* strategies that have been proposed to tackle the islanding problem. Hereafter, we explain the rationale behind the distributed solution of the islanding problem that we propose and introduce the distributed power imbalance estimator, which plays an important role for the migration decision-making. Subsequently, the distributed migration strategy is explained. We demonstrate analytically that our method finds, under some assumption on the network structure and in a finite number of migration steps, a partition of the power network such that the *average absolute power imbalance* remains within a certain bound from the total power imbalance of the power network, whose expression is given.

Finally, a summary of our results and discussion over their implications, complemented with possible future research directions, are drawn in Chapter 6.

In the Appendix A of the Thesis, a summary is included of unrelated work carried out during the PhD related with the modelling of the spread of COVID-19 in Italy and the proposal of containment strategies.

1.2 List of Publications

The results in this Thesis produced the following publications

- Lo Iudice F.*, Cardona-Rivera R.*, Grotta A., Coraggio M., di Bernardo M. Utilizing synchronization to partition power networks into microgrids, In preparation (Chapter 5).
- Della Rossa F.*, Salzano D.*, Di Meglio A.*, De Lellis F.*, Coraggio M., Calabrese C., Guarino A., Cardona-Rivera R., De Lellis P., Liuzza D., Lo Iudice F., Russo G., di Bernardo M. (2020). A network model of Italy shows that intermittent regional strategies can alleviate the COVID-19 epidemic. Nature communications, 11(1), 1-9 (Appendix A).

2 Compositional modelling of the power grid and the primary control layer.

A power grid is an ensemble of electric generators and loads interconnected by transmission lines (See Figure 2.1). The dynamics of each of these three different elements can be obtained from the physical laws describing their components. In this chapter, we derive the different dynamical models used to describe them based on first principles and then, we put these models together with the aid of graph theoretical tools to derive the **Power Grid Electrical Model**, which is the most detailed representation of a power grid that we can offer. After this, we introduce the primary control layer, which is in charge of controlling the power grid at the micro-scale, using the generators as the actuation of the network. We present an exhaustive review of the current modelling and control literature with the aim of giving a unified description of the power grid from a control theoretical point of view.

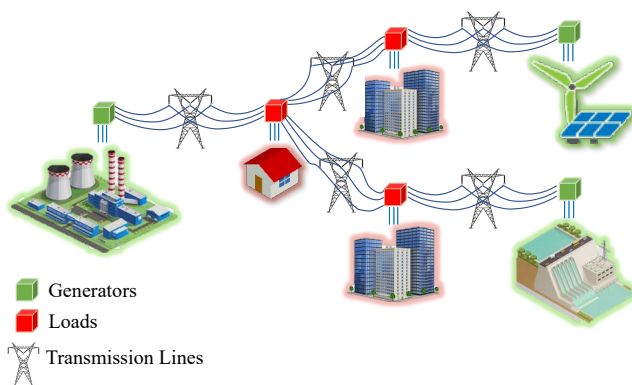


Figure 2.1: The power grid and its components

2.1 Preliminaries

In the following, we introduce a series of definitions and properties that are useful for the results in the following Chapters.

We consider three phase-symmetric AC variables $x(t)$ written in ABC-coordinates as

$$x(t) = \begin{bmatrix} x_a \\ x_b \\ x_c \end{bmatrix} := \bar{x}(t) \begin{bmatrix} \cos(\theta(t) + \phi) \\ \cos\left(\theta(t) + \phi - \frac{2\pi}{3}\right) \\ \cos\left(\theta(t) + \phi + \frac{2\pi}{3}\right) \end{bmatrix} \quad (2.1)$$

where $\bar{x}(t)$ is the amplitude of the signal at time t , $\theta(t)$ is a time varying phase and ϕ is a constant phase lag. Note that $x_a + x_b + x_c = 0 \forall t$.

We also define the four-dimensional variable

$$\mathbf{x} := \begin{bmatrix} x_a \\ x_b \\ x_c \\ x_r \end{bmatrix} = \begin{bmatrix} \bar{x}(t) \cos(\theta(t) + \phi) \\ \bar{x}(t) \cos\left(\theta(t) + \phi - \frac{2\pi}{3}\right) \\ \bar{x}(t) \cos\left(\theta(t) + \phi + \frac{2\pi}{3}\right) \\ x_r \end{bmatrix} \quad (2.2)$$

that considers the so-called rotor coordinate and the the AC variable $x(t)$ in (2.1).

2.1.1 Coordinate Transformations

A three-phase AC signal can also be represented in several transformed coordinates, i.e., the $\alpha\beta$ -coordinates, the *DQZ*-coordinates and the *Phasor representation* [64, 98]. The $\alpha\beta$ -coordinates can be defined as $x_{\alpha\beta} = T_{\alpha\beta}x$ with

$$T_{\alpha\beta} := \sqrt{\frac{2}{3}} \begin{bmatrix} 1 & -\frac{1}{2} & -\frac{1}{2} \\ 0 & \frac{\sqrt{3}}{2} & -\frac{\sqrt{3}}{2} \\ \frac{\sqrt{2}}{2} & \frac{\sqrt{2}}{2} & \frac{\sqrt{2}}{2} \end{bmatrix}. \quad (2.3)$$

As the third component of the product $T_{\alpha\beta}x(t)$ is always zero for all possible values of $\theta(t)$, the $\alpha\beta$ -transformation projects the three-phase signal x onto \mathbb{R}^2 . In what follows, we use the rotation matrix:

$$\text{Rot}(\eta) := \begin{bmatrix} \cos(\eta) & -\sin(\eta) \\ \sin(\eta) & \cos(\eta) \end{bmatrix} \quad (2.4)$$

whose derivative with respect to η can be written as

$$\frac{\partial \text{Rot}(\eta)}{\partial \eta} = -J \text{Rot}(\eta) \quad (2.5)$$

with

$$J = \begin{bmatrix} 0 & 1 \\ -1 & 0 \end{bmatrix}. \quad (2.6)$$

The following matrixes will become useful

$$J_3 := \begin{bmatrix} 0 & 1 & 0 \\ -1 & 0 & 0 \\ 0 & 0 & 0 \end{bmatrix}, \quad (2.7)$$

$$\mathbf{J} = \begin{bmatrix} J_3 & \mathbb{0}_3 \\ \mathbb{0}_3^\top & 0 \end{bmatrix}, \quad (2.8)$$

with $\mathbb{0}_3 = [0, 0, 0]^\top$.

Given the $\alpha\beta$ -transformation matrix in (2.3) and the rotation matrix in (2.4), we introduce the DQZ-transformation matrix as

$$T_{dq}(\eta) := \begin{bmatrix} \text{Rot}(-\eta) & 0_{2 \times 1} \\ 0_{1 \times 2} & 1 \end{bmatrix} T_{\alpha\beta}, \quad (2.9)$$

where the product $T_{dq}(\eta)x(t)$ also projects any three phase signal x onto \mathbb{R}^2 . Notice that $T_{dq}(\eta)$ is an orthonormal transformation, so that $T_{dq}(\eta)^{-1} = T_{dq}(\eta)^\top$. Applying (2.9) to x in (2.1), we obtain the DQZ-representation of the signal x as

$$x_{dq} := \begin{bmatrix} x_d \\ x_q \\ x_0 \end{bmatrix} = T_{dq}(\eta)x = \sqrt{\frac{3}{2}} \bar{x}(t) \begin{bmatrix} \cos(\theta - \eta + \phi) \\ \sin(\theta - \eta + \phi) \\ 0 \end{bmatrix}. \quad (2.10)$$

The fact that the x_0 coordinate in (2.10) is zero $\forall t$ allows us to dismiss it when the DQZ-transformation is applied to symmetric AC variables as in (2.1), leading to the *DQ-coordinates* $x_{dq} = [x_d, x_q]^\top$.

From (2.10), a relationship between the time derivatives of variables expressed in ABC and DQZ-coordinates can be established. Specifically, we have

$$\dot{x}_{dq} = \dot{T}_{dq}(\eta)x + T_{dq}(\eta)\dot{x}.$$

From (2.5) we can write

$$\dot{T}_{dq}(\eta) = \dot{\eta}J_3T_{dq}(\eta)$$

and by using the inverse transform $x = T_{dq}(\eta)^\top x_{dq}$ we get

$$\dot{x}_{dq} = \dot{\eta}J_3x_{dq} + T_{dq}(\eta)\dot{x}. \quad (2.11)$$

We also define the *extended* DQZ-transformation $\mathbf{x}_{dqr} = T_{dqr}(\eta)\mathbf{x}$ for the four-dimensional variables in (2.2), with transformation matrix

$$T_{dqr}(\eta) = \begin{bmatrix} T_{dq}(\eta) & \mathbb{0}_3 \\ \mathbb{0}_3^\top & 1 \end{bmatrix}, \quad (2.12)$$

which yields the following expression for the time derivative of \mathbf{x}_{dqr}

$$\dot{\mathbf{x}}_{\text{dqr}} = \dot{\eta} \mathbf{J} \mathbf{x}_{\text{dqr}} + T_{\text{dqr}}(\eta) \dot{\mathbf{x}}. \quad (2.13)$$

Another representation of a three phase-symmetric AC signal can be obtained by using the Phasor representation, written as

$$\vec{X} := X(t)e^{j\phi} = X(t) \cos(\phi) + jX(t) \sin(\phi), \quad (2.14)$$

with $\vec{X} \in \mathbb{C}$ and $X(t)$ being the Root Mean Square (RMS) value of the signal in ABC-coordinates, defined as

$$X(t) := \sqrt{\frac{1}{T} \int_0^T x(t)^\top x(t) dt}. \quad (2.15)$$

Note that if \bar{x} is constant, we can write $X(t) = \frac{\bar{x}}{\sqrt{2}}$. The phasor in (2.14) can be written in terms of the DQZ-coordinates for a three phase-symmetric AC variable x . This relation is the *Phasor to DQ-coordinates transformation*, which reads

$$\vec{X} = \frac{\bar{x}}{\sqrt{2}} \cos(\phi) + j \frac{\bar{x}}{\sqrt{2}} \sin(\phi) = \frac{x_d}{\sqrt{3}} + j \frac{x_q}{\sqrt{3}}. \quad (2.16)$$

2.1.2 Power Definition

In this Thesis, we use the following definition of *instantaneous active and reactive power* [5, 133]

$$p(t) := v^\top i = v_{\text{dq}}^\top i_{\text{dq}}, \quad (2.17a)$$

$$q(t) := \|v \times i\| = v_{\text{dq}}^\top J_3 i_{\text{dq}}, \quad (2.17b)$$

with $v \in \mathbb{R}^3$ and $i \in \mathbb{R}^3$ being voltage and current signals in ABC-coordinates and v_{dq} and i_{dq} its DQZ-coordinates representation. If we assume v and i to possess the same structure as (2.1) and to possess the same time varying phase θ , we can write

$$v = \bar{v} \begin{bmatrix} \cos(\theta + \phi_v) \\ \cos(\theta + \phi_v - \frac{2\pi}{3}) \\ \cos(\theta + \phi_v + \frac{2\pi}{3}) \end{bmatrix}, \quad (2.18a)$$

$$i = \bar{i} \begin{bmatrix} \cos(\theta + \phi_i) \\ \cos(\theta + \phi_i - \frac{2\pi}{3}) \\ \cos(\theta + \phi_i + \frac{2\pi}{3}) \end{bmatrix}, \quad (2.18b)$$

with ϕ_v and ϕ_i as constant phase angles. Substituting (2.18) in (2.17) leads to

$$p = \frac{3}{2} \bar{v} \bar{i} \cos(\phi_v - \phi_i), \quad (2.19a)$$

$$q = \frac{3}{2} \bar{v} \bar{i} \sin(\phi_v - \phi_i). \quad (2.19b)$$

The *single-phase average active power* is defined as the mean value of the instantaneous quantity (2.17a) over a period T , defined as [160]:

$$P := \frac{1}{3T} \int_0^T p(t) dt. \quad (2.20)$$

In general $T = \frac{2\pi}{\omega_{\text{ref}}}$ with ω_{ref} being a desired common angular frequency of the three-phase AC signals on a power network.

Now, if we assume that \bar{v} and \bar{i} are constant we can write the voltage and current v and i in phasor representation as

$$\vec{V} = V (\cos(\phi_v) + j \sin(\phi_v)), \quad (2.21a)$$

$$\vec{I} = I (\cos(\phi_i) + j \sin(\phi_i)), \quad (2.21b)$$

with RMS values V and I for the voltage v and current i as in (2.15). Given these quantities, we can define the *apparent power*

$$\vec{S} := \vec{V} \vec{I}^* = P + jQ \quad (2.22)$$

with I^* being the conjugate of I and Q being the *reactive power per phase*, written as:

$$Q = \sqrt{S^2 - P^2}. \quad (2.23)$$

With this, and considering voltage and current signals as in (2.18) we can write the active and reactive power in (2.20) and (2.23) as

$$P = \frac{1}{2} \bar{v} \bar{i} \cos(\phi_v - \phi_i) = \text{Re}(\vec{V} \vec{I}^*), \quad (2.24a)$$

$$Q = \frac{1}{2} \bar{v} \bar{i} \sin(\phi_v - \phi_i) = \text{Im}(\vec{V} \vec{I}^*). \quad (2.24b)$$

Given the Phasor to DQ-coordinates transformation in (2.16) and the expressions in (2.18) we define the **active and reactive power** in terms of the DQZ-coordinates as

$$P = \frac{p}{3} = \frac{1}{3} (v_d i_d + v_q i_q), \quad (2.25a)$$

$$Q = \frac{q}{3} = \frac{1}{3} (v_d i_q - v_q i_d). \quad (2.25b)$$

Note that both (2.24) and (2.25) assume that \bar{v} and \bar{i} are constant.

2.1.3 Useful Identities

As it will become useful for some computations, we consider the harmonic addition identity as [173]:

$$a \cos(x) + b \sin(x) = \operatorname{sgn}(a) \sqrt{a^2 + b^2} \cos\left(x + \arctan\left(-\frac{b}{a}\right)\right). \quad (2.26)$$

2.2 Generator models

2.2.1 The synchronous machine

Synchronous Machines (SM) are devices that transform mechanical energy into electrical energy relying on Faraday's law of electromagnetic induction. Inside a SM, a rotating magnetic field induces a time varying voltage on static coils. These machines are generally made of two main parts, a stator and a rotor [98]. The *rotor* is a mechanical device that transmits the mechanical energy coming from a flywheel rotating at an angular frequency ω_m and is surrounded by a DC magnetic field with N_p poles. These magnetic poles are generated by a coil array called the field windings or by a set of permanent magnets. The purpose of the rotor is to magnetically induce three-phase AC currents with angular frequency ω on the *stator*, the latter being formed by a set of coils (one per phase). The magnetic field coupling between the rotor and the stator allows the transformation of mechanical energy into electrical energy. Both the electrical and mechanical angular frequencies, ω_m and ω , are related through the expression $\omega_m = \frac{N_p}{2} \omega$.

Considering a flywheel dynamics with mechanical damping [44, 142, 166], we can write the rotor's rotational motion dynamic, as

$$\dot{\theta} = \omega_m, \quad (2.27a)$$

$$M\dot{\omega}_m = -D\omega_m - \tau_e + \tau_m, \quad (2.27b)$$

where M is the inertia constant, D is a mechanical friction coefficient and θ is the angular position of the rotor. In the following, we consider a two-pole SM for simplicity, implying that $\omega_m = \omega$. The mechanical torque τ_m is an input coming from an external power source, a steam turbine for example, whose output is controllable. The electrical torque τ_e is induced by the magnetic field inside the coils but, before giving its expression, the magnetic field dynamics must be introduced.

We consider a SM with a single-field winding [31, 71], which is a simplification of the more general Three-Damper-Winding model in [142]. This simplification assumes that the aggregated effect of the damper windings can be modelled by only one flux linkage λ_r and is valid for cylindrical rotor SMs which are widely used in thermal, gas and nuclear power generation [31], (See Figure (2.2)). The main variables of interest on the magnetic

field dynamics are the **flux linkages** $\boldsymbol{\lambda} \in \mathbb{R}^4$, representing the total magnetic field passing through each of the coils of the stator (λ_a, λ_b and λ_c) and the rotor coil (λ_r) of the SM. Assuming no subharmonics on the magnetic field, the flux linkages evolve according to the dynamics [31, 71]

$$\dot{\boldsymbol{\lambda}} = -RL^{-1}(\theta)\boldsymbol{\lambda} + \mathbf{v}, \quad (2.28)$$

with $\mathbf{v} \in \mathbb{R}^4$ being the vector of the voltages on the stator (v_a, v_b and v_c) and rotor (v_r) coil terminals (see Figure (2.2)), R the electrical resistance of these coils and $L(\theta)$ the **inductance matrix**, that describes a linear relation between the flux linkages and the winding currents $\mathbf{i} \in \mathbb{R}^4$ according to

$$\boldsymbol{\lambda} = L(\theta)\mathbf{i}. \quad (2.29)$$

Note that all of the three variables $\boldsymbol{\lambda}, \mathbf{v}$ and \mathbf{i} are four-dimensional variables as in (2.2).

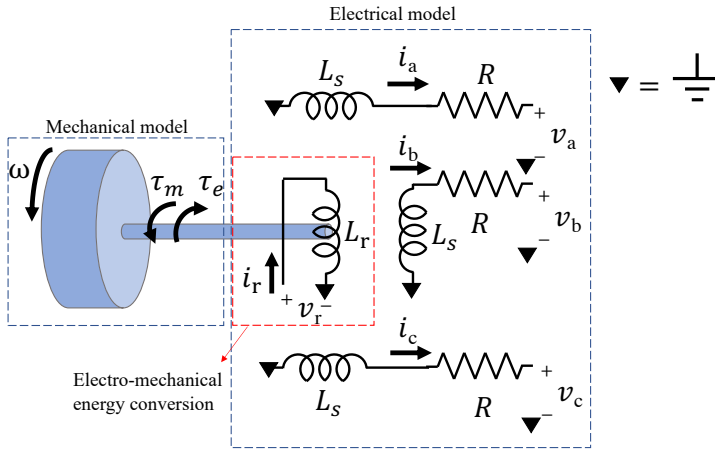


Figure 2.2: Representation of the synchronous machine model described by equations (2.27) to (2.29)

Remark 2.1. Notice that model (2.28) is written in the so-called *motor convention* [44], which implies that currents \mathbf{i} must change sign when considering the generator model.

In what follows, we use the definition of inductance matrix given in [71, Appendix C] for a three-phase SM without saliency terms and for the sake of simplicity, we apply the extended DQZ-transformation (2.12). Multiplying both sides of (2.28) by $T_{\text{dqr}}(\theta)$ and using (2.13) yields

$$\dot{\boldsymbol{\lambda}}_{\text{dqr}} = -RL_{\text{dqr}}^{-1}\boldsymbol{\lambda}_{\text{dqr}} + \omega\mathbf{J}\boldsymbol{\lambda}_{\text{dqr}} + \mathbf{v}_{\text{dqr}}, \quad (2.30)$$

with \mathbf{J} as in (2.8). The matrix $L_{\text{dqr}} = T_{\text{dqr}}(\theta)L(\theta)T_{\text{dqr}}(\theta)^\top$ is the inductance matrix in DQZ-coordinates [71] given by

$$L_{\text{dqr}} = \begin{bmatrix} L_{\text{d}} & 0 & 0 & L_{\text{e}} \\ 0 & L_{\text{q}} & 0 & 0 \\ 0 & 0 & L_{\text{sl}} & 0 \\ L_{\text{e}} & 0 & 0 & L_{\text{r}} \end{bmatrix} \quad (2.31)$$

where L_{d} , L_{q} are the direct- and quadrature- synchronous inductances, that are equal in the absence of saliency terms $L_{\text{d}} = L_{\text{q}} = L_{\text{s}}$, with L_{s} being the stator inductance. L_{sl} is the armature windings leakage inductance L_{r} being the field winding self-inductance and $L_{\text{e}} = \sqrt{\frac{3}{2}}L_{\text{sr}}$ with L_{sr} being the stator-to-rotor mutual inductance magnitude.

Remark 2.2. In a more general setting, the direct- and quadrature synchronous inductances in (2.31) are $L_{\text{d}} = L_{\text{sl}} + \frac{3}{2}(L_{\text{s0}} + L_{\text{g}})$ and $L_{\text{q}} = L_{\text{sl}} + \frac{3}{2}(L_{\text{s0}} - L_{\text{g}})$ with L_{s0} accounting for the space-fundamental component of air-gap inductance, and L_{g} a term accounting for the presence of salient poles [71].

The main connection between the mechanical and electrical models (2.27) and (2.28) is the electrical torque τ_e , whose expression can be derived from the energy conservation law in the SM coupling magnetic field [142], given by

$$H_{\text{g}} = H_{\text{e}} + H_{\text{m}},$$

where H_{g} , H_{e} and H_{m} are the stored energy on the magnetic field, the electrical and the electromechanical energy, respectively. Since the time derivative of the stored magnetic energy can be written as [71, 142]

$$\dot{H}_{\text{g}} = \underbrace{\mathbf{i}^\top \dot{\boldsymbol{\lambda}}}_{\text{Electrical power}} + \underbrace{\tau_e \omega}_{\text{Electro-Mechanical Power}} \quad (2.32)$$

and the total derivative of $H_{\text{g}}(\boldsymbol{\lambda}, \theta)$ is

$$\dot{H}_{\text{g}}(\boldsymbol{\lambda}, \theta) = \frac{\partial H_{\text{g}}(\boldsymbol{\lambda}, \theta)}{\partial \boldsymbol{\lambda}} \dot{\boldsymbol{\lambda}} + \frac{\partial H_{\text{g}}(\boldsymbol{\lambda}, \theta)}{\partial \theta} \omega. \quad (2.33)$$

By comparing (2.32) and (2.33), the electrical torque can be computed as

$$\tau_e = \frac{\partial H_{\text{g}}(\boldsymbol{\lambda}, \theta)}{\partial \theta}. \quad (2.34)$$

Now, as the stored magnetic energy can be expressed as $H_{\text{g}}(\boldsymbol{\lambda}, \theta) = \frac{1}{2} \mathbf{i}^\top L(\theta) \mathbf{i}$ [71], one can write (2.34) as

$$\tau_e = \frac{1}{2} \mathbf{i}^\top \frac{\partial L(\theta)}{\partial \theta} \mathbf{i} = \frac{1}{2} \mathbf{i}_{\text{dqr}}^\top \mathbf{J} L_{\text{dqr}} \mathbf{i}_{\text{dqr}}, \quad (2.35)$$

with \mathbf{J} as in (2.8). This allows us to write the electromechanical torque expression in DQZ-coordinates as

$$\tau_e = -L_e \dot{i}_r i_q.$$

Although the SM model (2.30) comes from physical laws, it is not suitable for control design because the flux linkage λ_{dqr} is difficult to measure directly. To avoid this, the linear relation (2.29), written in DQZ coordinates as

$$\boldsymbol{\lambda}_{dqr} = L_{dqr} \mathbf{i}_{dqr}, \quad (2.36)$$

can be exploited to rewrite the flux linkage dynamics (2.30) as

$$L_{dqr} \dot{\mathbf{i}}_{dqr} = -R \mathbf{i}_{dqr} + \omega \mathbf{J} L_{dqr} \mathbf{i}_{dqr} + \mathbf{v}_{dqr}. \quad (2.37)$$

Now, rewriting (2.37) in scalar form, we get

$$L_d \dot{i}_d + L_e \dot{i}_r = -R i_d + \omega L_q i_q + v_d \quad (2.38a)$$

$$L_q \dot{i}_q = -R i_q - \omega L_d i_d - \omega L_e i_r + v_q \quad (2.38b)$$

$$L_{sl} \dot{i}_0 = -R i_0 + v_0 \quad (2.38c)$$

$$L_r \dot{i}_r + L_e \dot{i}_d = -R i_r + v_r \quad (2.38d)$$

Notice that defining a field winding voltage control action as

$$v_r = L_r \dot{i}_r + L_e \dot{i}_d + \kappa (i_r - i_r^*) \quad (2.39)$$

for some positive κ and given a suitable reference value i_r^* , from (2.38d), we can guarantee $\dot{i}_r = 0$ [31, 56]. Selecting v_r as in (2.39) further simplifies the SM model (2.38). Also notice that (i) equation (2.38c) represents a stable linear system whose input is $v_0 = 0$ for three-phase stator voltages v_a, v_b and v_c of the form in (2.1) and that (ii) the dynamics of the other state variables in (2.38) are independent of i_0 and v_0 . Then, we can safely disregard (2.38c). Also consider that we can obtain the SM model in *generator notation* by applying $i_d = -i_d$ and $i_q = -i_q$ [142]. With this in mind, we can then write the following simplified model of the SM in DQ-coordinates:

$$\dot{\theta} = \omega \quad (2.40a)$$

$$M \dot{\omega} = -D \omega - L_e \dot{i}_r i_q + \tau_m \quad (2.40b)$$

$$L_d \dot{i}_d = -R i_d + \omega L_q i_q - v_d \quad (2.40c)$$

$$L_q \dot{i}_q = -R i_q - \omega L_d i_d + \omega L_e \dot{i}_r - v_q. \quad (2.40d)$$

2.2.2 The voltage source converter

Voltage Source Converters (VSC) are devices that serve as interface between a DC power source, typically a renewable energy source [115, 158] and the three-phase AC network. In this Thesis, we choose the VSC architecture depicted in Figure 2.3 for explanatory purposes [16, 158, 178]. It is composed of three main stages, the **DC power stage**, the **power electronics stage** responsible of the DC/AC conversion and the **AC power stage**. To obtain a model of the selected architecture of the VSC, we start by noting that the three-phase AC output current $i = [i_a, i_b, i_c]^T$ of the **AC power stage** must fulfill Kirchhoff's Voltage Law (KVL), i.e. [26, 178],

$$L_f \dot{i} = -Ri + v_{sw} - v \quad (2.41)$$

where L_f and R are the inductance and resistance of the output resistive-inductive filter of the VSC and $v = [v_a, v_b, v_c]^T$ is the three-phase output voltage.

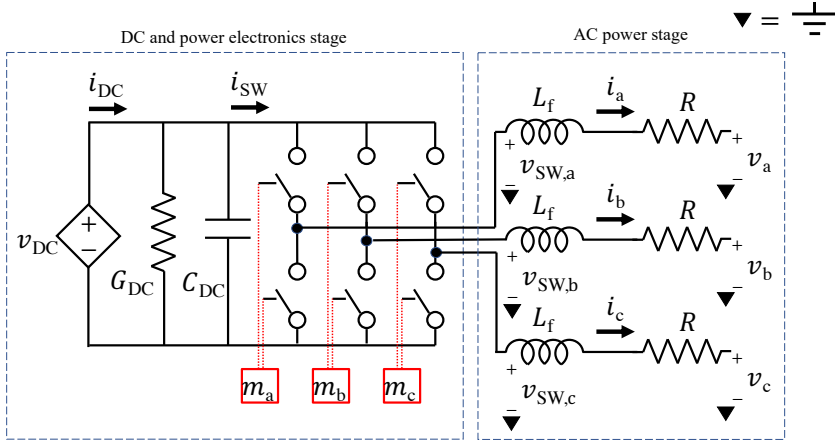


Figure 2.3: Representation of the voltage source converter model described by equations (2.46)

The switching voltage v_{sw} in (2.41) is a piece-wise smooth control signal depending on the commutation patterns used to drive the **power electronics stage** and depends directly on the DC voltage. It is normal practice to consider that the commutation patterns are generated via a Pulse-Width-Modulation strategy with a high frequency carrier, whose harmonics are discarded, allowing the use of an averaged version of v_{sw} [178]. Considering that the selected VSC architecture (see Figure 2.3) has 6 lossless switches with only two logical values, we can write the average-switching voltage as [178]

$$v_{sw} = \frac{1}{2} v_{DC} m \quad (2.42)$$

where v_{DC} is the DC voltage from the power source of the VSC and $m = [m_a, m_b, m_c]^T$ such that $\|m\| \leq 1$ is the averaged amplitude of the modulating signal which allows to

transform the DC signal from the power source into a three-phase AC signal.

The **DC power stage** dynamics, instead, are mainly dominated by the voltage of the DC power source $v_{\text{DC}} \in \mathbb{R}$ and can be obtained by using Kirchhoff's Current Law (KCL), i.e.,

$$C_{\text{DC}}\dot{v}_{\text{DC}} = -G_{\text{DC}}v_{\text{DC}} - i_{\text{sw}} + i_{\text{DC}} \quad (2.43)$$

where C_{DC} and G_{DC} are the capacitance and admittance at the input of the VSC, and $i_{\text{DC}} \in \mathbb{R}$ is the current drawn from the DC power source and $i_{\text{sw}} \in \mathbb{R}$ is the switching input current to the power electronics. Using the expression for v_{sw} given in (2.42), from (2.45), the average-switching current becomes

$$i_{\text{sw}} = \frac{1}{2}m^{\text{T}}i. \quad (2.44)$$

Now, as we consider a lossless energy conversion process, the input and output power of the **power electronics stage** must be the same, which implies

$$v_{\text{DC}}i_{\text{sw}} = v_{\text{sw}}^{\text{T}}i. \quad (2.45)$$

Finally, substituting (2.44) in (2.43), and (2.42) in (2.41), the complete model of the VSC in ABC-coordinates can be written as

$$C_{\text{DC}}\dot{v}_{\text{DC}} = -G_{\text{DC}}v_{\text{DC}} - \frac{1}{2}m^{\text{T}}i + i_{\text{DC}} \quad (2.46a)$$

$$L_{\text{f}}\dot{i} = -Ri + \frac{1}{2}mv_{\text{DC}} - v \quad (2.46b)$$

The VSC model (2.46) can be expressed in DQZ-coordinates by applying the transformation in (2.9) as $T_{\text{dq}}(\theta)$, with θ being the phase angle of the voltage v , yielding

$$C_{\text{DC}}\dot{v}_{\text{DC}} = -G_{\text{DC}}v_{\text{DC}} - \frac{1}{2}m_{\text{dq}}^{\text{T}}i_{\text{dq}} + i_{\text{DC}} \quad (2.47a)$$

$$L_{\text{f}}\dot{i}_{\text{dq}} = -(RI_3 - \omega L_{\text{f}}J_3)i_{\text{dq}} + \frac{1}{2}m_{\text{dq}}v_{\text{DC}} - v_{\text{dq}} \quad (2.47b)$$

with $I_3 \in \mathbb{R}^{3 \times 3}$ the identity matrix and J_3 as in (2.7). In scalar form we obtain

$$C_{\text{DC}}\dot{v}_{\text{DC}} = -G_{\text{DC}}v_{\text{DC}} - \frac{1}{2}m_{\text{dq}}^{\text{T}}i_{\text{dq}} + i_{\text{DC}} \quad (2.48a)$$

$$L_{\text{f}}\dot{i}_{\text{d}} = -Ri_{\text{d}} + \omega L_{\text{f}}i_{\text{q}} + \frac{1}{2}m_{\text{d}}v_{\text{DC}} - v_{\text{d}} \quad (2.48b)$$

$$L_{\text{f}}\dot{i}_{\text{q}} = -Ri_{\text{q}} - \omega L_{\text{f}}i_{\text{d}} + \frac{1}{2}m_{\text{q}}v_{\text{DC}} - v_{\text{q}} \quad (2.48c)$$

$$L_{\text{f}}\dot{i}_0 = -Ri_0 - v_0 \quad (2.48d)$$

As it has been done for the SM, notice that (i) equation (2.48d) represents a stable linear system whose input is $v_0 = 0$ for three-phase stator voltages v_a, v_b and v_c of the form in (2.1) and that (ii) the dynamics of the other state variables in (2.48) are independent of i_0 and v_0 . Then, we can safely disregard (2.48d), obtaining the following final model of the VSC in DQ-coordinates:

$$C_{\text{DC}}\dot{v}_{\text{DC}} = -G_{\text{DC}}v_{\text{DC}} - \frac{1}{2}m_{\text{dq}}^{\text{T}}i_{\text{dq}} + i_{\text{DC}} \quad (2.49\text{a})$$

$$L_{\text{f}}\dot{i}_{\text{d}} = -Ri_{\text{d}} + \omega L_{\text{f}}i_{\text{q}} + \frac{1}{2}m_{\text{d}}v_{\text{DC}} - v_{\text{d}} \quad (2.49\text{b})$$

$$L_{\text{f}}\dot{i}_{\text{q}} = -Ri_{\text{q}} - \omega L_{\text{f}}i_{\text{d}} + \frac{1}{2}m_{\text{q}}v_{\text{DC}} - v_{\text{q}} \quad (2.49\text{c})$$

A summary of all the variables and parameters can be found in Table 2.1.

2.2.3 Comparing the generator models

The generator models (2.40) and (2.46) arise from quite different physical laws. However, they share several relevant structural similarities as both systems are made of three stages, power supply, energy storage, and power conversion, that share the same purposes. [56, 129, 166]. Here we discuss both similarities and differences in these three stages.

- **Power supply stage:** regardless of the nature of the generator, external power must be fed to it, whether it is the mechanical torque τ_{m} for a SM or the DC current i_{DC} for a VSC. These external inputs play the crucial role of ensuring power balance as they are the power source of the network itself. These variables have different limitations due to the availability of the power source, being, in the case of the DC input of VSCs, the maximum current ratings defined by the design of the VSC and the stochasticity of the power generation conditions like the weather define the actual power limitations. On the other hand, the SMs case is slightly different as their power supply is controllable within the range defined by technological limitations.
- **Energy storage stage:** both SMs and VSCs are characterized by energy storage devices guaranteeing robustness of the energy conversion. In SMs, the kinetic energy is stored in the rotor thanks to its large inertia M , while in VSCs, the DC electrical energy is stored on the capacitance C_{DC} . As the inertia provided by the flywheel is many orders of magnitude greater than the one provided by the DC capacitors, SMs are more robust to disturbances compared to VSCs. This must be compensated with appropriate control actions in the case of the VSCs.
- **Power conversion stage:** this stage is responsible for converting the external input into AC power whose frequency must be compatible with that of the grid. SMs convert mechanical energy into AC electrical energy through the magnetic coupling between the rotor and the stator, while VSCs convert DC electrical energy into AC electrical energy thanks to the modulation of the switching sequences of the power electronics.

Remark 2.3. In some special cases, both systems become *structurally equivalent* from a dynamical systems point of view. This happens when the modulating signal m is designed to confer a virtual inertia to the frequency of the AC signals of the VSC, emulating the mechanical coupling of a SM (2.27) [183].

Both in SMs and VSCs, the energy storage and the power conversion stages are inherently linked and determine the performance of the power grid as a whole. To show this in a quantitative fashion, we derive next the power balance equations for both types of generators. We start by introducing the total energy in systems (2.30) and (2.46) [56, 71] as:

$$H_{\text{SM}} = \frac{1}{2}M\omega^2 + \frac{1}{2}\boldsymbol{\lambda}_{\text{dqr}}^{\text{T}}L_{\text{dqr}}^{-1}\boldsymbol{\lambda}_{\text{dqr}} \quad (2.50\text{a})$$

$$H_{\text{VSC}} = \frac{1}{2}C_{\text{DC}}v_{\text{DC}}^2 + \frac{1}{2}L_{\text{f}}i_{\text{dq}}^{\text{T}}i_{\text{dq}} \quad (2.50\text{b})$$

with (2.50) being the Hamiltonian functions of both SM and VSC in DQZ-coordinates and representing the total energy of both systems. The power balances of both devices can be obtained by differentiating (2.50a) and (2.50b) with respect to time, which yields

$$\dot{H}_{\text{SM}} = \omega M\dot{\omega} + \boldsymbol{\lambda}_{\text{dqr}}^{\text{T}}L_{\text{dqr}}^{-1}\dot{\boldsymbol{\lambda}}_{\text{dqr}} \quad (2.51\text{a})$$

$$\dot{H}_{\text{VSC}} = v_{\text{DC}}C_{\text{DC}}\dot{v}_{\text{DC}} + L_{\text{f}}i_{\text{dq}}^{\text{T}}\dot{i}_{\text{dq}} \quad (2.51\text{b})$$

Substituting the expressions of $\dot{\omega}$, $\dot{\boldsymbol{\lambda}}_{\text{dqr}}$, \dot{v}_{DC} and \dot{i}_{dq} from (2.30) and (2.47) in the power balances (2.51), and using the flux linkage and current relation (2.36) to write the expression in terms of the output current \mathbf{i}_{dqr} , we obtain

$$\dot{H}_{\text{SM}} = -D\omega^2 + \omega L_{\text{e}}i_{\text{r}}i_{\text{q}} + \omega\tau_{\text{m}} - R\mathbf{i}_{\text{dqr}}^{\text{T}}\mathbf{i}_{\text{dqr}} + \omega\mathbf{i}_{\text{dqr}}^{\text{T}}\mathbf{J}L_{\text{dqr}}\mathbf{i}_{\text{dqr}} + \mathbf{i}_{\text{dqr}}^{\text{T}}\mathbf{v}_{\text{dqr}} \quad (2.52\text{a})$$

$$\dot{H}_{\text{VSC}} = -G_{\text{DC}}v_{\text{DC}}^2 + v_{\text{DC}}i_{\text{DC}} - i_{\text{dq}}^{\text{T}}(RI_2 - \omega L_{\text{f}}J_3)i_{\text{dq}} - i_{\text{dq}}^{\text{T}}v_{\text{dq}} \quad (2.52\text{b})$$

As it can be shown that $\mathbf{i}_{\text{dqr}}^{\text{T}}\mathbf{J}L_{\text{dqr}}\mathbf{i}_{\text{dqr}} = -L_{\text{e}}i_{\text{r}}i_{\text{q}}$, then the terms $\omega L_{\text{e}}i_{\text{r}}i_{\text{q}}$ and $\omega\mathbf{i}_{\text{dqr}}^{\text{T}}\mathbf{J}L_{\text{dqr}}\mathbf{i}_{\text{dqr}}$ in (2.52a) cancel each other out. Then, decomposing the dot product $\mathbf{i}_{\text{dqr}}^{\text{T}}\mathbf{v}_{\text{dqr}}$ as $i_{\text{dq}}^{\text{T}}v_{\text{dq}} + i_{\text{r}}v_{\text{r}}$ we can recast the expression of the power balances of the generators as

$$\dot{H}_{\text{SM}} = \underbrace{i_{\text{dq}}^{\text{T}}v_{\text{dq}}}_{\text{Power Output}} + \underbrace{i_{\text{r}}v_{\text{r}} + \omega\tau_{\text{m}}}_{\text{Power Input}} - \underbrace{(D\omega^2 + R\mathbf{i}_{\text{dqr}}^{\text{T}}\mathbf{i}_{\text{dqr}})}_{\text{Power Losses}} \quad (2.53\text{a})$$

$$\dot{H}_{\text{VSC}} = \underbrace{v_{\text{DC}}i_{\text{DC}}}_{\text{Power Input}} - \underbrace{i_{\text{dq}}^{\text{T}}v_{\text{dq}}}_{\text{Power Output}} - \underbrace{(G_{\text{DC}}v_{\text{DC}}^2 + i_{\text{dq}}^{\text{T}}(RI_2 - \omega L_{\text{f}}J_3)i_{\text{dq}})}_{\text{Losses}}. \quad (2.53\text{b})$$

Substituting the right-hand side of (2.51) as the left-hand side of (2.53), and (i) neglecting the power losses terms in (2.53), (ii) considering that in (2.51) the dynamics of the flux linkage λ_{dq} are faster than the frequency dynamics $\dot{\omega}$ (current dynamics i_{dq} faster than voltage dynamics v_{DC} in the VSC's case), (iii) assuming that the power consumption of

the field windings are small ($i_r v_r \approx 0$) and that the SM is in generator representation (i_{dq} changes sign), we obtain the relations

$$\underbrace{\omega M \dot{\omega}}_{\text{Kinetic energy rate}} \approx \underbrace{\omega \tau_m}_{\text{Power Input}} - \underbrace{i_{dq}^T v_{dq}}_{\text{Power Output}} \quad (2.54a)$$

$$\underbrace{v_{DC} C_{DC} \dot{v}_{DC}}_{\text{DC energy source rate}} \approx \underbrace{v_{DC} i_{DC}}_{\text{Power Input}} - \underbrace{i_{dq}^T v_{dq}}_{\text{Power Output}} \quad (2.54b)$$

The approximations in (2.54) show that power imbalances generate a variation in the energy stored in the flywheel of the SMs and in the DC condenser of the VSCs respectively. In the case of SMs, an increase (decrease) of the power output will decelerate (accelerate) the flywheel, generating a decrease (increase) of the SM electrical frequency. While the large inertia M of SMs partly mitigates the frequency variations, the frequency requirements are such that these variations can still jeopardize the correct functioning of the grid thus eliciting the need of a frequency control feedback loop for the SM. Note also that in (2.54) the power output depends on the power at the terminals of the generators as we have $p = i_{dq}^T v_{dq}$ as defined in (2.17a). This fact will be of great usefulness when deriving a simplified network model.

2.3 Load models

The transmitted power is delivered to power consuming devices known as loads. Their modeling is dependent on the scale of the power network that is being evaluated. At a small scale, loads can be modeled as the parallel aggregation of passive electrical elements like resistors, inductors and capacitors, and time varying power demanding devices [17, 63]. Using the KCL on the schematic proposed in Figure 2.4, a load model can be written as

$$C_1 \dot{v}_a + \frac{1}{R_1} v_a + \frac{1}{L_1} \int_{t_0}^t v_a(\tau) d\tau + p_{la}(t) v_a^{-1} = -i_a, \quad (2.55)$$

where the dynamics of the phases b and c are also ruled by the same expression. Here, R_1, C_1 and L_1 are the resistance, capacitance and inductance of the passive elements, $p_l(t)$ is the time dependant power demand, $i = [i_a, i_b, i_c]^T$ is the output current to the aggregated loads and $v = [v_a, v_b, v_c]^T$ is the bus voltage.

Although most of the loads are composed of these elements, their aggregate behavior is not completely captured by the model (2.55) due to the presence of more complex devices like heating and cooling machinery, synchronous motors, etc [136]. To overcome this problem, loads can be modelled by giving expressions (static or dynamic) for the active and reactive average load power consumption P_l and Q_l in terms of the nodal voltage magnitude \bar{v} and frequency ω at steady state. Examples of load models that follow this structure are, among others, the **ZIP model** [17, 136] and the **Exponential Recovery Model** [83, 90].

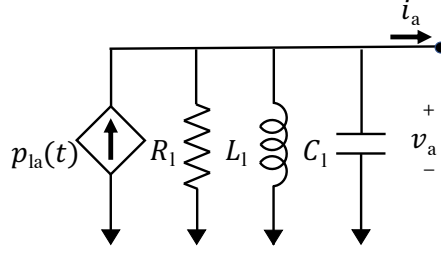


Figure 2.4: Load model with passive electrical elements and power source $p_l(t)$, described by (2.55). Note that here we show only one of the three circuits of the three-phase AC load as all of them are equal when assuming balanced circuits.

The main issue of these models is that the active and reactive power consumption P_1 and Q_1 must be translated in three-phase currents and voltages i and v at the input of the aggregate loads, as in (2.55). A load current expression can be given in DQZ-coordinates. From (2.25) we can write

$$i_{dq} = \frac{3}{\|v_{dq}\|^2} \begin{bmatrix} v_d & -v_q \\ v_q & v_d \end{bmatrix} \begin{bmatrix} P_1 \\ Q_1 \end{bmatrix}. \quad (2.56)$$

For a more exhaustive review on load modelling, the reader is referred to [17, 136].

2.4 Transmission lines model

Transmission Lines (TL) are electrical conductors used to transmit electrical power from the generators to the loads. Although transmission line characteristics vary depending on the amount of power that they must transmit, the dynamic behavior of the lines is taken into account through a series arrangement of inductive-resistive elements and parasitic capacitances at its endpoints. In three-phase systems, two components of the system are connected through three transmission lines, each of them carrying the signal of one phase. This is known as the π -model of a transmission line [63, 98], given by

$$L_t \dot{i}_t = -R_t i_t + v_1 - v_2 \quad (2.57a)$$

$$C_1 \dot{v}_1 = -G_1 v_1 - i_t + i_1 \quad (2.57b)$$

$$C_2 \dot{v}_2 = -G_2 v_2 + i_t + i_2, \quad (2.57c)$$

where (2.57a) determines the dynamics of the TL conductor, and (2.57b)-(2.57c) the dynamics at its end-points, most commonly known as *buses*. The variable $i_t = [i_{t,a}, i_{t,b}, i_{t,c}]^T$ represent the currents flowing on each of the three conductors, parameters L_t and R_t are the inductance and resistive losses of the TL, variable $v_k = [v_{a,k}, v_{b,k}, v_{c,k}]^T$ with $k \in \{1, 2\}$ represents the voltage at the buses of the TL and parameters C_k and G_k are shunt capacitances and impedances representing parasitic losses. We consider a

balanced system, so that the parameters are equal for all phases. The bus input current $\dot{i}_k = [\dot{i}_{a,k}, \dot{i}_{b,k}, \dot{i}_{c,k}]^T$ depends on the component attached to bus k , that is, they are equal to the Stator Terminal currents on the SM, the Output filter's current on the VSC or the output load current. A graphical representation of the model is provided in Figure 2.5.

As stated before, models in DQZ-coordinates become useful for analysis and control design. To write a DQZ-coordinates version of (2.57), we must apply the transformation matrix (2.9) on a common reference frame (network reference frame) $x_{dq} = T_{dq}(\omega_{ref}t)x$ to all TL of the network [142], yielding

$$L_t \dot{i}_{t,DQ} = -(R_t I_2 - \omega_{ref} L_t J) i_{t,DQ} + v_{1,dq} - v_{2,dq} \quad (2.58a)$$

$$C_1 \dot{v}_{1,dq} = -(G_1 I_2 - \omega_{ref} C_1 J) v_{1,dq} - \dot{i}_{t,DQ} + \dot{i}_{1,dq} \quad (2.58b)$$

$$C_2 \dot{v}_{2,dq} = -(G_2 I_2 - \omega_{ref} C_2 J) v_{2,dq} + \dot{i}_{t,DQ} + \dot{i}_{2,dq}, \quad (2.58c)$$

with $I_2 \in \mathbb{R}^{2 \times 2}$ the identity matrix and J as in (2.6). Note that in (2.58) we also can dismiss the zero coordinate of each of the equations, allowing us to written $i_{t,DQ} = [i_{t,D}, i_{t,Q}]^T$, $v_{k,dq} = [v_{k,d}, v_{k,q}]^T$ and $i_{k,dq} = [i_{k,d}, i_{k,q}]^T$. Note also that the DQZ-transformation used in (2.58) is different from the DQZ-transformation applied to the SM and VSC models (2.40) and (2.49) and the load model (2.56). For this reason, when coupling generators/loads to the TL model, we must apply the Bus-Network transformation (or Machine-Network transformation) $x_{dq} = T_{BN} x_{dq}$, which reads [142]:

$$T_{BN}(\delta) = T_{dq}(\omega_{ref}t) T_{dq}(\theta)^T = \begin{bmatrix} \cos(\delta) & -\sin(\delta) & 0 \\ \sin(\delta) & \cos(\delta) & 0 \\ 0 & 0 & 1 \end{bmatrix}. \quad (2.59)$$

with $\delta = \theta - \omega_{ref}t$. This transformation is applied to the generator/ load output current $\dot{i}_{k,dq}$ to that we obtain the terms $\dot{i}_{k,dq}$ in (2.58b) and (2.58c) and we apply its inverse $T_{BN}^{-1}(\delta) = T_{BN}^T(\delta)$ (to the bus voltages $v_{k,dq}$, so to obtain $v_{k,dq}$ that links the transmission line dynamics with the generator models (2.40) and (2.49). Note that the last row and column of $T_{BN}(\delta)$ in (2.59) are not considered when the zero coordinate of x_{dq} is dismissed.

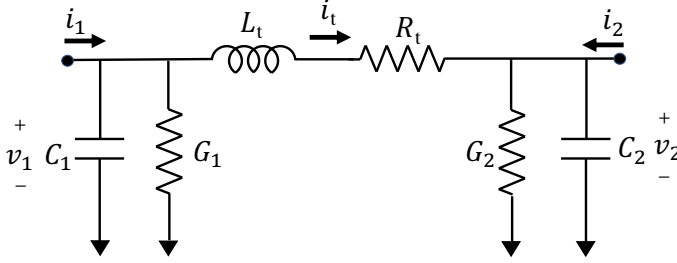


Figure 2.5: Transmission Line model

2.5 The electrical model of the power grid

The connection of a set of TLs, between geographically distant generators and loads can be interpreted from a graph theoretical point of view. As a starting point we emphasise that, in the power network literature, the terms nodes and edges are commonly replaced with the terms *Buses* and *Branches*.

The electrical model of the power grid can then be defined as a connected graph $\mathcal{G}(\mathcal{V}, \mathcal{E})$ where generators and loads are considered as a set of N nodes (buses) $\mathcal{V} \equiv \{1, \dots, N\}$ and TLs are considered as a set of M edges (branches) $\mathcal{E} \equiv \{\{k_1, h_1\}, \dots, \{k_M, h_M\}\}$ and a mapping $a \rightarrow \{k_a, h_a\}$ that assigns an index $a \in \{1, \dots, M\}$ to each edge $\{k_a, h_a\} \in \mathcal{E}$ with $k_a, h_a \in \mathcal{V}$. The node pairs $\{k_a, h_a\}$ of the edge set have an associated positive direction so that the current (and as a consequence the power) flow is positive from k_a to h_a . With this in mind, and based on (2.58a), a model of the **transmission network** conductors can be written in DQZ-coordinates as

$$L_{t(k,h)} \dot{i}_{t,\text{DQ}(k,h)} = -(R_{t(k,h)} I_2 - \omega_{\text{ref}} L_{t(k,h)} J) i_{t,\text{DQ}(k,h)} + v_{k,\text{dq}} - v_{h,\text{dq}} \quad \forall \{k, h\} \in \mathcal{E} \quad (2.60)$$

with $L_{t(k,h)}$ and $R_{t(k,h)}$ being the inductance and resistance parameters of the transmission line $\{k, h\}$ and $i_{t,\text{DQ}(k,h)}$ is the current flowing from bus k to bus h , with $i_{t,\text{DQ}(k,h)} = -i_{t,\text{DQ}(h,k)}$. The variables $v_{k,\text{dq}}$ and $v_{h,\text{dq}}$ represent the voltage drops in each of its endpoints whose dynamics are described by equations (2.58b) and (2.58c) and that can be written for each node in \mathcal{V} as

$$C_k \dot{v}_{k,\text{DQ}} = -(G_k I_2 - \omega_{\text{ref}} C_k J) v_{k,\text{DQ}} - \sum_{a=1}^M e_{k,a} i_{t,\text{DQ}(k,h_a)} + i_{k,\text{DQ}} \quad \forall k \in \mathcal{V} \quad (2.61)$$

with C_k and G_k being the parasitic capacitance and admittance parameters of the k -th bus, and $e_{k,a}$ the element (k, a) of the incidence matrix $E \in \mathbb{R}^{N \times M}$ defined as

$$e_{k,a} = \begin{cases} 1 & \{k, h_a\} \in \mathcal{E} \\ -1 & \{h_a, k\} \in \mathcal{E} \\ 0 & \text{otherwise} \end{cases}$$

which also represents the graph $\mathcal{G}(\mathcal{V}, \mathcal{E})$. Note that $e_{k,a}$ is positive if the current $i_{t,\text{DQ}}(k, h_a)$ is assumed to flow from k to h_a and negative otherwise. Finally $i_{t,\text{DQ}}$ represents the current injected (drawn) from the network by a generator (or load) connected to a bus k . A graphical representation of this network model can be seen in Figure 2.6

The complete transmission network model (2.60) and (2.61) can be written in matrix form by using the approach in [15, 63], leading to

$$\begin{aligned} \mathbf{L}_t \dot{\underline{i}}_{t,\text{DQ}} &= -\mathbf{Z}_t \underline{i}_{t,\text{DQ}} + (E \otimes I_3)^\top \underline{v}_{\text{dq}} \\ \mathbf{C} \dot{\underline{v}}_{\text{dq}} &= -\mathbf{Y}_0 \underline{v}_{\text{DQ}} - (E \otimes I_3) \underline{i}_{t,\text{DQ}} + \underline{i}_{\text{dq}}, \end{aligned} \quad (2.62)$$

being \otimes the Kronecker matrix product, with $\underline{i}_{t,\text{DQ}} = [i_{t,\text{DQ}}^\top(k_1, h_1), \dots, i_{t,\text{DQ}}^\top(k_M, h_M)]^\top$ the TL's current vector, $\underline{v}_{\text{dq}} = [v_{1,\text{dq}}^\top, \dots, v_{N,\text{dq}}^\top]^\top$ the bus voltage vector and the input current vector $\underline{i}_{\text{dq}} = [i_{1,\text{dq}}, \dots, i_{N,\text{dq}}]$. Here we define diagonal matrices \mathbf{L}_t , \mathbf{R}_t , \mathbf{G} and \mathbf{C} (see Table 2.1 for more details) and matrices $\mathbf{Z}_t = \mathbf{R}_t \otimes I_2 - \omega_{\text{ref}}(\mathbf{L}_t \otimes J)$ and $\mathbf{Y}_0 = \mathbf{G} \otimes I_2 - \omega_{\text{ref}}(\mathbf{C} \otimes J)$. Note that $\mathbf{Z}_t = \text{diag}(Z_{t,1}, \dots, Z_{t,M})$ and $\mathbf{Y}_0 = \text{diag}(Y_{0,1}, \dots, Y_{0,N})$ are block diagonal with blocks

$$Z_{t,a} = \begin{bmatrix} R_{t(k_a, h_a)} & -\omega_{\text{ref}} L_{t(k_a, h_a)} \\ \omega_{\text{ref}} L_{t(k_a, h_a)} & R_{t(k_a, h_a)} \end{bmatrix} \quad (2.63)$$

$$Y_{0,k} = \begin{bmatrix} G_k & -\omega_{\text{ref}} C_k \\ \omega_{\text{ref}} C_k & G_k \end{bmatrix} \quad (2.64)$$

All variables and parameters are summarized in Table 2.1. Until now, we have discussed the modelling of the power network elements and how they interact with the power network. To complete the model of a real power network, we have to consider next the different schemes used to control the generators, which are the main drivers of the network.

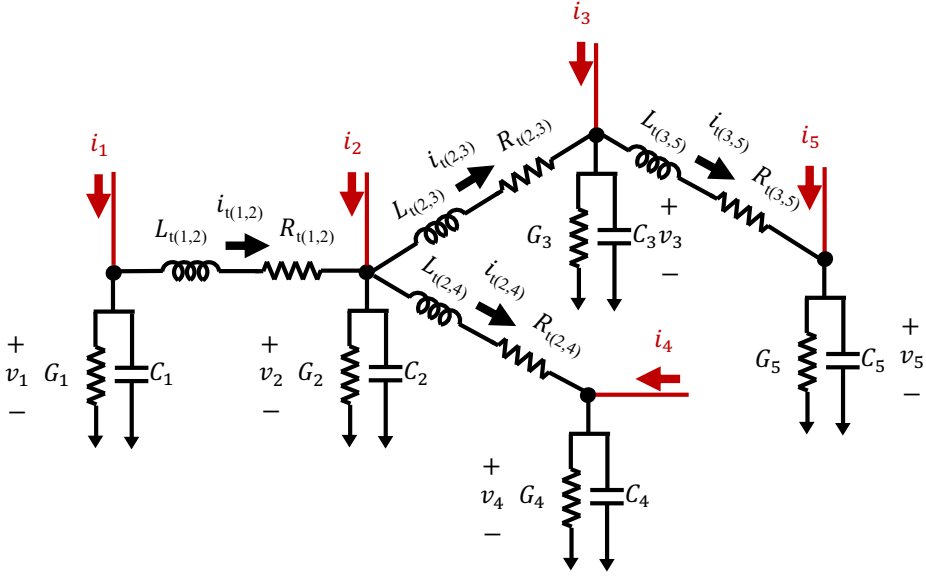


Figure 2.6: Graphical representation of the transmission lines network model described by equations (2.60) and (2.61). The nodal current inputs i_k are highlighted in red

2.6 Generator's control: a primary regulation layer

Until now, we have presented the open-loop dynamics of the generators but, to be placed into the grid, they require a set of local controllers that constitute the so called *Primary Layer* of the control architecture of the power network. Complementing the open-loop generator dynamics given in Section (2.2) with the controllers introduced in this section yields a closed-loop model of the power network. In what follows, we give the control specifications for the SMs and the VSCs that can be classified as

2.6.1 Steady state specifications

- **Compliant three-phase AC signals** All nodal voltage and input current signals of the network, i.e. i^* and v^* , must be three-phase AC signals at steady state, that is

$$v = \bar{v}(t) \begin{bmatrix} \cos(\theta(t) + \phi_v) \\ \cos(\theta(t) + \phi_v - \frac{2\pi}{3}(t)) \\ \cos(\theta(t) + \phi_v + \frac{2\pi}{3}(t)) \end{bmatrix} \quad (2.65a)$$

Component	Variable/Parameter	Name
Synchronous Machines	θ	SM rotor angular position
	ω_m	SM mechanical angular frequency
	ω	SM electrical angular frequency
	τ_m	Mechanical torque
	τ_e	Induced electrical torque
	i_r	Rotor windings excitation current
	$L(\theta)$	SM inductance matrix
	$v = [v_a, v_b, v_c]^T$	Stator terminal voltages
	$\mathbf{v} = [v^T, v_r]^T$	SM windings terminal voltages
	$i = [i_a, i_b, i_c]^T$	Stator terminal currents
	$\mathbf{i} = [i^T, i_r]^T$	SM windings terminal current
	$\lambda = [\lambda_a, \lambda_b, \lambda_c, \lambda_r]^T$	SM windings flux linkages
	M	Inertia constant
	D	Damping constant
	R	Stator/output resistance (SM/VSC)
	L_s	Armature windings inductance
L_{sl}	Armature windings leakage inductance	
L_{sr}	Stator-to-rotor inductance	
L_r	Field windings self-inductance	
Voltage Source Converters	v_{DC}	VSC source voltage
	i_{DC}	VSC source current
	v_{sw}	Power electronics output voltage
	i_{sw}	Power electronics output current
	$v = [v_a, v_b, v_c]^T$	Output filter's terminal voltages
	$i = [i_a, i_b, i_c]^T$	Output filter's terminal currents
	$m = [m_a, m_b, m_c]^T$	Power electronics modulation
	R	Output filter's resistance
	L_f	Output filter's inductance
	C_{DC}	DC stage capacitor
	G_{DC}	DC stage admittance
Loads	$p_l = [p_{la}, p_{lb}, p_{lc}]^T$	Time dependant power demand
	$v = [v_a, v_b, v_c]^T$	Load's terminal voltages
	$i = [i_a, i_b, i_c]^T$	Load's currents
	Pl	Average active power
	Ql	Average reactive power
	R_l	Load's resistance
	L_l	Load's impedance
	C_l	Load's capacitance

Table 2.1: Summary of variables and parameters in Chapter 1

$$i = \bar{i}(t) \begin{bmatrix} \cos(\theta(t) + \phi_i) \\ \cos(\theta(t) + \phi_i - \frac{2\pi}{3}) \\ \cos(\theta(t) + \phi_i + \frac{2\pi}{3}) \end{bmatrix}, \quad (2.65b)$$

Component	Variable/Parameter	Name	
Transmission Lines	$v_k = [v_{a,k}, v_{b,k}, v_{c,k}]^T$	Buses voltages	
	$i_k = [i_{a,k}, i_{b,k}, i_{c,k}]^T$	Bus input current	
	$i_{t(k,h)} = [i_{t,a(k,h)}, i_{t,b(k,h)}, i_{t,c(k,h)}]^T$	Transmission line current	
	$R_{t(k,h)}$	Transmission line's resistance	
	$L_{t(k,h)}$	Transmission line's inductance	
	C_k	Bus parasitic capacitance	
	G_k	Bus parasitic admittance	
	$e_{k,a}$	Incidence matrix element	
	Network elec- tri- cal model	N	Number of buses
		M	Number of transmission lines
\mathcal{V}		Power grid's node set	
\mathcal{E}		Power grid's edge set	
$\mathcal{G}(\mathcal{V}, \mathcal{E})$		Power grid's graph	
$\underline{i}_t = [i_{t(k_1, h_1)}^T, \dots, i_{t(k_M, h_M)}^T]^T$		TL currents stack vector	
$\underline{v} = [v_1^T, \dots, v_N^T]^T$		Bus voltages stack vector	
$\underline{i} = [i_1^T, \dots, i_N^T]$		TL input currents stack vector	
E		Network incidence matrix	
$\mathbf{R}_t = \text{diag}(R_{t(k_1, h_1)}, \dots, R_{t(k_M, h_M)})$		TL resistive terms matrix	
$\mathbf{L}_t = \text{diag}(L_{t(k_1, h_1)}, \dots, L_{t(k_M, h_M)})$		TL inductive terms matrix	
$\mathbf{C} = \text{diag}(C_1, \dots, C_N)$		Bus parasitic capacitance matrix	
$\mathbf{G} = \text{diag}(G_1, \dots, G_N)$		Bus parasitic admittance matrix	
$\mathbf{Z}_t = \mathbf{R}_t \otimes I_2 - \omega_{\text{ref}}(\mathbf{L}_t \otimes J)$	TL impedance matrix		
$\mathbf{Y}_0 = \mathbf{G} \otimes I_2 - \omega_{\text{ref}}(\mathbf{C} \otimes J)$	TL nodal admittance matrix		

Table 2.2: Summary of variables and parameters in Chapter 1

for constant phases ϕ_v and ϕ_i and time varying phase $\theta(t)$ and amplitudes $\bar{i}(t)$ and $\bar{v}(t)$.

- **Power set-point following** In nominal conditions, a generator must satisfy active and reactive power demands

$$\lim_{t \rightarrow \infty} p = p^* \quad (2.66a)$$

$$\lim_{t \rightarrow \infty} q = q^* \quad (2.66b)$$

with p and q representing the instantaneous active and reactive power computed with (2.17) and p^* and q^* being desired set-points.

- **Common frequency and voltage set-point following** to guarantee the power set-point following specifications in (2.66), the whole power system must have the same frequency ω_{ref} and each buses must follow a given voltage set-point \bar{v}^* . This translates in

$$\lim_{t \rightarrow \infty} \dot{\theta}(t) = \omega_{\text{ref}} \quad (2.67a)$$

$$\lim_{t \rightarrow \infty} \bar{v}(t) = \bar{v}^* \quad (2.67b)$$

Note that we do not give any specification related with the current magnitude \bar{i} as from (2.19) we can write at regime

$$p^* = \frac{3}{2} \bar{v}^* \bar{i}^* \cos(\phi_v - \phi_i) \quad (2.68a)$$

$$q^* = \frac{3}{2} \bar{v}^* \bar{i}^* \sin(\phi_v - \phi_i) \quad (2.68b)$$

which implies that \bar{i}^* is guaranteed at regime as the values of p^* , q^* , \bar{v}^* , ϕ_v and ϕ_i are already guaranteed by fulfilling specifications (2.65), (2.66) and (2.67),

Remark 2.4. *The reactive power specification in (2.66b) and the voltage magnitude specification in (2.67b) cannot always be simultaneously fulfilled. For this reason, these specifications are commonly fulfilled by capacitive-inductive banks and FACTS (Flexible AC Transmission Systems) devices [156] in the case of a SM, which are beyond the scope of this thesis. In the VSCs, a trade-off can be imposed to ensure one of the specifications, and this is why VSCs operate in two different modes, being voltage control or reactive power control [66].*

2.6.2 Perturbed steady state specifications

Power imbalances coming from the power grid generate frequency (and voltage) drifts on the generator terminals with respect to their nominal value ω_{ref} (\bar{v}^*), which also propagate to the power source, changing the turbine rotational speed in the case of the SM or the DC voltage on the VSC. In some circumstances, these disturbances make the power systems stabilize onto an equilibrium point with common frequency ω_0 (bus voltages \bar{v}_0) different from its nominal value.

When that occurs, it is desired that under a *perturbed steady state* ω_0 (\bar{v}_0), the closed-loop generator changes its active power (reactive power) by an amount inversely proportional to the steady state frequency difference $\Delta\omega = \omega_0 - \omega_{\text{ref}}$ (nodal voltage magnitude difference $\Delta\bar{v} = \bar{v}_0 - \bar{v}^*$), with change rates

$$\frac{\Delta p}{\Delta\omega} = -\kappa_p \quad (2.69a)$$

$$\frac{\Delta q}{\Delta\bar{v}} = -\kappa_q \quad (2.69b)$$

where $\kappa_p \in \mathbb{R}_{>0}$ and $\kappa_q \in \mathbb{R}_{>0}$ are known as the **effective gains** of the power source and their inverse is known as the **droop slopes** [110]. These specifications apply when

the frequency (and voltage) deviations are inside a narrow operating interval close to its nominal value $|\omega - \omega_{\text{ref}}| \leq |\omega_{\text{max}} - \omega_{\text{min}}|$ ($|\bar{v} - \bar{v}^*| \leq |\bar{v}_{\text{max}} - \bar{v}_{\text{min}}|$). Commonly we will have [48, 49, 110]:

$$\frac{|\omega_{\text{max}} - \omega_{\text{min}}|}{2\pi} \leq 2\text{Hz} \quad (2.70a)$$

$$\frac{|\bar{v}_{\text{max}} - \bar{v}_{\text{min}}|}{\bar{v}^*} \leq 20\%. \quad (2.70b)$$

The intervals in (2.70) represent safety operation ranges that, if violated, require coordinated actions among the power network nodes like, load shedding or generator tripping [110]. In general, a **deadband** is defined around the nominal frequency ω_{ref} (nominal voltage \bar{v}^*) for actuators protection, so that small power imbalances are adjusted by the inertial response of the coupled SMs, without the need of any additional power injection (see Figure (2.7)). It is recommended that the deadband must have a maximum width of ± 0.036 Hz [48].

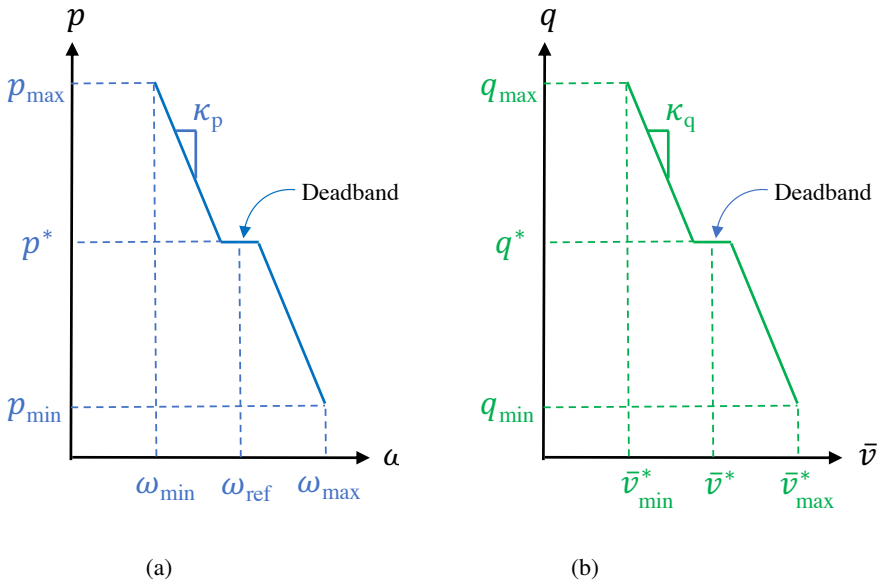


Figure 2.7: (a) Active power p vs frequency ω and (b) reactive power q vs voltage magnitude \bar{v} relations that fulfill the small signal specifications in (2.69)

2.6.3 Transient specifications

Reliability is indeed a crucial issue for power grids, and in this framework it translates into transient specifications for the control system. The controllers must reject any kind of *large disturbances*, like short circuits on transmission lines, load shedding, or non-forecasted weather conditions, which give rise to nonlinear phenomena [37, 132]. Although many control strategies have been proposed to tackle these sources of instability [128, 169, 176] the transient stabilization of the power system is still an open problem for both the SM and VSC control [88, 180].

2.6.4 Transient specifications for low inertia power systems

The introduction of renewable energy sources like solar plants or wind turbines have led to the decrease of the total mechanical inertia of the power systems. This is so, because, most of these energy sources have low inertia as the wind turbines (compared with steam turbines) or even do not rely on the electro-mechanical energy conversion provided by SM like solar plants, and are instead interfaced with the network through VSCs. In addition to this problem, note that nuclear and coal based power plants have been decommissioned in the last years, lowering even more the overall inertia of the grid [115].

As inertia decreases, the inertial response of the SMs of the power network are not enough to reject disturbances and primary controllers are activated more frequently. To avoid the further worsening of these problems, generators connected to low inertia power systems must fulfill the specifications [49, 115]:

$$\left| \frac{d\omega}{dt} \right| < \alpha \quad (2.71)$$

where $\alpha \in \mathbb{R}_{>0}$ representing a maximum frequency rate of change. The specification (2.71) is normally fulfilled by SM-based generation due to the flywheel's mechanical inertia.

Remark 2.5. The left hand side of (2.71) is estimated by the ROCOF (Rate-of-Change-of-Frequency), defined as:

$$\frac{d\omega}{dt} \approx \text{ROCOF}_{\Delta t} = \frac{1}{2\pi} \frac{\omega(t_0 + \Delta t) - \omega(t_0)}{\Delta t} \quad (2.72)$$

where t_0 determines the beginning of a failure producing high power imbalance and Δt a desired prediction time interval (generally $\Delta t \in [0.1, 0.5]$ sec) [49]

In the following, the control actions deployed for the fulfillment of the previously introduced specifications are explained. We provide Table 2.3 as a guide.

Component	Control Strategy	Control Specification
Synchronous Machines	Frequency Control	Frequency specification (2.67a), active power specification (2.66a) and droop specification (2.69a)
	AVR and PSS	Voltage specification (2.67b)
	FACTS	Reactive power specification (2.66b)
Voltage Source Converters	DC voltage control	Active power specification (2.66a)
	Power Electronics Control	Voltage specification (2.67b), Frequency specification (2.67a), Reactive power specification (2.66b), droop specifications (2.69) and transient specification (2.71)

Table 2.3: Summary of the control strategies of the SMs and the VSCs and its relation with the control specifications that they fulfill.

2.6.5 Primary control of synchronous machines

As shown in section 2.6.1, A generator must fulfill specifications (2.65) to (2.67), to be able to transfer power to the network. In particular, the SM achieves this if the primary controllers guarantee consistent steady state values for the input torque τ_m , and the rotor winding excitation current i_r , i.e.

$$\lim_{t \rightarrow \infty} i_r = i_r^* \quad (2.73a)$$

$$\lim_{t \rightarrow \infty} \tau_m = \tau_m^* \quad (2.73b)$$

with τ_m^* being the desired torque set-point and i_r^* a steady state value of the rotor windings current. In what follows, we define nominal operating condition values for the inputs i_r^* and τ_m^* for the SM so that these specifications are satisfied. Consider the SM dynamics in DQ-coordinates (2.40). At steady state, we will have that:

$$0 = v_d^* + Ri_d^* - \omega_{\text{ref}} L_q i_q^* \quad (2.74a)$$

$$\omega_{\text{ref}} L_e i_r^* = v_q^* + Ri_q^* + \omega_{\text{ref}} L_d i_d^* \quad (2.74b)$$

As the specification (2.65) must be fulfilled, we must provide terminal voltages $v_{dq}^* = \sqrt{\frac{3}{2}} \bar{v}^* [\cos(\phi_v), \sin(\phi_v)]^\top$ and currents $i_{dq}^* = \sqrt{\frac{3}{2}} \bar{i}^* [\cos(\phi_i), \sin(\phi_i)]^\top$, which allow us to write (2.74b) as

$$\bar{i}_r^* = \sqrt{\frac{3}{2}} \frac{1}{\omega_{\text{ref}} L_e} (\bar{v}^* \sin(\phi_v) + \bar{i}^* (R \sin(\phi_i) + \omega_{\text{ref}} L_d \cos(\phi_i))) \quad (2.75)$$

and by defining the complex impedance $Z_d = R + j\omega_{\text{ref}} L_d$ and using the harmonic addition identity (2.26) we can write

$$\bar{i}_r^* = \sqrt{\frac{3}{2}} \frac{1}{\omega_{\text{ref}} L_e} (\bar{v}^* \sin(\phi_v) + \bar{i}^* |Z_d| \sin(\phi_i + \angle Z_d)) \quad (2.76)$$

With this in mind, we can also write (2.74a) as

$$\bar{v}^* \cos(\phi_v) + \bar{i}^* |Z_q| \cos(\phi_i + \angle Z_q) = 0 \quad (2.77)$$

with the complex impedance $Z_q = R + j\omega_{\text{ref}} L_q$. As it is not always guaranteed that there is a value \bar{i}^* that fulfills (2.68), (2.76) and (2.77), the reactive power set-point specification (2.66b) is often fulfilled by auxiliary devices, as noted earlier in Remark 2.4.

Finally, the steady state value τ_m^* that guarantees the fulfillment of the frequency specification (2.66), which can be computed through equations (2.40a) at steady state, is

$$\tau_m^* = D\omega_{\text{ref}} + \sqrt{\frac{3}{2}} L_e \bar{i}_r^* \bar{i}^* \sin(\phi_i). \quad (2.78)$$

By replacing \bar{i}_r^* from (2.76) and \bar{v}^* from (2.77) in (2.78) we obtain:

$$\tau_m^* = D\omega_{\text{ref}} + \frac{p^*}{\omega_{\text{ref}}} + \frac{3}{2} \bar{i}^{*2} (|Z_q| \cos(\phi_i) \cos(\phi_i + \angle Z_q) + |Z_d| \sin(\phi_i) \sin(\phi_i + \angle Z_d)). \quad (2.79)$$

with p^* as in (2.68a). In the absence of saliency terms ($Z_d = Z_q$) and using the harmonic addition identity in (2.26), (2.79) reduces to

$$\tau_m^* = D\omega_{\text{ref}} + \frac{p^*}{\omega_{\text{ref}}} + \frac{3}{2\omega_{\text{ref}}} \bar{i}^{*2} R. \quad (2.80)$$

The steady state torque τ_m^* ensures constant rotor frequency ($\dot{\omega} = 0$) and, as a consequence, that the steady state solution of (2.40a) is $\theta(t)^* = \omega_{\text{ref}} t + \theta_0$. Note that by multiplying (2.79) by ω_{ref} on both sides we obtain

$$p_m^* = \omega_{\text{ref}} \tau_m^* = p^* + D\omega_{\text{ref}}^2 + \frac{3}{2} \bar{i}^{*2} R. \quad (2.81)$$

which implies that the total mechanical power p_m^* fed into the SM depends on the active power set-point p^* and on the internal electrical and mechanical losses.

However, in real operating conditions, the actual power demand is seldom, if ever, equal to its desired value p^* . The primary control layer of a SM, a typical architecture of which is depicted in Figure 2.8, represents the grid's first line of defense against perturbations. Consider a SM connected to the power network. From the power network voltage dynamics in (2.61), power imbalances due to changes in the current flows $i_{t(k,h)}$ propagate on a SM through a variation in the output current i which, according to (2.58), causes a perturbation in the output voltage v (voltage drops are associated with load increases, and viceversa). This perturbation propagates through the stator windings of the SM according to (2.40c) and (2.40d), eventually varying the electrical torque τ_e and thus generating a drift of the rotor frequency ω from its nominal value ω_{ref} (see (2.27)).

The role of the primary control layer is to adapt the mechanical power fed to the SM through the torque τ_m and the field current i_r so that the output active, p , satisfy the actual power demand of the grid (encompassed on the power set-points p^*) while keeping the rotor frequency ω and the output voltage magnitude \bar{v} at their nominal values specified by (2.67a) and (2.67b). To do so, two different control loops are leveraged (see Fig. 2.8), one denoted as the **frequency control loop**, and another one composed of the **automatic voltage regulator** and the **power system stabilizer**. We will review the main approaches to the design of these control loops in what follows.

Frequency Control

The frequency control loop is responsible of increasing the mechanical input power $p_m = \omega\tau_m$ (see (2.53a)) fed to the SM to satisfy the power specification (2.66a) and to restore the rotor frequency ω_{ref} , fulfilling specification (2.67a). The SM primary frequency control can be written as

$$p_m = p_m^* + \kappa_p(\omega_{\text{ref}} - \omega) \quad (2.82)$$

with p_m^* as in (2.81). A proper choice of the gain κ_p allows for the fulfillment of droop specification defined in (2.69a). Note that the controller in (2.82) is a simplification of the SM frequency control architecture as it does not consider any Turbine-Governor dynamics, i.e., dynamics on the power source of the SM and the actuators used to control it [112, 135, 139].

Remark 2.6. *The proportional controller (2.82) does not ensure perfect regulation of the frequency. Proper integral control is needed for this task, as explained in Section 4.2.1.*

Automatic Voltage Regulator and Power System Stabilizer

The *automatic voltage regulator* is in charge of ensuring voltage set-point following specification (2.67b) by ensuring a proper field winding voltage v_r at steady state, which provides the required steady state excitation current i_r^* . Traditionally, this is accomplished through the proportional controller [98]

$$v_r = \kappa_e(\bar{v}^* - \bar{v}) + u_{\text{PSS}}, \quad (2.83)$$

where the gain κ_e is tuned based on a linearization of the SM model (2.38) about the equilibrium corresponding to the nominal operating point defined in section 2.6.1. However, the automatic voltage regulator alone induces undesired oscillations in the rotor frequency ω due to the simultaneous action of the frequency control loop. The task of dampening these oscillations is left to an auxiliary control loop, the *power system stabilizer* u_{PSS} , which is commonly in charge of fulfilling transient stability specifications and is designed as a phase compensator in the traditional architecture portrayed in Figure 2.8.

These two control loops can be designed either sequentially or together, with the PI control technique in [35], robust control techniques such as H^∞ control [23], LQG regulators [123, 138], MPC [141], or self-tuning control [67, 77, 84] having been leveraged in the past to account for the changes in the parameters of the linearized system due to variations of the operating point of the SM. More recently this problem has been tackled by translating it into an optimization problem [27] or through adaptive dynamic programming [20].

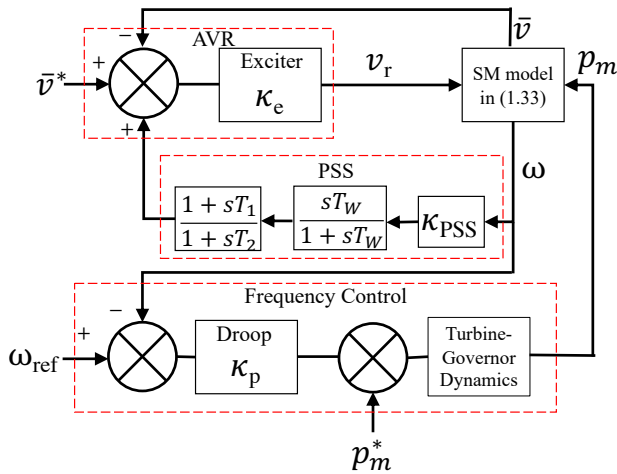


Figure 2.8: SM's control architecture. From top to bottom: Automatic Voltage Regulator, Power System Stabilizer and Frequency Controller.

2.6.6 Primary control of voltage source converters

In the case of the VSC, the fulfillment of specifications (2.65) to (2.67) depends on defining consistent steady state values for the DC input current i_{DC} and the modulation signal m such that

$$\lim_{t \rightarrow \infty} i_{\text{DC}} = i_{\text{DC}}^* \quad (2.84a)$$

$$\lim_{t \rightarrow \infty} m_{\text{dq}} = m_{\text{dq}}^* \quad (2.84b)$$

$$(2.84c)$$

with i_{DC}^* being an DC-input current set-point and $m_{\text{dq}}^* = [m_{\text{d}}^*, m_{\text{q}}^*]^{\text{T}}$ set-points for the modulation signal m in DQ-coordinates. In what follows, we derive expressions for i_{DC}^* , m_{dq}^* .

Consider the output current dynamics of the VSC in (2.49b) and (2.49c). At steady state, we have

$$m_{\text{d}}^* = \frac{2}{v_{\text{DC}}^*} (v_{\text{d}}^* + R i_{\text{d}}^* - \omega_{\text{ref}} L_{\text{f}} i_{\text{q}}^*), \quad (2.85a)$$

$$m_{\text{q}}^* = \frac{2}{v_{\text{DC}}^*} (v_{\text{q}}^* + R i_{\text{q}}^* + \omega_{\text{ref}} L_{\text{f}} i_{\text{d}}^*). \quad (2.85b)$$

By assuming the three-phase voltage and current signals v and i as specified by (2.65) and (2.67), we can write $v_{\text{dq}}^* = \sqrt{\frac{3}{2}} \bar{v}^* [\cos(\phi_v), \sin(\phi_v)]^{\text{T}}$ and currents $i_{\text{dq}}^* = \sqrt{\frac{3}{2}} \bar{i}^* [\cos(\phi_i), \sin(\phi_i)]^{\text{T}}$, and allow us to write (2.85) as

$$m_{\text{d}}^* = \frac{2}{v_{\text{DC}}^*} \sqrt{\frac{3}{2}} (\bar{v}^* \cos(\phi_v) + R \bar{i}^* \cos(\phi_i) - \omega_{\text{ref}} L_{\text{f}} \bar{i}^* \sin(\phi_i))$$

$$m_{\text{q}}^* = \frac{2}{v_{\text{DC}}^*} \sqrt{\frac{3}{2}} (\bar{v}^* \sin(\phi_v) + R \bar{i}^* \sin(\phi_i) + \omega_{\text{ref}} L_{\text{f}} \bar{i}^* \cos(\phi_i))$$

Defining the complex impedance $Z_{\text{f}} = R + j\omega_{\text{ref}} L_{\text{f}}$ and using the harmonic addition identity in (2.26) we get

$$m_{\text{d}}^* = \frac{2}{v_{\text{DC}}^*} \sqrt{\frac{3}{2}} (\bar{v}^* \cos(\phi_v) + \bar{i}^* |Z_{\text{f}}| \cos(\phi_i + \angle Z_{\text{f}})) \quad (2.86a)$$

$$m_{\text{q}}^* = \frac{2}{v_{\text{DC}}^*} \sqrt{\frac{3}{2}} (\bar{v}^* \sin(\phi_v) + \bar{i}^* |Z_{\text{f}}| \sin(\phi_i + \angle Z_{\text{f}})) \quad (2.86b)$$

$$(2.86c)$$

Now, the DC stage model of the VSC in (2.49a) is, at steady state

$$i_{\text{DC}}^* = G_{\text{DC}}v_{\text{DC}}^* + \frac{1}{2} (m_{\text{d}}^*i_{\text{d}}^* + m_{\text{q}}^*i_{\text{q}}^*)$$

Considering three-phase voltage and current signals v and i as specified in (2.65) in DQ-coordinates and the steady state value of the modulation signal in (2.86), we can then write

$$i_{\text{DC}}^* = G_{\text{DC}}v_{\text{DC}}^* + \frac{p^*}{v_{\text{DC}}^*} + \frac{3}{2v_{\text{DC}}^*} \bar{i}^{*2} R$$

with p^* as in (2.68a) and the steady state DC voltage v_{DC}^* being a parameter dependent on the power source design.

Until now, we have just considered the static behavior of the VSC. Similar to the mechanism described in the case of the SM, power imbalances propagate inside the VSC through changes on the terminal voltage v which then propagates to the Output filter's current i according to (2.46b) and to the DC source voltage v_{DC} due to the dependence of (2.46a) on i . To reject disturbances, the VSCs are controlled by a cascaded control architecture that uses the modulation signal m and the DC-current i_{DC} . This cascaded architecture is described next.

Cascaded control of the VSC

The VSC's control architecture is composed of two main stages being the **DC voltage control** and the **Cascaded AC voltage/current control**. To compensate this DC voltage drift from its nominal value, the **DC voltage control** generates DC current set-points i_{DC} that the power source must follow in order to generate more power and, at the same time, satisfy (2.66a) (See Figure 2.9). An example of this controller is taken from [158]

$$i_{\text{DC}}^* = \underbrace{k_{\text{DC}}(v_{\text{DC}}^* - v_{\text{DC}})}_{\text{DC voltage control}} + \underbrace{\frac{p^*}{v_{\text{DC}}^*}}_{\text{Power Injection}} + \underbrace{G_{\text{DC}}v_{\text{DC}} + \frac{v_{\text{DC}}i_{\text{sw}} - p}{v_{\text{DC}}^*}}_{\text{Losses}}. \quad (2.87)$$

The disturbances can also be compensated defining control strategies for the modulation signal m , as it affects the Output-Filter's current i according to (2.46b). The **Cascaded AC voltage/current control** is a cascaded control architecture (See Figure 2.9) that computes switching patterns m for the power electronics of the VSC, so that they fulfill the steady state specifications (2.86) and it is composed of three main stages introduced as follows. The **AC Voltage Control Stage** produces current set-points $\hat{i}(t)$ that compensate disturbances coming from the terminal voltage v of the VSC. The current set-point computation and is done through two main control paradigms, which will be explained later in detail. The **AC Current Control Stage** computes switching voltage set-points $\hat{v}_{\text{sw}}(t)$ that compensate disturbances propagating on the output current i , by ensuring that it follows the set-point $\hat{i}(t)$. This can be done by solving a tracking control problem through the PI controller in DQ-coordinates [140]

$$\widehat{v}_{sw,dq} = v_{dq} + Zi_{dq} + \kappa_{sw1} (\widehat{i}_{dq} - i_{dq}) + \kappa_{sw2} \int_0^t (\widehat{i}_{dq}(\tau) - i_{dq}(\tau)) d\tau, \quad (2.88)$$

where $Z = RI_2 - \omega_{ref}L_fJ$, $I_2 \in \mathbb{R}^{2 \times 2}$ is the identity matrix, J is as in (2.6) and R and L_f as in (2.46). Parameters κ_{sw1} and κ_{sw2} are the proportional and integral control gains of the controller. Finally, The **Modulation Stage** computes the modulation signal m based on (2.88), as

$$m = \frac{2}{v_{DC}^*} T_{dq}(\widehat{\theta})^T \widehat{v}_{sw,dq} \quad (2.89)$$

with the DQ-transformation matrix $T_{dq}(\widehat{\theta})$ as defined in (2.9) (the last row of $T_{dq}(\widehat{\theta})$ is dismissed as $\widehat{v}_{sw,dq}$ is in DQ-coordinates) and $\widehat{\theta}$ an estimate of the phase θ of the bus voltage v . For the computation of $\widehat{\theta}$ and the \widehat{i} , two main paradigms have been proposed, the **Grid-Following** and the **Grid-Forming control**.

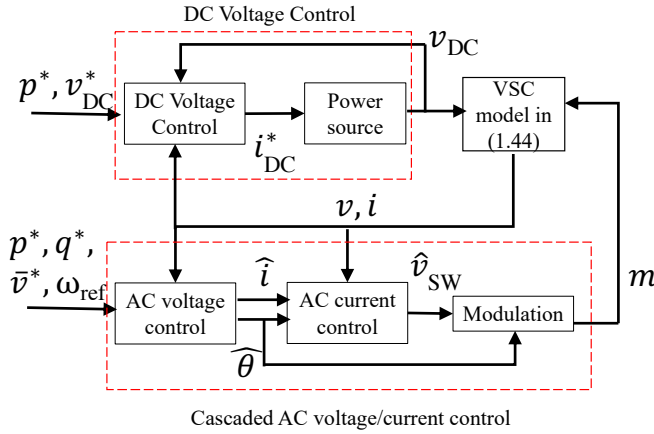


Figure 2.9: VSC's control architecture. From Top to Bottom: DC Voltage Controller and Cascaded AC voltage/current controller

Grid-Following control

In this control architecture, it is assumed that the terminal voltage v is a three-phase AC signal as in (2.1), with constant and known amplitude \bar{v} and phase $\theta = \omega_0 t + \theta_0$, being ω_0 a common frequency among the nodes of the network, close to the nominal one ω_{ref} . With this assumption, the specifications (5.15) and (2.69a) are fulfilled by directly measuring the phase θ of v . A general Grid-Following control architecture has three main stages [50] (See Figure 2.10).

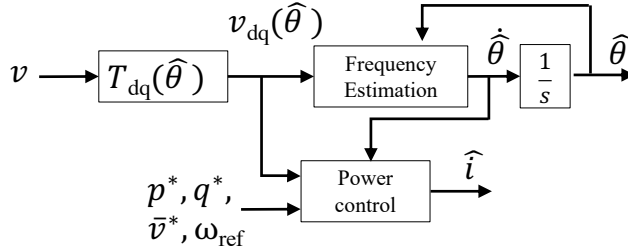


Figure 2.10: Grid-Following control

- **Frequency estimation:** this stage is in charge of obtaining a frequency estimate $\dot{\hat{\theta}}$ from the direct measurement of the output voltage v . This is commonly accomplished through a PLL (Phase-locked loop) architecture [41, 140] that estimates the bus frequency as

$$\dot{\hat{\theta}} = \omega_{\text{ref}} + \kappa_{\theta 1} v_q(\hat{\theta}) + \kappa_{\theta 2} \int_0^t v_q(\hat{\theta}(\tau)) d\tau \quad (2.90)$$

with $v_q(\hat{\theta})$ being the Q -component of the bus voltage v , computed with $T_{dq}(\hat{\theta})$, which can be written as

$$v_q(\hat{\theta}) = \sqrt{\frac{3}{2}} \bar{v} \sin(\theta(t) - \hat{\theta}(t) + \phi_v)$$

with $\theta(t)$ being the current time varying phase of the terminal voltage v and ϕ_v a constant phase shift. Parameters $\kappa_{\theta 1}$ and $\kappa_{\theta 2}$ are proportional and integral gains of the PLL (See Figure 2.9). Note that the estimate $\dot{\hat{\theta}}$ (2.90) allows the VSC to fulfill specification (2.67a) when $\theta = \theta^* = \omega_{\text{ref}} t$.

- **Power control:** in order to fulfill specifications (2.66a) and (2.66b), Grid-Following VSCs are controlled as current sources, by generating current set-point \hat{i} to match the required power injections p^* and q^* . This set-point is computed in DQ-coordinates as

$$\hat{i}_{dq} = \underbrace{Y v_{dq}}_{\substack{\text{Bus} \\ \text{Losses}}} + \frac{1}{v_d} [u_p, u_q]^T \quad (2.91)$$

where $v_d = \sqrt{\frac{3}{2}} \bar{v} \cos(\theta(t) - \hat{\theta}(t) + \phi_v)$ is the D -coordinate of the terminal voltage v_{dq} computed with $T_{dq}(\hat{\theta})$, $Y = GI_2 - \omega_{\text{ref}}CJ$ is the admittance of the capacitive and resistive parasitic terms in (2.58) representing the bus losses, with $I_2 \in \mathbb{R}^{2 \times 2}$ as the identity matrix and J as in (2.6). Finally, the variables u_p and u_q represent **Droop Control** inputs

$$\begin{aligned} u_p &= p^* + \kappa_p(\omega_{\text{ref}} - \dot{\hat{\theta}}) \\ u_q &= q^* + \kappa_q(\bar{v}^* - v_d). \end{aligned} \quad (2.92)$$

Notice that (2.66b) is fulfilled by using the Grid Following control, because the steady state voltage specification in (2.67b) is approximately guaranteed by the network. Also note that, under a proper choice of parameters κ_p and κ_q , the small signal specifications in (2.69) can also be satisfied.

Grid-Forming control

This control architecture is born from the necessity of the VSCs to fulfill steady state frequency and voltage specifications (2.67a) and (2.67b) in the cases when the network is not robust enough to allow the fulfillment of them by direct measurement of the terminal voltage v . In this control paradigm, VSCs are controlled to operate as ideal three-phase AC voltage sources with amplitude \bar{v}^* and frequency ω_{ref} at regime [157]. In doing so, two main control stages are used. The **AC Voltage Set-Point Generation** stage computes the AC voltage set-point \hat{v} which is then fed into the **AC Voltage Control** stage, which ensures that the VSC's terminal voltage v follows the voltage reference \hat{v} (See Figure 2.11).

- **AC Voltage Set-Point Generation** As stated before, this stage computes terminal voltage set-points \hat{v} that allow the VSC to fulfill specifications (2.67a) and (2.67b). These set-points can be written in ABC-coordinates as as

$$\hat{v} = \bar{\bar{v}} \begin{bmatrix} \cos(\hat{\theta}) \\ \cos(\hat{\theta} - \frac{2\pi}{3}) \\ \cos(\hat{\theta} + \frac{2\pi}{3}) \end{bmatrix} \quad (2.93)$$

with $\bar{\bar{v}}$ and $\hat{\theta}$ being its amplitude and phase. Many approaches have been proposed to compute \hat{v} [158] and we introduce here some of the most common.

- **Droop control** This control strategy is designed with the purpose to resemble the droop characteristic of the SM frequency controller in (2.82), so that

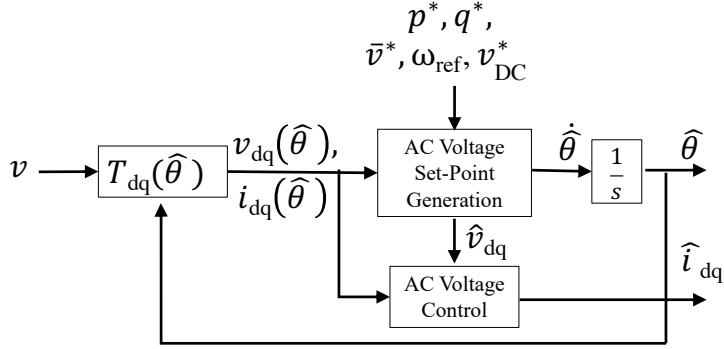


Figure 2.11: Grid-Forming control

the small signal specification (2.69a) can also be fulfilled. In doing so, the frequency is computed as:

$$\dot{\hat{\theta}} = \omega_{\text{ref}} + \frac{1}{\kappa_p}(p - p^*). \quad (2.94)$$

with p being the active power in (2.17a), the power set-point p^* is as in (2.68a) and a proper choice of κ_p allows the VSC to fulfill the small signal specification (2.69b). On this control strategy, a trade-off can be sought between the steady state specifications (2.66b) and (2.67b) and, to do so, the voltage magnitude reference \hat{v} is computed in two modes:

* **Voltage magnitude regulation mode**

$$\hat{v} = k_{v1}(\bar{v}^* - \bar{v}) + k_{v2} \int_0^t (\bar{v}^* - \bar{v}(\tau)) d\tau \quad (2.95)$$

with \bar{v} being the terminal voltage magnitude, \bar{v}^* is a desired steady state voltage amplitude and k_{v1} and k_{v2} are proportional and integral gains for the controller,

* **Reactive power sharing mode:**

$$\hat{v} = \bar{v}^* + \frac{1}{\kappa_q}(q - q^*) \quad (2.96)$$

with q^* being the reactive power set-point in (2.66b) a proper choice of κ_q allows the VSC to fulfill the small signal specification (2.69b).

- **Virtual synchronous machine control:** The VSC's frequency is controlled in order to replicate the phase and frequency dynamics of a SM, [65, 183]:

$$\dot{\hat{\theta}} = \hat{\omega} \quad (2.97a)$$

$$\hat{M}\hat{\omega} = \frac{1}{\omega_{\text{ref}}}(p^* - p) + \kappa_p(\omega_{\text{ref}} - \hat{\omega}) \quad (2.97b)$$

where \hat{M} is a parameter determining the virtual inertia and the term $1/\kappa_p$ defines a virtual damping constant. The voltage reference magnitude \hat{v} can be computed through two alternative modes

- * **Voltage magnitude regulation mode**

$$\hat{v} = \hat{\omega}\kappa_{v1}(\bar{v}^* - \bar{v}) + \hat{\omega}\kappa_{v2} \int_0^t (\bar{v}^* - \bar{v}(\tau)) d\tau \quad (2.98)$$

where k_{v1} and k_{v2} are proportional and integral gains for the controller

- * **Reactive power sharing Mode:**

$$\hat{v} = \hat{\omega}\hat{L}\hat{i}_r \quad (2.99a)$$

$$\dot{\hat{i}}_r = \frac{1}{\hat{L}} \left(q^* - q + \frac{1}{\kappa_q}(\bar{v}^* - v_d) \right) \quad (2.99b)$$

with \hat{i}_r as a virtual analogous of a rotor winding current and \hat{L} a virtual inductance parameter.

- **Matching Control:** This control strategy replicates the power-frequency relation of the SM, by exploiting structural similarities between both devices. In doing so, it is assumed that the phase is proportional to the input DC voltage v_{DC} [16]:

$$\hat{\theta} = \kappa_\theta v_{\text{DC}} \quad (2.100)$$

where $\kappa_\theta = \omega_{\text{ref}}/v_{\text{DC}}^*$ is the frequency-to-DC-voltage ratio at steady state and v_{DC} . This control strategy leaves the frequency regulation to the **DC voltage control** in (2.87). In this strategy, the voltage magnitude reference \hat{v} is computed as in (2.95) (or (2.96) for reactive power sharing). This is done with the purpose to match the switching voltage v_{sw} in (2.42) with the term $\omega \mathbf{J}L_{\text{dq}}\mathbf{i}_{\text{dq}}$ in (2.37).

Remark 2.7. *The VSC control is still an open problem. Recently, new approaches for the control of the VSC have been proposed, like the **Dispatchable***

virtual oscillator control in [146]

- **AC voltage control loop:** This control loop is in charge of generating current set-points for i in DQZ-coordinates by using the voltage set-point v_{trac} . It is computed as:

$$\hat{i}_{\text{dq}} = i_{\text{dq}} + Y v_{\text{dq}} + \kappa_{i1} (\hat{v}_{\text{dq}} - v_{\text{dq}}) + \kappa_{i2} \int_0^t (\hat{v}_{\text{dq}}(\tau) - v_{\text{dq}}(\tau)) d\tau \quad (2.101)$$

with $Y = GI_2 - \omega_{\text{ref}}CJ$ is the admittance of the capacitive and resistive parasitic terms in (2.58) representing the bus losses, with $I_2 \in \mathbb{R}^{2 \times 2}$ as the identity matrix and J as in (2.6). Here, i_{dq} and v_{dq} are the output filter's current and the terminal voltage in DQ-coordinates, computed with $T_{\text{dq}}(\hat{\theta})$ and κ_{i1} and κ_{i2} are proportional and integral gains of the controller in (2.101).

2.7 Summary

In this Chapter, we introduced an unified approach to completely describe the power grid from a micro-scale and control theoretical point of view. We derived the dynamic models for each of the power network components. We also described how these components interact and introduced the electrical model of the power network with the aid of graph theoretical tools. After this, we explained the control goals of the primary control layer and gave formal control specifications in terms of the electrical model of the power network. This then allowed us to map each of the power network control specifications in detailed control specifications for each of the SMs and the VSCs. Finally, we introduced the most common control strategies used to satisfy these control specifications.

In what follows, we introduce a simpler power network model known as the Swing Equation, that becomes instrumental in understanding of additional control problems of the power network.

3 Network model of the power grid

So far, we focused on describing the constitutive components of the power network from a **micro-scale** point of view. Studying the complex behavior of the power network is of interest for modelling and control purposes as the availability and feasibility of the production and transmission of the required power does not depend on each agent itself (generator or load) but on the collective dynamics of the whole ensemble of generators and loads. An example of this is that the emergent frequency synchronization phenomenon on the power network is still used as a proxy for the coordination of power generation and demand, with the caveat that synchrony is only preserved under small phase deviations and absence of large disturbances [122, 124]. Still, there is a need of new modeling and control tools that consider the network complex dynamics and topology for the control design.

In this Chapter, we introduce the modelling strategies of the power network modelled as a complex multi-agent system [73]. To do so, we introduce the **Swing Equation** as a simplified network model of the power grid, but that still preserves its complex dynamics. We then present the main assumptions that allow the Power Grid Electrical Model (introduced in Chapter 2) to be simplified into the Swing Equation. We show analytically that this approach is valid for a network of synchronous machines by means of singular perturbation tools. Also, we explain how this approach can be extended to encompass any generator and load model. In so doing, we provide a novel framework that maps all the components of the Power Grid Electrical Model into the Swing Equation by associating each component with a set of parameters. Finally, we review additional simplified models of the power grid, based on further simplifications of the Swing Equation.

3.1 The swing equation: a network model of the power grid

On the secondary layer, the main feature that must be captured by a model is the link between frequency deviations and power imbalance. This can be done by modeling the power grid as a network of coupled oscillators, each representing either a generator or a load, interconnected by edges capturing the effect of transmission lines. The coupled oscillators dynamics used to model the secondary layer are represented by the **Swing Equation** [21, 125], that can be written by using the graph notation introduced in Section 2.5, as

$$\begin{aligned} \tilde{M}_k \ddot{\delta}_k + \tilde{D}_k \dot{\delta}_k &= \tilde{P}_k - \sum_{h=1}^N \sigma_{kh} \sin(\delta_k - \delta_h - \gamma_{kh}) + u_k \quad \forall k \in \mathcal{V}_{\text{sec}} \\ \tilde{M}_k \ddot{\delta}_k + \tilde{D}_k \dot{\delta}_k &= \tilde{P}_k - \sum_{h=1}^N \sigma_{kh} \sin(\delta_k - \delta_h - \gamma_{kh}) \quad \forall k \in \mathcal{V} \setminus \mathcal{V}_{\text{sec}} \end{aligned} \quad (3.1)$$

where $\dot{\delta}_k = \omega_k - \omega_{\text{ref}}$ is the frequency deviation from the nominal frequency ω_{ref} at node k and the parameters \tilde{M}_k and \tilde{D}_k represent the inertia and damping constant, similar to the parameters defined for SMs in (2.27) (see Table 3.1). The normalized power $\tilde{P}_k = \frac{P_k}{S_{\text{base}}}$ is produced by a generator if $\tilde{P}_k > 0$, $k \in \mathcal{V}_g$ and is consumed by a load if $\tilde{P}_k < 0$, $k \in \mathcal{V}_l$, with the active power P_k as in (2.24a) and S_{base} known as the nominal volt-amperes in each phase of the power network. The parameter $\sigma_{kh} = \tilde{V}_k \tilde{V}_h |\tilde{Y}_{kh}|$ represents a coupling gain between nodes $k, h \in \mathcal{V}$, depending on the normalized bus voltage magnitudes $\tilde{V}_k = \frac{V_k}{V_{\text{base}}}$, with $V_k = \frac{\bar{v}_k^*}{\sqrt{2}}$ being the RMS value of the voltage magnitude \bar{v}_k^* at steady-state, that fulfills the specification (2.67b) and V_{base} the nominal voltage magnitude. The coupling gain σ_{kh} also depends on the normalized complex admittance $\tilde{Y}_{kh} = Y_{kh} \frac{V_{\text{base}}}{I_{\text{base}}}$ with $Y_{kh} = G_{kh} + jB_{kh}$ with real and imaginary terms G_{kh} , B_{kh} (the latter also known as susceptance), I_{base} is the nominal current of the power network and $\gamma_{kh} = \frac{\pi}{2} - \arctan\left(\frac{B_{kh}}{G_{kh}}\right)$ is a constant phase shift. Finally, u_k is the secondary control input and $\mathcal{V}_{\text{sec}} \subset \mathcal{V}$ is the set of nodes that have secondary control capabilities.

The right-hand side of the swing equation (3.1) represents the power flow on the grid, where the sum of the sine functions represents the power that node k transmits or receives through neighboring **transmission lines**. The effect of the latter is captured by the coupling constants σ_{kh} , representing the maximum power that can be transmitted through the line $\{k, h\} \in \mathcal{E}$ and by the phase angle γ_{kh} . At steady-state, equation (3.1) must satisfy the **AC Power Flow Equations**:

$$\tilde{P}_k - \sum_{h=1}^N \sigma_{kh} \sin(\delta_k^* - \delta_h^* - \gamma_{kh}) = 0 \quad (3.2a)$$

$$\tilde{Q}_k + \sum_{h=1}^N \sigma_{kh} \cos(\delta_k^* - \delta_h^* - \gamma_{kh}) = 0 \quad (3.2b)$$

with δ_k^* being a suitable phase angle at regime, $\tilde{Q}_k = \frac{Q_k}{S_{\text{base}}}$ is a normalized reactive power steady-state value, with Q_k as in (2.24b). The importance and usefulness of the AC Power Flow equations will be highlighted in Section 4.3.

Model (3.1) and the AC Power Flow Equations in (3.2) assume that (i) the primary control layer is capable of ensuring a steady output voltage magnitude $V_k = \frac{\bar{v}_k^*}{\sqrt{2}}$, with \bar{v}_k^* fulfilling the primary voltage specification in (2.67b), and (ii) that the active and reactive

power are $P_k = \frac{p_k^*}{3}$ and $Q_k = \frac{q_k^*}{3}$, with p_k^* and q_k^* satisfying specification in (2.66) in each of the network buses. It also assumes time-scale separation between the frequency and voltage magnitude dynamics.

In what follows, we will discuss the relation between the power network electrical model introduced in Chapter 1 and the swing equation in (3.1).

3.1.1 From the electrical power network model to the swing equation

Model (3.1) has been derived under the main assumptions that the primary control layer (i) guarantees small frequency deviations $\delta_k := \omega_k - \omega_{\text{ref}}$ and the fulfillment of voltage and power specifications (2.66) and (2.67b) (ii) it keeps the power system in a stable regime and (iii) the times-scale of the dynamics of the electrical components are faster than the times-scale of the frequency dynamics. This set of assumptions are known as the **Quasi steady-state assumption**. In what follows, we show a sketch proof of the derivation of the Swing Equation, based on these assumptions and on the electrical model of the power grid.

We consider, for the sake of simplicity, a power network where there is a SM connected to each of its buses. From the power balance in (2.53a) the Hamiltonian time derivative for each of the SM in generator convention reads

$$\dot{H}_{\text{SM}k} = \underbrace{\omega_k \tau_{mk} + i_{rk} v_{rk}}_{\text{Power Input}} - \underbrace{i_{\text{dq}k}^{\text{T}} v_{\text{dq}k}}_{\text{Power Output}} - \underbrace{(D_k \omega_k^2 + R_k \mathbf{i}_{\text{dq}k}^{\text{T}} \mathbf{i}_{\text{dq}k})}_{\text{Power Losses}} \quad \forall k \in \mathcal{V} \quad (3.3)$$

Now, recalling the time derivative of the SM's Hamiltonian in (2.51) and the linear flux linkage-current relation in (2.29) we can write the left hand side of (3.3) as

$$\omega_k M_k \dot{\omega}_k + \mathbf{i}_{\text{dq}k}^{\text{T}} L_{\text{dq}rk} \dot{\mathbf{i}}_{\text{dq}rk} = \omega_k \tau_{mk} + i_{rk} v_{rk} - p_k - (D_k \omega_k^2 + R_k \mathbf{i}_{\text{dq}k}^{\text{T}} \mathbf{i}_{\text{dq}k}) \quad \forall k \in \mathcal{V} \quad (3.4)$$

with $p_k = i_{\text{dq}k}^{\text{T}} v_{\text{dq}k}$ being the instantaneous active power that the SM injects into the network, as defined in (2.17). As the inertia constant M_k is much greater by several orders of magnitude than the elements of the inductance matrix $L_{\text{dq}rk}$, we can consider fast dynamics of the current $\mathbf{i}_{\text{dq}rk}$, which implies we can approximate it by using its steady-state value $\mathbf{i}_{\text{dq}rk}^*$ [39, 95, 153]. With this in mind and rearranging terms in (3.4) in a convenient manner we can write

$$\omega_k M_k \dot{\omega}_k + D_k \omega_k^2 \approx \omega_k \tau_{mk} + i_{rk}^* v_{rk}^* - R_k \mathbf{i}_{\text{dq}rk}^{*\text{T}} \mathbf{i}_{\text{dq}rk}^* - p_k \quad (3.5)$$

As the terminal currents i must fulfill specification (2.65), we can write, by using the DQ-transformation matrix $T_{\text{dq}}(\theta_k)$, the current $i_{\text{dq}k}^* = \sqrt{\frac{3}{2}} \bar{i}_k^* [\cos(\phi_{i,k}), \sin(\phi_{i,k})]^{\text{T}}$. With this, we can rewrite the term $R_k \mathbf{i}_{\text{dq}rk}^{*\text{T}} \mathbf{i}_{\text{dq}rk}^*$ in (3.5) as

$$R_k \mathbf{i}_{\text{dq}rk}^{*\text{T}} \mathbf{i}_{\text{dq}rk}^* = R_k i_{\text{dq}k}^{*\text{T}} i_{\text{dq}k}^* + R_k i_{rk}^{*2} = \frac{3}{2} R_k \bar{i}_k^{*2} + R_k i_{rk}^{*2}. \quad (3.6)$$

From (2.38d) we have that at equilibrium $i_{rk}^* v_{rk}^* = R_k i_{rk}^{*2}$, leading to

$$\omega_k M_k \dot{\omega}_k + D_k \omega_k^2 \approx \omega_k \tau_{mk} - \frac{3}{2} R_k \bar{i}_k^{*2} - p_k. \quad (3.7)$$

Now, by multiplying both sides of equation (3.7) by $\frac{\omega_{\text{ref}}}{\omega_k}$, we obtain

$$\omega_{\text{ref}} M_k \dot{\omega}_k + \omega_{\text{ref}} D_k \omega_k \approx \omega_{\text{ref}} \tau_{mk} - \frac{\omega_{\text{ref}}}{\omega_k} \left(\frac{3}{2} R_k \bar{i}_k^{*2} + p_k \right). \quad (3.8)$$

By considering that the electrical frequency is close to its steady-state value $\omega_k \approx \omega_{\text{ref}}$, we can write

$$\omega_{\text{ref}} M_k \dot{\omega}_k + \omega_{\text{ref}} D_k \omega_k \approx p_{mk} - \frac{3}{2} R_k \bar{i}_k^{*2} - p_k, \quad (3.9)$$

with $p_{mk} \approx \omega_{\text{ref}} \tau_{mk}$. Replacing p_{mk} by the primary frequency controllers (2.82) in each SM, written as

$$p_{mk} = p_{mk}^* + \kappa_{pk} (\omega_{\text{ref}} - \omega_k), \quad (3.10)$$

and applying the change of variable $\delta_k = \omega_k - \omega_{\text{ref}}$, we obtain

$$\omega_{\text{ref}} M_k \ddot{\delta}_k + (\kappa_p + \omega_{\text{ref}} D_k) \dot{\delta}_k \approx p_{mk}^* - D_k \omega_{\text{ref}}^2 - \frac{3}{2} R_k \bar{i}_k^{*2} - p_k \quad (3.11)$$

Then, by replacing p_{mk}^* from (2.81) we have

$$\omega_{\text{ref}} M_k \ddot{\delta}_k + (\kappa_{pk} + \omega_{\text{ref}} D_k) \dot{\delta}_k \approx p_k^* - p_k \quad (3.12)$$

Our purpose now is to give an expression for p_k that depends only on the phase differences between nodes of the network and line parameters. To do so, consider the transmission line network model (2.62).

Assuming fast dynamics on the bus voltages v_{DQ} and line currents i_{LDQ} , the following linear steady-state map relation between the steady-state currents i_{DQ}^* and voltages v_{DQ}^* can be derived as

$$i_{\text{DQ}}^* = \mathbf{Y} v_{\text{DQ}}^* \quad (3.13)$$

where $\mathbf{Y} = \mathbf{Y}_0 + \mathbf{Y}_{\text{TL}}$ is known as the **admittance matrix** of the power network, which is composed of the **Shunt admittance matrix** \mathbf{Y}_0 as defined in (2.64), and the **TL admittance matrix** $\mathbf{Y}_{\text{TL}} := (E \otimes I_3) \mathbf{Y}_t (E \otimes I_3)^\top$ with $\mathbf{Y}_t := \mathbf{Z}_t^{-1}$ and \mathbf{Z}_t being as defined in (2.63). We can write the block terms of the **admittance matrix** as

$$\mathbf{Y}_{(k,h)} = \begin{cases} -\mathbf{Y}_{t(k,h)} & k \neq h \wedge \{k, h\} \in \mathcal{E} \\ \mathbf{Y}_0 + \sum_{h=1}^N \mathbf{Y}_{t(k,h)} & k = h \\ \mathbf{0}_{3 \times 3} & \text{otherwise} \end{cases} \quad (3.14)$$

where $\mathbf{Y}_{(k,h)}$ may also be written in the following compact form

$$\mathbf{Y}_{(k,h)} = \begin{bmatrix} G_{kh} & -B_{kh} \\ B_{kh} & G_{kh} \end{bmatrix} \quad (3.15)$$

with $G_{kh}, B_{kh} \in \mathbb{R}$. Expanding the scalar terms of expression in (3.13) we obtain

$$i_{\text{DQ}k}^* = \sum_{h=1}^N \mathbf{Y}_{(k,h)} v_{\text{DQ}h}^* \quad (3.16)$$

By considering the current-voltage relation (3.16) and the Bus-Network transformation (2.59), the instantaneous active power at steady-state can be written as

$$p_k = i_{\text{dq}k}^{*\text{T}} v_{\text{dq}k}^* = i_{\text{DQ}k}^{*\text{T}} v_{\text{DQ}k}^* = \sum_{h=1}^N v_{\text{DQ},h}^{*\text{T}} \mathbf{Y}_{(k,h)}^{\text{T}} v_{\text{DQ},k}^* \quad (3.17)$$

As we are interested on the frequency deviation dynamics, we assume nodal steady-state voltages

$$v_k = \bar{v}_k^* \begin{bmatrix} \cos(\theta_k(t)) \\ \cos(\theta_k(t) - \frac{2\pi}{3}) \\ \cos(\theta_k(t) + \frac{2\pi}{3}) \end{bmatrix} \quad (3.18)$$

which only satisfy (2.65a) and the voltage specification (2.67b) as required by the Quasy-steady-state assumption and that can be written in the network reference frame DQ-coordinates by using the transformation matrix $T_{\text{dq}}(\omega_{\text{ref}}t)$, leading to $v_{\text{DQ}k}^* = \sqrt{3}V_k[\cos(\delta_k), \sin(\delta_k)]^{\text{T}}$ with $V_k = \frac{\bar{v}_k^*}{\sqrt{2}}$ being the RMS value of the amplitude \bar{v}_k^* at steady-state and $\delta_k = \theta_k - \omega_{\text{ref}}t$ the phase deviation. Notice that we dismissed the zero coordinate in $v_{\text{DQ}k}$.

Replacing the nodal voltages $v_{\text{DQ}k}$ in (3.17) we obtain the expression

$$p_k = 3 \sum_{h=1}^N V_k V_h (G_{kh} \cos(\delta_k - \delta_h) + B_{kh} \sin(\delta_k - \delta_h))$$

which can be further simplified into

$$p_k = 3 \sum_{h=1}^N V_k V_h |Y_{kh}| \sin(\delta_k - \delta_h - \gamma_{kh}) \quad (3.19)$$

with $Y_{kh} = G_{kh} + jB_{kh} \in \mathbb{C}$ being a representation of the admittance matrix term $\mathbf{Y}_{(k,h)}$ in (3.15) and $\gamma_{kh} = \frac{\pi}{2} - \arctan\left(\frac{B_{kh}}{G_{kh}}\right)$ as a constant phase angle. Replacing (3.19) into (3.12) yields

$$\omega_{\text{ref}} M_k \ddot{\delta}_k + (\kappa_{\text{pk}} + \omega_{\text{ref}} D_k) \dot{\delta}_k \approx p_k^* - 3 \sum_{h=1}^N V_k V_h |Y_{kh}| \sin(\delta_k - \delta_h - \gamma_{kh}) \quad (3.20)$$

Finally, by using the normalized inertia constant $\tilde{M}_k = \frac{\omega_{\text{ref}} M_k}{3S_{\text{base}}}$, the normalized damping constant $\tilde{D}_k = \frac{\kappa_{pk} + \omega_{\text{ref}} D_k}{3S_{\text{base}}}$, the normalized input power $\tilde{P}_k = \frac{P_k^*}{3S_{\text{base}}}$, the normalized admittance $\tilde{Y}_{(k,h)} = Y_{(k,h)} \frac{I_{\text{base}}}{\tilde{V}_{\text{base}}}$ and the normalized voltage $\tilde{V}_k = \frac{V_k}{\tilde{V}_{\text{base}}}$, and considering secondary control inputs $u_k \forall k \in \mathcal{V}_{\text{sec}}$ we can write the power network model as

$$\begin{aligned} \tilde{M}_k \ddot{\delta}_k + \tilde{D}_k \dot{\delta}_k &= \tilde{P}_k - \sum_{h=1}^N \sigma_{kh} \sin(\delta_k - \delta_h - \gamma_{kh}) + u_k \quad \forall k \in \mathcal{V}_{\text{sec}} \\ \tilde{M}_k \ddot{\delta}_k + \tilde{D}_k \dot{\delta}_k &= \tilde{P}_k - \sum_{h=1}^N \sigma_{kh} \sin(\delta_k - \delta_h - \gamma_{kh}) \quad \forall k \in \mathcal{V} \setminus \mathcal{V}_{\text{sec}} \end{aligned} \quad (3.21)$$

with $\sigma_{kh} = \tilde{V}_k \tilde{V}_h |\tilde{Y}_{kh}|$. A notation and terminology summary can be found in Table 3.1 and in what follows, we drop the normalized parameters notation, yielding

$$\begin{aligned} \tilde{M}_k \ddot{\delta}_k + \tilde{D}_k \dot{\delta}_k &= P_k - \sum_{h=1}^N \sigma_{kh} \sin(\delta_k - \delta_h - \gamma_{kh}) + u_k \quad \forall k \in \mathcal{V}_{\text{sec}} \\ \tilde{M}_k \ddot{\delta}_k + \tilde{D}_k \dot{\delta}_k &= P_k - \sum_{h=1}^N \sigma_{kh} \sin(\delta_k - \delta_h - \gamma_{kh}) \quad \forall k \in \mathcal{V} \setminus \mathcal{V}_{\text{sec}} \end{aligned} \quad (3.22)$$

with $V_k = \tilde{V}_k$, $P_k = \tilde{P}_k$, $G_{kk} = \tilde{G}_{kk}$ and $Y_{kh} = \tilde{Y}_{kh}$ for the sake of simplicity.

Although this sketch proof is based on a network with SM dynamics, it has been demonstrated that the dynamics of a wide variety of power network components can be approximated to an oscillator like dynamics with a structure similar to that in (3.22). In what follows, we provide a framework that maps each of these components into the Swing Equation.

Remark 3.1. Note that in the power network literature, all normalized quantities in (3.21) have units p.u. (Per Unit).

Remark 3.2. The simplification used in step (3.8), in which $\frac{\omega_{\text{ref}}}{\omega} \approx 1$ has been criticized as it can lead to misleading results in stability analysis [30, 119]

Remark 3.3. Exploiting the fact that the admittance terms $\mathbf{Y}_{(k,h)}$ can be written as a complex number $Y_{kh} \in \mathbb{C}$, these last complex admittances can also be written in matrix form $\tilde{\mathbf{Y}} \in \mathbb{C}^{M \times M}$, known as the admittance matrix of the power network. The linear relation between current and voltage in (3.13) in phasor representation can be written as

$$\vec{\mathbf{I}} = \tilde{\mathbf{Y}} \vec{\mathbf{V}} \quad (3.23)$$

with phasor stack vectors $\vec{\mathbf{I}} = [\vec{I}_1, \dots, \vec{I}_k, \dots, \vec{I}_N]$, $\vec{\mathbf{V}} = [\vec{V}_1, \dots, \vec{V}_k, \dots, \vec{V}_N]$ and elements $\vec{I}_k = \frac{i_{Dk}}{\sqrt{3}} + j\frac{i_{Qk}}{\sqrt{3}}$ and $\vec{V}_k = \frac{v_{Dk}}{\sqrt{3}} + j\frac{v_{Qk}}{\sqrt{3}}$

Quantity	Name	Value
\tilde{M}_k	Inertia constant	$\frac{\omega_{\text{ref}} M_k}{3S_{\text{base}}}$
\tilde{D}_k	Damping constant	$\frac{\kappa_{pk} + \omega_{\text{ref}} D_k}{3S_{\text{base}}}$
\tilde{P}_k	Bus active power	$\frac{P_k^*}{3S_{\text{base}}}$
\tilde{Y}_{kh}	TL admittance	$\tilde{G}_{kh} + j\tilde{B}_{kh}$
\tilde{V}_k	Bus voltage magnitude	$\frac{\bar{v}_k^*}{\sqrt{2}V_{\text{base}}}$
σ_{kh}	Maximum TL's power exchange	$\tilde{V}_k \tilde{V}_h \left \tilde{Y}_{kh} \right $
δ_k	Phase deviation	$\theta_k - \omega_{\text{ref}} t$
γ_{kh}	Constant phase deviation	$\frac{\pi}{2} - \arctan\left(\frac{B_{kh}}{G_{kh}}\right)$

Table 3.1: Parameters summary of the Swing Equation in (3.21) and their relation with parameters of power grid's electrical model

3.1.2 Modelling power network components with the swing equation

There is a wide range of power network components that can be modelled by using the swing equation in (3.22) [21, 117, 125, 145]. This is mainly done by selecting proper values of \tilde{M}_k , \tilde{D}_k and P_k . In what follows, it is shown how different types of generators and loads can be modelled with the swing equation.

Generators

The generators are modelled by assuming positive nodal power values $P_k > 0$, $\forall k \in \mathcal{V}_g \subset \mathcal{V}$ and, depending on the generator's type, we may choose the Swing Equation's parameters as follows.

- **Synchronous Machines:** generator buses with SM dynamics $\forall k \in \mathcal{V}_{\text{SM}} \subset \mathcal{V}$ are modelled with parameters $\tilde{M}_k = \frac{\omega_{\text{ref}} M_k}{3S_{\text{base}}}$ and $\tilde{D}_k = \frac{\kappa_{pk} + \omega_{\text{ref}} D_k}{3S_{\text{base}}}$.
- **Voltage Source Converters:** generator buses with VSC dynamics $\forall k \in \mathcal{V}_{\text{VSC}} \subset \mathcal{V}$ are modelled depending on the primary controller structure.
 - **Virtual synchronous machine control:** in the case of VSCs controlled as Virtual SMs ($\forall k \in \mathcal{V}_{\text{VSC2}} \subset \mathcal{V}_{\text{VSC}}$), the parameter \tilde{M}_k is proportional to the virtual inertia \hat{M}_k in (2.97), that is $\tilde{M}_k = \frac{\omega_{\text{ref}} \hat{M}_k}{3S_{\text{base}}}$ and \tilde{D}_k is proportional to the droop slope of the primary control $\tilde{D}_k = \frac{\kappa_{pk}}{3S_{\text{base}}}$.

- **Grid-Forming control:** nodes with VSCs that are controlled with Grid-Forming strategies that do not introduce virtual inertia ($\forall k \in \mathcal{V}_{\text{VSC1}} \subset \mathcal{V}_{\text{VSC}}$) can be modelled with parameters $\tilde{M}_k = 0$ and $\tilde{D}_k = \frac{r_{pk}}{3P_{\text{base}}}$.
- **Grid-Following control:** nodes with VSCs that are controlled with Grid-Following strategies ($\forall k \in \mathcal{V}_{\text{VSC0}} \subset \mathcal{V}_{\text{VSC}}$) can be modelled with parameters $\tilde{M}_k = 0$ and $\tilde{D}_k = 0$.

Loads

Loads can be modelled by assuming negative nodal power values $P_k \leq 0, \forall k \in \mathcal{V}_l \subset \mathcal{V}$ and, depending on the load's type, we may choose the Swing Equation's parameters as follows.

- **Synchronous Motors** ($\forall k \in \mathcal{V}_{l2} \subset \mathcal{V}$): in this case, the parameter \tilde{M}_k is proportional to the inertia constant of the synchronous motors $\tilde{M}_k = \frac{\omega_{\text{ref}} \tilde{M}_k}{3S_{\text{base}}}$ and \tilde{D}_k is proportional to the damping constant $\tilde{D}_k = \frac{\omega_{\text{ref}} D_k}{3S_{\text{base}}}$.
- **Frequency-dependent loads** ($\forall k \in \mathcal{V}_{l1} \subset \mathcal{V}$): as explained in Section 2.3, aggregated loads can have frequency dependent dynamics [21] and can be modelled by defining the parameters $\tilde{M}_k = 0$ and $\tilde{D}_k = \frac{\omega_{\text{ref}} D_{lk}}{3S_{\text{base}}}$, being D_{lk} the load's damping coefficient.
- **Resistive loads** ($\forall k \in \mathcal{V}_{l0} \subset \mathcal{V}$): in the case of purely resistive loads, we have $\tilde{M}_k = 0$ and $\tilde{D}_k = 0$.

In Table 3.2 we provide a summary of the parameter choices and associated components modelled by (3.22). Different choices of these parameters lead to a DAE (Differential Algebraic Equations) models of the form

$$\tilde{M}_k \ddot{\delta}_k + \tilde{D}_k \dot{\delta}_k = P_k - P_{e,k} + u_k \quad \forall k \in \mathcal{V}_2 \quad (3.24a)$$

$$\tilde{D}_k \dot{\delta}_k = P_k - P_{e,k} + u_k \quad \forall k \in \mathcal{V}_1 \quad (3.24b)$$

$$0 = P_k - P_{e,k} + u_k \quad \forall k \in \mathcal{V}_0 \quad (3.24c)$$

with $P_{e,k}$ given by

$$P_{e,k} = \sum_{h=1}^N \sigma_{kh} \sin(\delta_k - \delta_h - \gamma_{kh}) \quad (3.25)$$

with nodes sets associated with second-order differential equations in set $\mathcal{V}_2 \equiv \mathcal{V}_{\text{SM}} \cup \mathcal{V}_{\text{VSC2}} \cup \mathcal{V}_{l2}$, of first order differential equations in set $\mathcal{V}_1 \equiv \mathcal{V}_{\text{VSC1}} \cup \mathcal{V}_{l1}$ and algebraic equations in set $\mathcal{V}_0 \equiv \mathcal{V}_{\text{VSC0}} \cup \mathcal{V}_{l0}$. Note that equation (3.24b) considers the presence of secondary controllers also for controllable loads in the case of demand control for frequency regulation, as it has been proposed in [61, 111]. In the absence of secondary controllers ($k \in \mathcal{V} \setminus \mathcal{V}_{\text{sec}}$), we have $u_k = 0$. An example of the modelling capabilities and reduction of the Swing Equation is depicted in Figure 3.1.

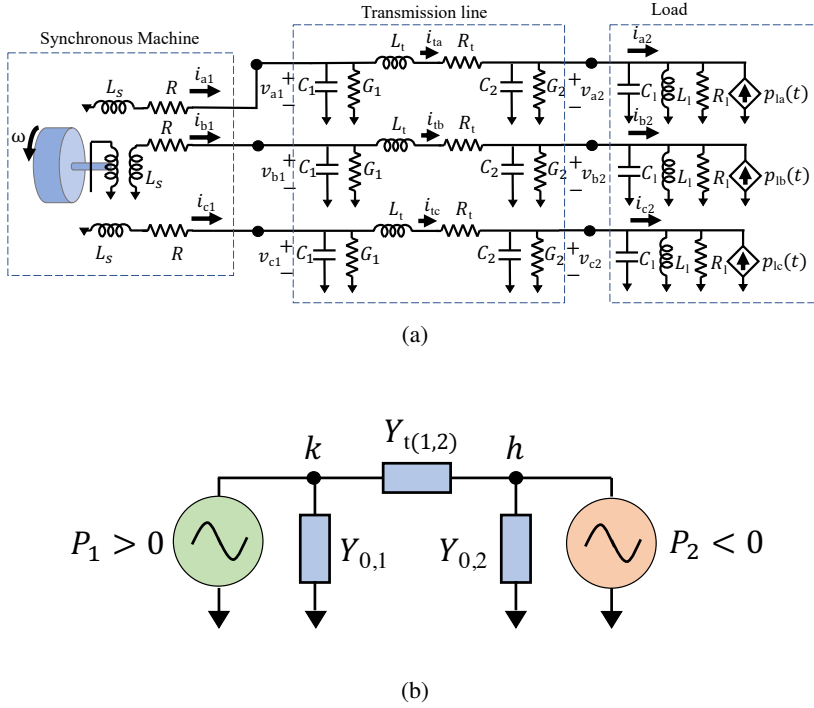


Figure 3.1: (a) A SM providing power $P_1 > 0$ to a three phase load with power consumption $P_2 < 0$ (b) The equivalent model obtained by using the Swing equation (3.22), with $Y_{0,k}, Y_{t(1,2)} \in \mathbb{C}$ being complex admittances representing $Y_{0,k}$ and $Y_{t(1,2)}$ in (3.14).

Remark 3.4. In some modelling approaches, there is particular interest in considering the frequency dynamics inside the stator windings [125, 142]. In doing so, it is assumed that the generator can be modelled by two nodes, the internal node $k' \in \mathcal{V}'_{SM}$, which models the internal voltage of the SM as an AC voltage source with magnitude $E_{k'}$, and the terminal node $k \in \mathcal{V}_{SM}$, with terminal voltage magnitude V_k which is connected to the network. These two nodes are connected with each other through the **transient reactance**, defined as

$$X_{sk} = j\omega_{\text{ref}} L_{sk} \quad (3.26)$$

which represents the internal impedance of the stator windings produced by the inductance $L_d = L_q = L_s$. The frequency dynamics can be modelled using (3.22) as

$$\tilde{M}_{k'} \ddot{\delta}_{k'} + \tilde{D}_{k'} \dot{\delta}_{k'} = P_{k'} - E_{k'} V_k Y_{sk} \sin(\delta_{k'} - \delta_k) + u_k \quad \forall k' \in \mathcal{V}'_{SM} \quad (3.27a)$$

$$\tilde{D}_k \dot{\delta}_k = P_k - P_{e,k} + u_k \quad \forall k \in \mathcal{V}_I \quad (3.27b)$$

$$0 = P_k - P_{e,k} + u_k \quad \forall k \in \mathcal{V}_0 \cup \mathcal{V}_{SM} \quad (3.27c)$$

with admittance $Y_{sk} = \frac{I_{base}}{X_{sk} V_{base}}$, X_{sk} as in (3.26) and $P_{e,k}$ as in (3.25). A representation of this modelling approach is depicted in Figure (3.2)

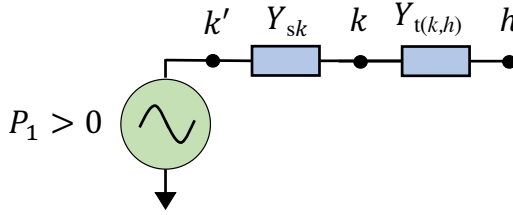


Figure 3.2: Transient reactance Y_{sk} and generator terminal node k'

3.1.3 Further simplifications

The power network model (3.24) can be difficult to use for analysis and control design and thus several approaches have been presented in the literature to simplify it. Here, we summarize the most relevant ones.

Effective Network model (EN)

The effective network model considers loads as purely resistive and performs a Shur Complement based simplification of the admittance matrix \vec{Y} in (3.23), known as the Kron Reduction method [57, 125]. To explain how this is achieved, let us particularize (3.24) to the case of nodes with second order dynamics $\mathcal{V}_2 \equiv \mathcal{V}_{SM} \cup \mathcal{V}_{VSC2} \cup \mathcal{V}_{I2}$ and static nodes $\mathcal{V}_0 \equiv \mathcal{V}_{VSC0} \cup \mathcal{V}_{I0}$, i.e. [125]

$$\tilde{M}_k \ddot{\delta}_k + \tilde{D}_k \dot{\delta}_k = P_k - P_{e,k} + u_k \quad \forall k \in \mathcal{V}_2, \quad (3.28a)$$

$$0 = P_k - P_{e,k} + u_k \quad \forall k \in \mathcal{V}_0. \quad (3.28b)$$

Component	Type	\tilde{M}_k	\tilde{D}_k	Nodes set
Generator $P_k > 0$, $k \in \mathcal{V}_g$	SM	$\frac{\omega_{\text{ref}}}{3P_{\text{base}}} M_k$	$\frac{\omega_{\text{ref}} D_k + \kappa_{p,k}}{3P_{\text{base}}}$	\mathcal{V}_{SM}
	VSC+VSM control	$\frac{\omega_{\text{ref}}}{3P_{\text{base}}} M_k$	$\frac{\kappa_{p,k}}{3P_{\text{base}}}$	$\mathcal{V}_{\text{VSC2}}$
	VSC+Grid-forming control	0	$\frac{\kappa_{p,k}}{3P_{\text{base}}}$	$\mathcal{V}_{\text{VSC1}}$
	VSC+Grid-following control	0	0	$\mathcal{V}_{\text{VSC0}}$
Loads $P_k < 0$, $k \in \mathcal{V}_l$	Synchronous motors	$\frac{\omega_{\text{ref}}}{3P_{\text{base}}} M_k$	$\frac{\omega_{\text{ref}}}{3P_{\text{base}}} D_k$	\mathcal{V}_l
	Linear power-frequency dependence	0	$\frac{\omega_{\text{ref}}}{3P_{\text{base}}} D_k$	$\mathcal{V}_{l1} \cup \mathcal{V}_{\text{ter1}}$
	Resistive loads	0	0	$\mathcal{V}_{l0} \cup \mathcal{V}_{\text{ter0}}$

Table 3.2: Modelling power network elements with the Swing Equation (3.21)

Based on the model in (3.28), the Kron Reduction method is then used to eliminate the rows and columns of the admittance matrix \vec{Y} that represent the static nodes (3.28b), so that the following model of the grid can be derived

$$\tilde{M}_k \ddot{\delta}_k + \tilde{D}_k \dot{\delta}_k = P_k - G_{\text{EN},kk} V_k^2 - \sum_{h=1, k \neq h}^N \sigma_{\text{EN},kh} \sin(\delta_k - \delta_h - \gamma_{\text{EN},kh}) + u_k \quad \forall k \in \mathcal{V}_2 \quad (3.29)$$

with parameters

$$\sigma_{\text{EN},kh} = V_k V_h |Y_{\text{EN},kh}|, \quad (3.30a)$$

$$\gamma_{\text{EN},kh} = \frac{\pi}{2} - \tan^{-1} \left(\frac{\text{Im}(Y_{\text{EN},kh})}{\text{Re}(Y_{\text{EN},kh})} \right), \quad (3.30b)$$

that take into account the resistive effect of the nodes in $\mathcal{V}_{\text{VSC0}} \cup \mathcal{V}_{l0}$ with the admittance parameters $Y_{\text{EN},kh}$, which are the elements of the Kron reduced matrix

$$\vec{Y}_{\text{EN}} = \vec{Y}^{\alpha\alpha} - \vec{Y}^{\alpha\beta} (\vec{Y}^{\beta\beta})^{-1} \vec{Y}^{\beta\alpha}$$

for a suitable partitioning of the admittance matrix

$$\vec{Y} = \begin{bmatrix} \vec{Y}^{\alpha\alpha} & \vec{Y}^{\alpha\beta} \\ \vec{Y}^{\beta\alpha} & \vec{Y}^{\beta\beta} \end{bmatrix}$$

where $\vec{Y}^{\alpha\alpha}$ represents the admittance terms between second-order buses such that $Y_{kh}^{\alpha\alpha} = Y_{kh}$ with $k, h \in \mathcal{V}_2$, $Y_{kh}^{\alpha\beta} = Y_{hk}^{\beta\alpha} = Y_{kh}$ such that $k \in \mathcal{V}_2, h \in \mathcal{V}_0$ and finally $Y_{kh}^{\beta\beta} = Y_{kh}$ with $k, h \in \mathcal{V}_0$.

The use of the Kron reduction method leads to a smaller network representation, as the nodes corresponding to loads are eliminated, and their admittance terms considered through the parameters of the reduced network topology. Moreover, note that the resultant network topology is not representative of the physical one. and it always becomes all-to-all if transient reactances (3.26) are considered, something that is not convenient to carry out for stability analysis based on network topological properties.

Structure preserving (SP)

The Structure Preserving model was first introduced in [21] and its main assumption is that aggregated loads have frequency dependent dynamics. This leads to the simplified model

$$\tilde{M}_k \ddot{\delta}_k + \tilde{D}_k \dot{\delta}_k = P_k - P_{e,k} + u_k \quad \forall k \in \mathcal{V}_2 \quad (3.31a)$$

$$\tilde{D}_k \dot{\delta}_k = P_k - P_{e,k} + u_k \quad \forall k \in \mathcal{V}_1 \quad (3.31b)$$

with $\mathcal{V}_2 \equiv \mathcal{V}_{SM} \cup \mathcal{V}_{VSC2} \cup \mathcal{V}_{I2}$ and $\mathcal{V}_1 \equiv \mathcal{V}_{VSC1} \cup \mathcal{V}_{ter1} \cup \mathcal{V}_{I1}$. This model does not have any algebraic equations, which avoids the use of the Kron reduction, so that the network structure remains intact.

Lossless transmission line assumption

It is common to assume that the resistive terms of the transmission lines are small $G_{kh} \approx 0$, neglecting resistive power losses. This assumption is considered valid for high voltage power networks, but has been extensively used for the analysis and control of power networks as it simplifies their analytical treatment [60, 62]. From (3.24), it leads to the simplified model

$$\tilde{M}_k \ddot{\delta}_k + \tilde{D}_k \dot{\delta}_k = P_k - \tilde{P}_{e,k} + u_k \quad \forall k \in \mathcal{V}_2 \quad (3.32a)$$

$$\tilde{D}_k \dot{\delta}_k = P_k - \tilde{P}_{e,k} + u_k \quad \forall k \in \mathcal{V}_1 \quad (3.32b)$$

$$0 = P_k - \tilde{P}_{e,k} + u_k \quad \forall k \in \mathcal{V}_0 \quad (3.32c)$$

with

$$\tilde{P}_{e,k} = \sum_{h=1}^N \tilde{\sigma}_{kh} \sin(\delta_k - \delta_h) \quad (3.33)$$

and $\tilde{\sigma}_{kh} = V_k V_h B_{kh}$ and B_{kh} a susceptance term.

The Microgrid The introduction of power sources based on renewable energies has served as a pivot to propose power network architectures that are more independent from transmission network operators. This is so, because these energies can be exploited in a distributed manner, with infrastructures in the order of KW or MW. One of the main characteristics of this architecture, is its lack of inertia due to the small amount, or even absence of flywheels for mechanical energy storage. In general a microgrid can be modelled as a special case of model (3.24) which, in its most restrictive case, only considers VSCs and resistive loads and can be given as:

$$\tilde{D}_k \dot{\delta}_k = P_k - P_{e,k} + u_k \quad \forall k \in \mathcal{V}_{\text{VSC1}} \quad (3.34a)$$

$$0 = P_k - P_{e,k} + u_k \quad \forall k \in \mathcal{V}_{\text{VSC0}} \cup \mathcal{V}_{\text{I0}} \quad (3.34b)$$

3.2 Summary

In this chapter, we gave simplified models for the power grid as a complex multi-agent system. First, we presented the Swing Equation as a simplified model of the power network. We also showed how a series of simplifications of the electrical model of the power network, mainly based on singular perturbation tools, lead us to the swing equation. These simplification steps also provided us the blueprints to provide a mapping of the electrical power network model into the swing equation, summarized in Table 3.2 and being the main contribution of this Chapter. Finally, we gave further simplifications of the swing equations found in the power network literature.

In the next Chapter, we will explain the hierarchical architecture of the power network and the important role the Swing Equation has on its design.

4 The control architecture of the power network

Until now, we have shown different modelling approaches for the power grid varying in terms of complexity and variables of interest. Among them, we introduced the Swing Equation and the Power AC Flow Equations as simplified models of the power grid. In this chapter, we use these models to present two main control tasks that are critical for the coordination of the power grid; the secondary frequency control and the set-point computation. These tasks, together with the respective models used for its formulation and control design, constitute additional levels of abstraction of the power grid, commonly known as the secondary and tertiary layers. This Chapter gives a comprehensive description of such layers explaining how they are designed and their relationship with the primary layer.

4.1 The hierarchical control architecture power grid

different modelling tools for the power network frequency dynamics. Now, we explain the hierarchical control architecture used to provide frequency regulation and power flow.

The power network is subject to a wide range of disturbances that can trigger the activation of protective equipment [47, 48]. The most common protective measure used within the power network is the direct disconnection of transmission lines that transmit more power than its nominal value and the disconnection of generators and loads whose nodal frequency/voltage is beyond predefined ranges [48]. Unfortunately, these protective measures can lead to power imbalance.

The power imbalance between generation and demand due to a disturbance produces an increase of the frequency deviation and the computation of the control signals required for this compensation is the joint task of the three control layers, being the Primary Control layer described in Section 2.6 one of them. From a control perspective, additional control layers working at different times-scales are designed with the purpose of coordinating the power generation by providing appropriate set-points \bar{v}_k^* , p_k^* and q_k^* to the Primary Controllers of generators $k \in \mathcal{V}_g$, which are required to fulfill specifications (2.66) and

(2.67b) after a disturbance. These set-points have the following structure

$$p_k^* = 3(P_k + u_k) \quad k \in \mathcal{V}_g \quad (4.1a)$$

$$q_k^* = 3Q_k \quad k \in \mathcal{V}_g \quad (4.1b)$$

$$\bar{v}_k^* = \sqrt{2}V_k \quad k \in \mathcal{V} \quad (4.1c)$$

with P_k, Q_k and V_k being the active and reactive power and the Root Mean Square voltage as defined in (3.2) and u_k the secondary control input in (3.22), also known as the *generation reserve*. The computation of these set-points is distributed in two main control layers. The **Tertiary Layer** computes power and voltage set-points for the generators $P_k, Q_k \forall k \in \mathcal{V}_g$ and V_k that minimize the generation costs, fulfill the power demand $P_k, Q_k \forall k \in \mathcal{V}_l$ and satisfy generation and transmission constraints. These set-points are assumed to be valid for a minutes-to-hours times-scale (**macro-scale**). Note that $P_k, Q_k \forall k \in \mathcal{V}_l$ are considered parameters of the network as they determine the current loads power demand and can be measured or forecasted.

The **Secondary Layer**, instead, provides the frequency set-point following on a faster times-scale (seconds to minutes times-scale), through an integral control action u_k which is, in most cases, based on measurements of the nodal frequency deviations $\hat{\delta}_k = \omega_k - \omega_{\text{ref}}$. This integral controller must ensure satisfaction of the frequency specification (2.67a) in all the network buses, while satisfying power generation constraints.

We depict in Figure 4.1 the desired frequency response of the power network in which the primary frequency control is in charge of ensuring the stability of power network after the **Arresting** and **Rebound Periods**. After the power network has reached an equilibrium, the secondary controller compensates the steady-state error and ensures that the desired frequency value is reached at steady-state. After this, the tertiary control updates the set-points to compensate any power demand perturbations.

Summing up, the tertiary layer assigns power set-points to the generators based on some forecasted demand change while reliability of the power generation is ensured by the secondary layer by adjust these set-points on a faster time-scale. The actuation task is then performed by the primary layer, which thus ensures set-point following (See Figure 4.2). The main approaches for the control of the power network from a secondary and tertiary layer point of view are explained in what follows.

Remark 4.1. *Note that the tertiary layer also computes the voltage set-points $V_k \forall k \in \mathcal{V}_l$, as they can be modified by changing the turn ratios of the nodes equipped with controllable transformers.*

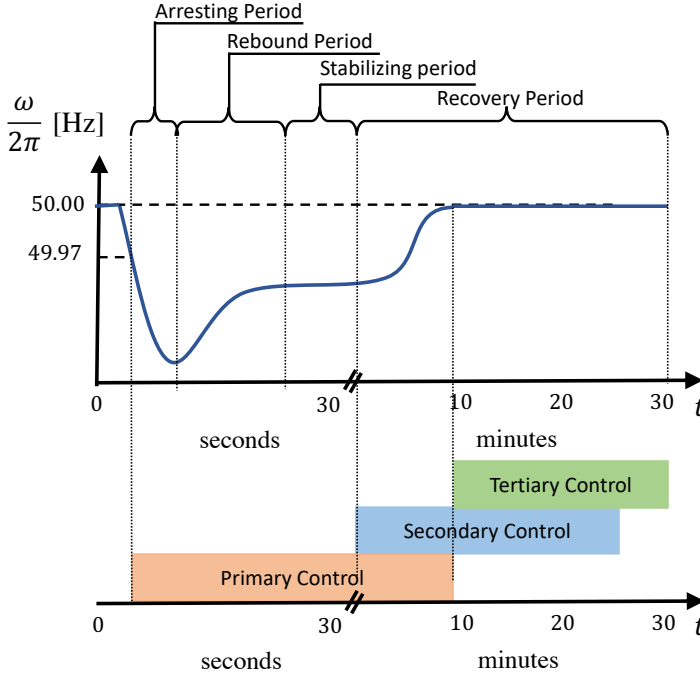


Figure 4.1: Desired frequency response of a power network to power demand disturbances. Adapted from [48]

4.2 The secondary control layer: frequency regulation

4.2.1 Secondary control specifications

From the network perspective, the satisfaction of the frequency specification (2.67a) depends on achieving the right balance between power generation and demand, that is, the power network must ensure that

$$\lim_{t \rightarrow \infty} \sum_{k \in \mathcal{V}} p_k(t) + \sum_{\{i,j\} \in \mathcal{E}} p_{\text{loss},\{i,j\}}(t) = 0 \quad (4.2)$$

with $p_k(t)$ be the instantaneous active power generated/consumed at node $k \in \mathcal{V}$ and $p_{\text{loss},(i,j)}(t)$ is the active power losses in the transmission line $(i,j) \in \mathcal{E}$. The mechanism that links the power balance (4.2) with the specification in (2.67a) will be made clearer in what follows. For instance, assume that primary controllers are able to ensure a synchronous steady-state frequency ω^* different from the nominal one ω_{ref} , that is

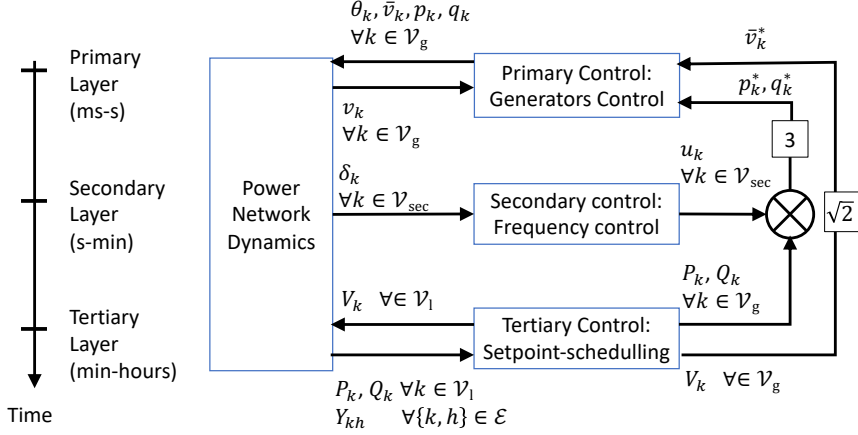


Figure 4.2: Control layers and their interaction with the power network

$$\lim_{t \rightarrow \infty} \omega_k = \omega^* \quad \forall k \in \mathcal{V}$$

At this synchronous regime, the dynamics in (3.24) become

$$\tilde{D}_k \dot{\delta}^* = P_k - P_{e,k}^* + u_k^* \quad \forall k \in \mathcal{V}_1 \cup \mathcal{V}_2 \quad (4.3a)$$

$$0 = P_k - P_{e,k}^* + u_k^* \quad \forall k \in \mathcal{V}_0 \quad (4.3b)$$

where $\dot{\delta}^* = \omega^* - \omega_{\text{ref}}$, is a state value of secondary control input $\forall k \in \mathcal{V}_{\text{sec}}$ and

$$P_{e,k}^* = \sum_{h=1}^N \sigma_{kh} \sin(\delta_k^* - \delta_h^* - \gamma_{kh}), \quad (4.4)$$

accounts for the transmitted power and transmission losses with $\delta_k^* = (\omega^* - \omega_{\text{ref}})t + \delta_k(0)$. Adding all equations in (4.3) over all buses on the network $k \in \mathcal{V}$ and solving for $\dot{\delta}^*$ we obtain [59]

$$\dot{\delta}^* = \frac{\sum_{k \in \mathcal{V}} (P_k - P_{e,k}^*) + \sum_{k \in \mathcal{V}_{\text{sec}}} u_k^*}{\sum_{k \in \mathcal{V}_2 \cup \mathcal{V}_1} \tilde{D}_k} \quad (4.5)$$

The term $\sum_{k \in \mathcal{V}} (P_k - P_{e,k}^*)$ accounts for the total power imbalance on the network. Under the assumption that the power demand $P_k < \forall k \in \mathcal{V}_1$ is known with high accuracy and that the power generation $P_k > \forall k \in \mathcal{V}_g$ is enough to satisfy this demand and the power losses, the power network fulfills specification (4.2) as $\sum_{k \in \mathcal{V}} (P_k - P_{e,k}^*) = 0$ and implies

at the same time that $u_k^* = 0 \forall k \in \mathcal{V}_{\text{sec}}$, as no secondary control would be needed. Note that the latter scenario is not always possible due to (i) disturbances coming from the power demand $P_k \forall k \in \mathcal{V}_1$, (ii) load model mismatch (iii) the primary control strategies in Section 2.6.5 and 2.6.6 are mainly proportional control strategies, producing frequency steady-state error by default. To ensure zero frequency deviation δ^* , proper secondary control signals u_k must be applied to the power network.

Remark 4.2. *It is commonly assumed that transmission lines are lossless ($G_{kh} \approx 0$) which leads to $\sum_{k \in \mathcal{V}} P_{e,k}^* \approx 0$ (see (3.33)) and the network frequency deviation can then be computed as [61]*

$$\delta^* = \frac{\sum_{k \in \mathcal{V}} P_k + \sum_{k \in \mathcal{V}_{\text{sec}}} u_k^*}{\sum_{k \in \mathcal{V}_2 \cup \mathcal{V}_1} \tilde{D}_k} \quad (4.6)$$

4.2.2 Secondary control problem statement

The main purpose of the secondary frequency control is to complement the primary controllers action by fulfilling the power balance specification (4.2). This becomes instrumental when the set-points $P_k \forall k \in \mathcal{V}_g$ are no longer accurate due to disturbances on the power demand $P_k \forall k \in \mathcal{V}_l$. To do so, the reserve power set-points u_k^* (steady-state secondary control values) must be computed so as to ensure that $\delta^* = 0$ in (4.6), while minimizing the operational cost of the generators, which can be written as an Optimal Economic Dispatch (OED) problem [98, Chapter 11], [182]

$$\begin{aligned} & \min_{u_k, k \in \mathcal{V}_{\text{sec}}} \sum_{k \in \mathcal{V}_{\text{sec}}} f_k(u_k^*) \\ & \text{s.t.} \\ & \sum_{k \in \mathcal{V}} P_k + \sum_{k \in \mathcal{V}_{\text{sec}}} u_k^* = 0 \end{aligned} \quad (4.7)$$

with $f_k(\cdot)$ being a function representing the operational cost of generator $k \in \mathcal{V}_g$ as a marginal cost of the power production. Note that the equality constraint of the optimization problem in (4.7) is the numerator of the steady-state synchronous frequency expression in (4.6). A suitable solution for the problem is to define an steady-state value of the secondary control input of the form [61, 118]:

$$u_k^* = -\frac{\lambda}{c_k} \quad (4.8)$$

where c_k is a marginal cost of the power production, λ is a Lagrange multiplier whose optimal value is

$$\lambda^* = \frac{\sum_{k \in \mathcal{V}} P_k}{\sum_{k \in \mathcal{V}_{\text{sec}}} c_k^{-1}} \quad (4.9)$$

This is demonstrated in what follows. A solution to the OED problem in (4.7) can be given through Lagrangian relaxation. We can define a Lagrangian function for the optimization problem (4.7) as

$$l(u_k^*) = \sum_{k \in \mathcal{V}_{\text{sec}}} f_k(u_k^*) + \lambda \left(\sum_{k \in \mathcal{V}} P_k + \sum_{k \in \mathcal{V}_{\text{sec}}} u_k^* \right) \quad (4.10)$$

with λ being a Lagrange multiplier. From the Dual feasibility condition we obtain:

$$\frac{\partial l(u_k^*)}{\partial u_k^*} = \frac{\partial f_k(u_k^*)}{\partial u_k^*} + \lambda = 0$$

which yields

$$\frac{\partial f_k(u_k^*)}{\partial u_k^*} = -\lambda \quad (4.11)$$

An interpretation of the result in (4.11) is that the marginal cost of the power generated for the secondary frequency control must be the same for all generators so that problem (4.7) becomes feasible. Assuming quadratic cost functions of the form

$$f_k(u_k^*) = \frac{1}{2} c_k u_k^{*2}$$

with $c_k \in \mathbb{R}$, the steady-state value of u_k^* that satisfies (4.11) is

$$u_k^* = -\frac{\lambda}{c_k} \quad (4.12)$$

Now, solving the dual optimization problem

$$\max_{\lambda} \phi(\lambda), \quad (4.13)$$

for the dual objective function

$$\phi(\lambda) = l\left(-\frac{\lambda}{c_k}\right) = -\frac{\lambda^2}{2} \sum_{k \in \mathcal{V}_{\text{sec}}} c_k^{-1} + \lambda \sum_{k \in \mathcal{V}} P_k,$$

we can derive an expression for the Lagrange multiplier by verifying the *First Order Stationarity Condition* of the dual problem (4.13), which reads

$$\frac{\partial \phi(\lambda^*)}{\partial \lambda} = -\lambda^* \sum_{k \in \mathcal{V}_{\text{sec}}} c_k^{-1} + \sum_{k \in \mathcal{V}} P_k = 0. \quad (4.14)$$

Solving (4.14) for λ^* lead to:

$$\lambda^* = \frac{\sum_{k \in \mathcal{V}} P_k}{\sum_{k \in \mathcal{V}_{\text{sec}}} c_k^{-1}} \quad (4.15)$$

Finally, from the optimal solution of the OED (4.12), we can write the optimal steady-state secondary control value as

$$u_k^* = -\frac{1}{c_k} \frac{\sum_{k \in \mathcal{V}} P_k}{\sum_{k \in \mathcal{V}_{\text{sec}}} c_k^{-1}} \quad (4.16)$$

The secondary control problem then reduces to find appropriate means of computing λ^* in (4.15) based on the total power imbalance of the $\sum_{k \in \mathcal{V}} P_k$. In most of the cases, the latter is difficult to measure and the frequency-power imbalance relation in (4.6) is exploited for its estimation.

Remark 4.3. In most of the control approaches λ is considered as an auxiliary control variable rather than a Lagrange multiplier, but its interpretation remains the same.

Remark 4.4. The optimization problem in (4.7) assumes that the condition $|\delta_k^* - \delta_h^*| \leq \pi/2$ holds for any optimal solution u_k

4.2.3 Secondary control design

The secondary control problem then translates an integral control problem that aims at compensating the power imbalance through frequency measurements on the power network, while satisfying (4.2) and (4.15) at steady-state. It has been carried out through three main approaches, being the **centralized**, the **decentralized** and the **distributed**, where the main difference between them is the number of integrators used to compute the control signal u_k and the presence or absence of a communication network among these controllers. A representation of these control paradigms is shown in Figure 4.3. In the following, the most representative frequency control algorithms are presented.

Centralized secondary control

The main characteristic of these strategies is that the Lagrange multiplier computation is done by a central controller. Some centralized approaches are explained in the following.

- **Automatic generation control (AGC)** the Automatic Generation Control has been the industry standard for secondary control over the past decades [87]. The main assumption done is that the power network is divided in clusters, known as Control Areas (CA) or Balancing Authorities (BA) that manage the control tasks of nodes inside it. These clusters are defined as subsets of the power network graph $\mathcal{G}_c(\mathcal{V}_c, \mathcal{E}_c) \subset \mathcal{G}(\mathcal{V}, \mathcal{E})$ with $c \in \{1, \dots, N_{CA}\}$ being the area index and N_{CA} is the number of clusters and are connected through an edge set

$$\mathcal{E}_{EX} = \mathcal{E} \setminus \bigcup_{\forall c} \mathcal{E}_c \quad (4.17)$$

defining a cut-set, composed of the edges or transmission lines that remain outside any defined cluster and are commonly known as *Tie Lines*. With this, the AGC strategy computes the Area Control Error (ACE) [12]

$$u_{ACE,c} = b_c \dot{\delta}_c + \sum_{c'=1}^{N_{CA}} \beta_{cc'} (P_{cc'}^* - P_{cc'}), \quad \forall c \in \{1, \dots, N_{CA}\} \quad (4.18)$$

where $\dot{\delta}_c$ is defined as the center of inertia's frequency of the CA c [97, 103, 142]

$$\dot{\delta}_c = \frac{\sum_{k \in \mathcal{V}_c} \tilde{M}_k \dot{\delta}_k}{\sum_{k \in \mathcal{V}_c} \tilde{M}_k} \quad (4.19)$$

and b_c being the bias factor of the control area c . Set-points $P_{cc'}^*$ are forecasted power exchanges between areas and $P_{cc'}$ are the current values of these exchanges,

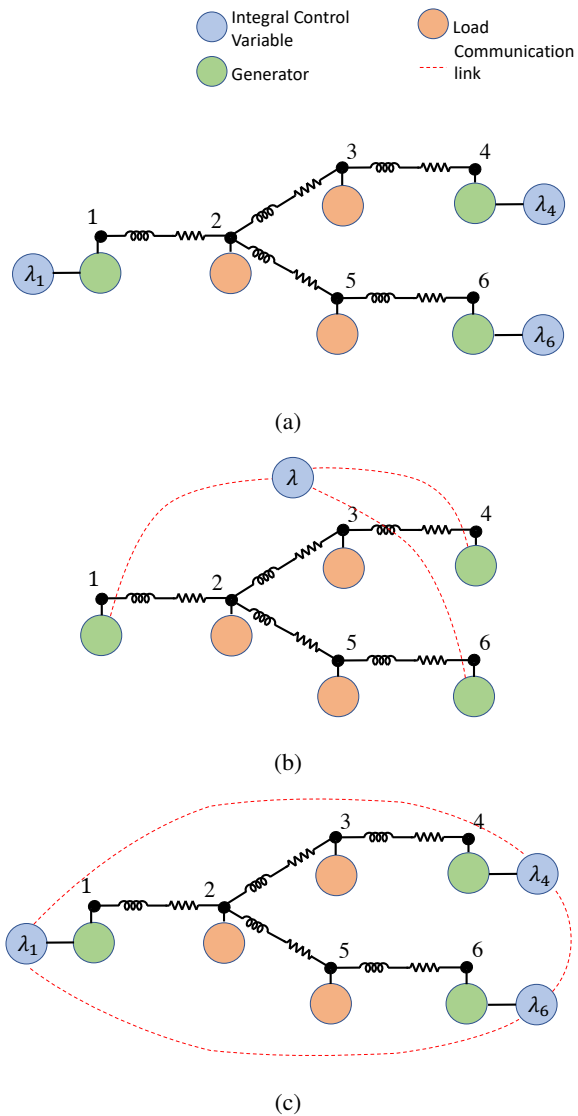


Figure 4.3: Secondary control design approaches (a) Decentralized (b) Centralized, (c) Distributed

which are actually the power flows on the tie lines and are defined as

$$P_{cc'} = \sum_{\substack{\forall k \in \mathcal{V}_c, \\ \forall k' \in \mathcal{V}'_c, \\ (k, k') \in \mathcal{E}_{EX}}} \sigma_{kk'} \sin(\delta_k - \delta'_k - \gamma_{kk'}) \quad (4.20)$$

Finally, in (4.18), $\beta_{cc'}$ is defined as

$$\beta_{cc'} = \begin{cases} 1 & \exists \{k, k'\} \in \mathcal{E}_{\text{EX}}, k \in \mathcal{V}_c, k' \in \mathcal{V}_{c'}, c \neq c' \\ 0 & \text{Otherwise} \end{cases} \quad (4.21)$$

with \mathcal{E}_{EX} as in (4.17). The Area Control Error (ACE) is then used to compute the auxiliary control variable of the area c as

$$\lambda_c = \kappa_{I,c} \int_0^t u_{\text{ACE},c}(\tau) d\tau, \quad \forall c \in \{1, \dots, N_{\text{CA}}\} \quad (4.22)$$

with $\kappa_{I,c}$ is the integral parameter. Finally, the value λ_c is broadcasted on the control area's generators, so that they are able to compute the AGC control signal

$$u_k = -\alpha_{c,k} \lambda_c, \quad k \in \mathcal{V}_{\text{sec},c}, \quad \forall c \in \{1, \dots, N_{\text{CA}}\} \quad (4.23)$$

where $\alpha_{c,k}$ is the participation factor of generator $k \in \mathcal{V}_{\text{sec},c}$ that must satisfy [12,36]

$$\sum_{k \in \mathcal{V}_{\text{sec}}} \alpha_{c,k} = 1$$

In the AGC architecture, the integral variable (4.22) solves the power balance specification (4.2) and an appropriate choice of the participation factors $\alpha_{k,c}$ solves the optimal Economic Dispatch Problem in (4.7). See Figure 4.4 for an AGC architecture example. A proper review on the AGC can be found in [97].

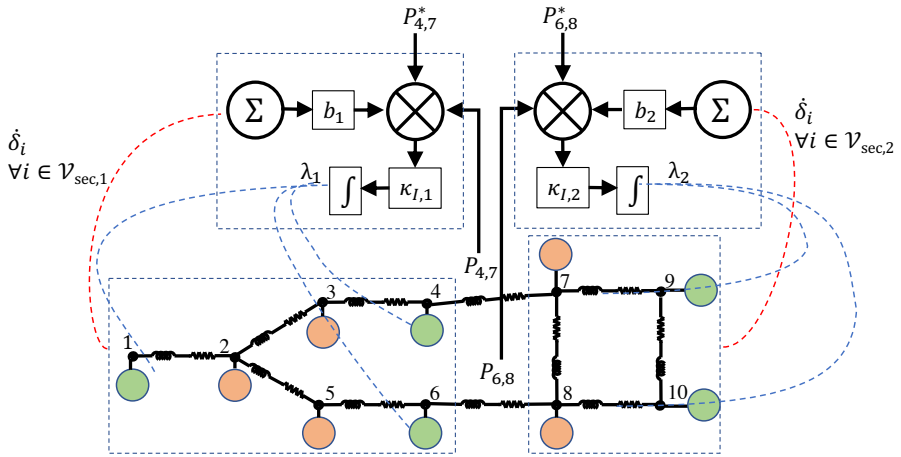


Figure 4.4: Automatic Generation Control architecture

- **Centralized averaging PI control (CAPI)**

Originally designed for the secondary frequency control VSCs dominated power networks (or the microgrid power network paradigm) [104, 147], this controller provides a stable synchronous solution on the model (3.34). It is defined as

$$u_k = -\alpha_k \lambda \quad \forall k \in \mathcal{V}_{\text{sec}} \quad (4.24a)$$

$$\dot{\lambda} = \kappa_I \sum_{k \in \mathcal{V}_{\text{sec}}} c_k \dot{\delta}_k \quad (4.24b)$$

with λ being an auxiliary control variable, $\delta_k = \omega_k - \omega_{\text{ref}}$ is the frequency deviation, κ_I is an integral parameter, c_k determines the response velocity of generator $k \in \mathcal{V}_g$ to frequency fluctuations and α_k determines its participation in secondary control. It was proven in [10, 62] that the CAPI controller can only fulfill the power balance requirements (4.2) provided that the parameters c_k , α_k and k_I are carefully tuned. These results were also extended in [28] for the case of lossy power network model and partial allocation of CAPI controllers.

- **Gather and broadcast frequency control**

This strategy was introduced in [61] and is intended to satisfy equal marginal costs specification (4.2) while achieving frequency regulation. This control strategy measures nodal frequency deviations δ_k to compute the auxiliary control variable

$$\dot{\lambda} = -\kappa_I \sum_{k \in \mathcal{V}_{\text{sec}}} c_k \dot{\delta}_k, \quad (4.25)$$

where k_I is an integral control parameter, and c_k determines the participation of each generator in frequency control, satisfying:

$$\sum_{k \in \mathcal{V}_{\text{sec}}} c_k = 1$$

The auxiliary control variable λ is then broadcasted to each generator participating in secondary frequency control and the secondary control input itself is computed locally by using the inverse of the marginal cost in (4.11) [61]

$$u_k = \frac{\partial f_k^{-1}(\lambda)}{\partial u_k^*} \quad (4.26)$$

where $\frac{\partial f_k^{-1}(\cdot)}{\partial u_k^*}$ is the inverse marginal cost function.

This control strategy is claimed to solve security issues of distributed control strategies because the operation cost functions $f_k(\cdot)$ of each generator are not broadcasted, allowing for fair power generation pricing and participation factor generation.

Decentralized secondary control

A generalized decentralized secondary frequency control requires that the integral control action applied on each generator must be only dependent on the generators local frequency, so that no communication protocols are needed. The simplest of its kind can be written as

$$u_k = -\lambda_k \quad k \in \mathcal{V}_{\text{sec}} \quad (4.27a)$$

$$\dot{\lambda}_k = \kappa_{I,k} \dot{\delta}_k \quad (4.27b)$$

where each generator participating in secondary control computes a local estimate λ_k of the Lagrange multiplier (auxiliary control variable).

The fully decentralized secondary frequency control in (4.27) has been a topic of intense debate [10, 162, 182] and main critic against it is that the power balance specification (4.2) cannot be fulfilled while also ensuring zero frequency deviation. In [174, 182] it has been demonstrated that in order to ensure the presence of a unique globally asymptotically stable equilibrium on a power network with decentralized secondary frequency control the conditions $k_{I,k} > 2 \sum_{h=1}^N \tilde{\sigma}_{kh} \forall k$ must be satisfied (with $\tilde{\sigma}_{kh}$ as in (3.33)), which leads to parameters $k_{I,k}$ that are too large and impractical and also do not solve the Economic Dispatch Problem in (4.7). It was also proven in [61] that decentralized frequency controllers are not robust to constant frequency measurement bias, although can be avoided by using phasor measurement units (PMU) [10]. In [174], a decentralized secondary frequency controller using a low pass filter (leaky integral controller) is proposed. It can satisfy the economic dispatch criteria in (4.7) but cannot achieve precise frequency control.

Distributed secondary control

The most representative distributed secondary frequency control is the *Distributed Averaging Proportional Integral control*. This controller uses per-to-per communication protocols between generators and a continuous time consensus averaging protocol is introduced to estimate the Lagrange multiplier λ [8, 10, 148]. A generalized DAPI architecture can be written as:

$$u_k = -\lambda_k \quad k \in \mathcal{V}_{\text{sec}} \quad (4.28a)$$

$$\dot{\lambda}_k = \kappa_{I1,k} \dot{\delta}_k + \kappa_{I2,k} \sum_{h \in \mathcal{V}_{\text{sec}}} a_{kh} (J_k(u_k) - J_h(u_h)) \quad (4.28b)$$

where $J_k(u_k) = \frac{\partial f_k(u_k)}{\partial u_k^*}$ is the marginal cost of power generation, $\kappa_{I1,k}$ and $\kappa_{I2,k}$ are integral control parameters and $a_{kh} = a_{hk} > 0$ the entries of the adjacency matrix \mathbf{A} describing the communication network topology [148, 162]. It is claimed in [56, 148] that

the auxiliary variables λ_k satisfy both specifications (4.2) and (4.8).

Even though DAPI controllers ensure frequency restoration while achieving economic dispatch, it was found in [11, 72, 159] that inappropriate tuning of the DAPI controller can lead to frequency instability in presence of measurement errors and disturbances. In [6] robustness under communication delays and bounded L2-gain performance is assessed. In [106], a novel distributed congestion control was presented, in order to eliminate overloading in TL in microgrids, while ensuring optimal dispatch and frequency regulation. Optimal frequency controllers considering operational constraints have been designed in [170, 171]. In [53, 91], a framework for the design of frequency controllers under load participation is presented. The network topology design of the DAPI controller has been studied in [177]. The effect of the controllers on the bus voltage dynamics and reactive power sharing have been also considered in [51, 144, 149, 162].

Other approaches

- **Sliding Mode Control approaches:** Some approaches like [114, 167] have considered the use of the sliding mode controller to ensure frequency restoration. This approach has been extended by [163, 164] in the form of decentralized and distributed sliding mode control strategies with turbine governor dynamics.
- **Multiplex networks approach:** in the series of works [9, 108, 109], Multiplex PI and PID controllers were proposed to ensure frequency regulation
- **Reinforcement learning** techniques have been proposed in [4, 78] for the secondary control problem solution.

A summary of the issues and approaches for the application of secondary control strategies on the microgrid can be found in [93].

4.3 The tertiary layer: set-point computation

The tertiary control layer is conceived to deploy planning and management task on the network, which are mainly concerned with the minimization of operational costs and fulfillment of safety requirements so that the operation of the network is reliable and stable. Specifically, power set-points $P_k, Q_k \forall k \in \mathcal{V}_g$ and voltage magnitude set-points $V_k \forall k \in \mathcal{V}$ must be computed so that the power demand $P_k, Q_k \forall k \in \mathcal{V}_l$ of the network is satisfied at the minimum generation cost while the physical and technological constraints like the transmission lines capacities, minimum and maximum power ratings in generators are fulfilled at regime.

4.3.1 Tertiary control specifications

Proper values of the set-points $P_k, Q_k \forall k \in \mathcal{V}_g$ and $V_k \forall k \in \mathcal{V}$ must be computed such that the power demand $P_k, Q_k \forall k \in \mathcal{V}_l$ is satisfied. As these set-points represent a desired operating point for each bus in the network, they must be computed such that the transmission of power is possible under the physical constraints of the network. For this reason, they must satisfy the AC Power Flow equations

$$P_k - \sum_{h=1}^N V_k V_h |Y_{kh}| \sin(\delta_k^* - \delta_h^* - \gamma_{kh}) = 0 \quad k \in \mathcal{V} \quad (4.29a)$$

$$Q_k + \sum_{h=1}^N V_k V_h |Y_{kh}| \cos(\delta_k^* - \delta_h^* - \gamma_{kh}) = 0 \quad k \in \mathcal{V} \quad (4.29b)$$

assuming that the power demand values $P_k, Q_k \forall k \in \mathcal{V}_l$ are known with accuracy. In (4.29), Y_{kh} and γ_{kh} are considered parameters of the network and $\delta_k^* \forall k \in \mathcal{V}$ phase angle differences at regime. Note that (4.29) encode the physical constraints of the transmission lines at regime and make evident the times-scale separation assumption of the tertiary control layers compared to other layers and the network dynamics, as only the algebraic expressions are used as the power network model. Note that if the set-points $P_k, Q_k \forall k \in \mathcal{V}_g$ and $V_k \forall k \in \mathcal{V}$ fulfill (4.29), they also satisfy the power imbalance specification (4.2) as, by summing up all terms in (5.3a) we obtain

$$\sum_{k \in \mathcal{V}} (P_k - P_{e,k}^*) = 0 \quad (4.30)$$

with $P_{e,k}^*$ as in (4.4). Here, (4.30) implies that if the set-points $P_k, Q_k \forall k \in \mathcal{V}_g$ and $V_k \forall k \in \mathcal{V}$ are computed properly, the secondary control action can be shut down until the power demand estimates $P_k, Q_k \forall k \in \mathcal{V}_l$ are not longer valid.

Aside from fulfilling the power transmission requirements (4.29), the set-points must also consider the technological limitations and stability of the power network, encoded in the following inequalities

$$P_k^{\min} \leq P_k \leq P_k^{\max} \quad k \in \mathcal{V}_g \quad (4.31a)$$

$$Q_k^{\min} \leq Q_k \leq Q_k^{\max} \quad k \in \mathcal{V}_g \quad (4.31b)$$

$$V_{\min} \leq V_k \leq V_{\max} \quad k \in \mathcal{V} \quad (4.31c)$$

$$|\delta_k^* - \delta_h^* - \gamma_{kh}| \leq \frac{\pi}{2} \quad \forall \{k, h\} \in \mathcal{E} \quad (4.31d)$$

$$|P_{kh}| \leq P_{kh}^{\max} \quad \forall \{k, h\} \in \mathcal{E} \quad (4.31e)$$

where (4.31a) and (4.31b) keep the active and reactive set-points within the ranges $[P_k^{\min}, P_k^{\max}]$ and $[Q_k^{\min}, Q_k^{\max}]$ of active and reactive power values that the generator $k \in$

\mathcal{V}_g can provide, (4.31c) and (4.31d) keep the nodal voltage and phase deviation values inside ranges that allow the power network to be stable at regime, and (4.31e) keeps the power transmitted through the transmission lines $P_{kh} = G_{kh} V_k^2 - V_k V_h |Y_{kh}| \sin(\delta_k - \delta_h - \gamma_{kh})$ below its maximum ratings P_{kh}^{\max} . In general, it is desired that the voltage remain close to the base voltage of the power system, which is captured by defining voltage range limits $V_{\min} = V_{\text{base}} - \Delta V_{\max}$ and $V_{\max} = V_{\text{base}} + \Delta V_{\max}$ with ΔV_{\max} being the maximum allowed voltage deviation. Note that (4.31e) limits the maximum phase deviation so that a stable phase-locked solution in the network dynamics in (3.24) can be obtained [58, 59].

4.3.2 Tertiary control problem statement

In its most general version, the tertiary control problem is defined as a Nonlinear Program known as the **AC Optimal Power Flow (OPF)** problem, written as [7, 33, 120]

$$\min_{\substack{P_k, Q_k \forall k \in \mathcal{V}_g \\ V_k, \delta_k^* \forall k \in \mathcal{V}}} \sum_{k \in \mathcal{V}_g} f_k(P_k) \quad (4.32a)$$

$$\text{s.t. } g_k(\mathbf{P}, \mathbf{Q}, \mathbf{V}, \boldsymbol{\delta}^*) = 0 \quad \forall k \in \mathcal{V} \quad (4.32b)$$

$$h_k(\mathbf{P}, \mathbf{Q}, \mathbf{V}, \boldsymbol{\delta}^*) \leq 0 \quad \forall k \in \mathcal{V} \quad (4.32c)$$

Here, the cost function $f_k(\cdot)$ represents the power generation cost of generator $k \in \mathcal{V}_g$ and $\mathbf{P}, \mathbf{Q}, \mathbf{V}$ and $\boldsymbol{\delta}^*$ are stack vectors for the active and reactive power, voltage magnitude and phase deviations, respectively. The equality constraints $g_k(\cdot)$ in (4.32b) are the power flow equations (4.29) and the inequality constraints $h_k(\cdot)$ are the technological and stability specifications in (4.31).

4.3.3 Tertiary control design

Solving the OPF problem can be cumbersome. Although the AC power flow is an accurate model of the transmission lines in steady-state, it makes of (4.32) a non-convex optimization problem and the computation of its feasible solutions is still an open problem [19]. This optimization problem has been solved with Nonlinear Programming [55, 79, 86, 102], Mixed Integer Linear Programming [32, 107] and Machine Learning techniques [18, 42]. With the purpose to avoid the complexity of the AC power flow equations, relaxations and approximations of them have been proposed allowing Linear Programming based relaxations [151, 152, 175] Reviews on this topic can be found in [74, 75, 117, 137].

All the previously proposed solutions are, at its core, based on centralized optimization methods. In the recent years, distributed optimization techniques have found application on the OPF problem due to the increase of distributed energy participation on the power network. The OPF problem has been solved in a distributed manner by using **Augmented Lagrange Decomposition** based methods as Analytical Target Cascading [113, 161],

Alternating Direction Method of Multipliers (ADMM) [29, 68, 154], Proximal Message Passing (PMP) [34, 96] and Auxiliary Problem Principle [43]. **Karush-Kuhn-Tucker (KKT) conditions** based distributed optimization methods have also been used to solve OPF problem, like Optimal Condition Decomposition [45] and Consensus+Innovation [54, 127]. See [89] and [117] for reviews on the topic.

4.4 Summary

In this chapter, we explained the hierarchical architecture of the power network. After explaining the role of Primary Control layer, we then showed how this layer cooperates with the Secondary and Tertiary layers to provide integral frequency control and set-point scheduling in a coordinated manner, so that a desired frequency response after disturbances is obtained. We also showed the role each of the control layer has in maintaining the network in a stable regime and how these layers exchange information to achieve this. We then gave a formalization for each of the control specifications that each layer has to fulfill. Finally, the most relevant control strategies for each of the layers are described.

In the next Chapter, we will focus on what happens to the power network when the hierarchical control architecture fails to maintain a stable regime and propose an algorithm that isolates portions of the power network in a distributed manner, so to contain failures and allow frequency stability and power dispatch inside them.

5 Self-organizing power network islanding

5.1 The power network islanding problem

In the previous Chapters, we have given a description of the power network models and its control architecture. Now, we consider the case in which the control architecture fails to maintain a stable regime and last resort strategies have to be deployed to ensure frequency stability and power dispatch across sections of the grid.

Among the different emergency containment strategies of the power network, we are particularly interested in the *Intentional Controlled Islanding* (ICI) strategies [1, 69, 70, 130, 155], i.e. algorithms to identify sections of the grid that can isolate and operate independently from it, such that power can be dispatched at least in some portions of the faulty grid.

In this Chapter, we give a formal description of the power network islanding specifications and introduce the islanding problem. After this, we propose a novel distributed power network partitioning algorithm to solve the ICI problem, designed to allow the network nodes to self-organize into islands. Specifically, the idea is for nodes of a power grid initially partitioned into some set of islands to migrate among them so as to (i) minimize the power imbalance of the islands and (ii) avoid large amounts of load shedding.

Our migration procedure modifies an initial partition of the grid, that can be computed through an offline method such as the slow coherency-based islanding [69, 179, 181], and updates it so to minimize the average absolute power imbalance of the grid. To do so, our migration algorithm is compounded with a *distributed dynamic estimator* allowing nodes to evaluate the power imbalance of an island (or microgrid) so to decide whether to migrate to/from it. This estimator relies on the ability of the nodes in each island of the grid to run in distributed fashion a virtual consensus dynamics parametrized so that the time derivatives of the node states converge to a common value that is proportional to the power imbalance of the island. Under suitable assumptions, we analytically show that our migrations strategy generates a sequence of partitions that converges in finite time to

a configuration whose average absolute power imbalance falls within a pre-computable bound of the minimal one. Moreover, we further validate our strategy by applying it to the IEEE 118 and IEEE 300 test systems, comparing the viable partitions we obtain to others suggested in previous papers in the literature. We formalize the ICI problem in the following.

5.2 Preliminaries

We define an *island* as a connected subgraph $\mathcal{M}_l = (\mathcal{V}_l, \mathcal{E}_l)$ of the power network graph $\mathcal{G}(\mathcal{V}, \mathcal{E})$ where $\mathcal{V}_l \subseteq \mathcal{V}$ is its node set and $\mathcal{E}_l = (\mathcal{V}_l \times \mathcal{V}_l) \cap \mathcal{E}$ its edge set. Given a set of nodes \mathcal{V}_l , we denote by $\mathcal{N}(\mathcal{V}_l)$ the set of neighbours of the nodes in \mathcal{V}_l , i.e. $\mathcal{N}(\mathcal{V}_l) := \{i \in \mathcal{V} \setminus \mathcal{V}_l \mid \exists j \in \mathcal{V}_l : \{i, j\} \in \mathcal{E}\}$ and by \mathcal{N}_i the set of all neighbours of node i . We say that island m is a neighbor of island l if and only if $\mathcal{N}(\mathcal{V}_m) \cap \mathcal{V}_l \neq \emptyset$.

A power network described by the graph \mathcal{G} is *partitioned* into n_μ islands, described by the subgraphs $\mathcal{M}_l, l = 1, \dots, n_\mu$, if the node sets $\mathcal{V}_1, \dots, \mathcal{V}_{n_\mu}$ are such that

- $\bigcup_{l=1}^{n_\mu} \mathcal{V}_l = \mathcal{V}$
- $\mathcal{V}_l \cap \mathcal{V}_m = \emptyset \forall m \neq l$
- $\bigcup_{l=1}^{n_\mu} \mathcal{E}_l = \mathcal{E} \setminus \{\{i, j\} \in \mathcal{E} \mid i \in \mathcal{V}_l, j \in \mathcal{V}_m, l \neq m\}$

We denote a partition of the set of nodes \mathcal{V} by $\Pi = \{\mathcal{V}_1, \dots, \mathcal{V}_{n_\mu}\}$ and by $\mathcal{G}^\Pi = (\mathcal{V}^\Pi, \mathcal{E}^\Pi)$ the graph, defined by the partition Π , whose i -th node is associated with the set \mathcal{V}_l of Π and whose edge set \mathcal{E}^Π is such that $\{l, m\} \in \mathcal{E}^\Pi$ if and only if $\mathcal{V}_l \cap \mathcal{N}(\mathcal{V}_m) \neq \emptyset$. Given a partition Π , a node i is defined as a *boundary node* of an island \mathcal{M}_l if $i \in \mathcal{V}_l$ and $\mathcal{N}_i \cap (\mathcal{V} \setminus \mathcal{V}_l) \neq \emptyset$. Finally, the *power imbalance* for each island \mathcal{M}_l is defined as

$$\bar{P}_l = \sum_{i \in \mathcal{V}_l} P_i, \quad (5.1)$$

whereas the overall grid's *power imbalance* is defined as

$$P_{\text{tot}} = \sum_{i=1}^n P_i = \sum_{l=1}^{n_\mu} \bar{P}_l. \quad (5.2)$$

with P_i being the nodal active power.

5.3 Islanding Specifications

Consider a power network subject to a major disturbance, product of line disconnection or generation/load disconnection such that stability cannot be guaranteed by the hierarchical control architecture. Suitable emergency islanding strategies must provide a partition Π of the power network that allow the islands \mathcal{M}_l to be stable and self-sufficient, so that re-synchronization to a frequency $\lim_{t \rightarrow \infty} \omega_i = \omega_l^* \forall i \in \mathcal{V}_l$, different from the nominal

frequency ω_{ref} , is possible. This translates, from the synchronous frequency expression in (4.5), in finding the partition $\Pi = \{\mathcal{V}_1, \dots, \mathcal{V}_{n_\mu}\}$ such that the post-fault equilibrium $\delta_i^*, \dot{\delta}_i^* \forall i \in \mathcal{V}_l$ satisfying

$$\dot{\delta}_i^* = \omega_l^* - \omega_{\text{ref}} = \frac{\bar{P}_l + P_{\text{loss},l}}{\sum_{i \in \mathcal{V}_l} \bar{D}_i} \quad \forall i \in \mathcal{V}_l \quad (5.3a)$$

$$P_{\text{loss},l} = - \sum_{k \in \mathcal{V}_l} G_{ii} V_i^2 - 2 \sum_{\forall \{i,j\} \in \mathcal{E}_l} V_i V_j G_{ij} \cos(\delta_i^* - \delta_j^*) \quad (5.3b)$$

is locally asymptotically stable. In (5.3), the disconnection of transmission lines due to a failure is considered by eliminating the disconnected line $\{i, j\}$ from the edge set \mathcal{E} and modifying the admittance terms Y_{ij} accordingly, while the disconnection of generators/loads is considered by eliminating its index from \mathcal{V} and any line connecting it to the network from \mathcal{E} . Note that edges that do not belong to the partition $\{i, j\} \notin \bigcup_{\mathcal{V}_l} \mathcal{E}_l$ are not considered in (5.3).

The partition Π must be computed before the *clearance time* t_{cl} of the power network's fault is reached, which is the time it takes the faulty power network's dynamics to reach the boundary of the basin of attraction of the post-fault desired equilibrium point defined in (5.3) [143].

5.4 Islanding Problem Formulation

Although the previous specifications represent the desired characteristic of an ICI strategy in an ideal setting, note that the clearance time and the basin of attraction boundary of the desired post-fault equilibrium point are not known a priori as they depend on the type and location of the fault and on the choice of partition Π . As computing both the clearance time and the basin of attraction for each possible failure and partition Π is computationally intensive for large-scale power networks, most of the ICI strategies aim at finding a partition $\Pi = \{\mathcal{V}_1, \dots, \mathcal{V}_{n_\mu}\}$ that solves one of the following simpler problems [69, 100]:

- **Average absolute power-imbalance minimization:** this formulation aims at finding a partition Π whose islands \mathcal{M}_l have the minimum absolute power imbalance $|\bar{P}_l|$, with \bar{P}_l as in (5.1) and is formulated as

$$\min_{\{\mathcal{V}_1, \dots, \mathcal{V}_{n_\mu}\}} \frac{1}{n_\mu} \sum_{l=1}^{n_\mu} |\bar{P}_l|. \quad (5.4)$$

The island's power imbalance \bar{P}_l is associated with the synchronous frequency deviation of the power network, as shown in (5.3a) from its nominal value, which in turn is related to the power network's frequency stability [56, 99]. Indeed, if the power fed into the grid exceeds the load's demand, then the frequency increases, while if the load's demand is higher than the power supply (lack of power), it

decreases. Variations of the frequency can lead the grid to operate with a high frequency deviation at regime causing potential faults and triggering the protection devices of the network.

The cost function in (5.4) has been used in previous works on power network partitioning, e.g. [69, 80, 105], as an indicator of the ability of a power system to satisfy the load demand, which is also known as *adequacy*.

- **Power-Flow disruption minimization:** which aims at finding a partition Π whose cut-set $\mathcal{E}_{\text{cut}} \equiv \{\mathcal{E} \setminus \bigcup_{\mathcal{V}_l} \mathcal{E}_l\}$ has the minimum sum of transmitted power in the pre-fault system. This problem can be formulated as:

$$\min_{\{\mathcal{V}_1, \dots, \mathcal{V}_{n_\mu}\}} \sum_{\{i,j\} \in \mathcal{E}_{\text{cut}}} \left(\frac{|P_{ij}| + |P_{ji}|}{2} \right), \quad (5.5)$$

with P_{ij} being the transmitted power from node i to node j through the line $\{i, j\}$. This transmitted power can be defined using the notation in (3.22) as

$$P_{ij} = G_{ij}V_i^2 - V_iV_j|Y_{ij}|\sin(\delta_i^* - \delta_j^* - \gamma_{ij}), \quad \forall \{i, j\} \in \mathcal{E} \quad (5.6a)$$

$$P_{ji} = -G_{ji}V_j^2 + V_iV_j|Y_{ij}|\sin(\delta_j^* - \delta_i^* - \gamma_{ij}), \quad \forall \{i, j\} \in \mathcal{E}. \quad (5.6b)$$

with $\delta_i \forall i \in \mathcal{V}$ satisfying the power flow equations (4.29). Solving the problem in (5.5) we attempt to achieve self sufficiency in the resultant islands, as the amount of power they would require from generators outside themselves is minimized.

Remark 5.1. Note that the expressions in (5.6) assume that the line current, and as a consequence the power, flows from node i to node j . Both P_{ij} and P_{ji} are different and its difference is the power loss of the transmission line

$$P_{\text{loss},ij} = P_{ij} - P_{ji} = G_{ij} (V_i^2 + V_j^2 - 2V_iV_j \cos(\delta_i^* - \delta_j^*)). \quad (5.7)$$

Note that fulfilling the requirement of computation time to be less than the clearance time translates into the need of designing algorithms to solve problems (5.4) and (5.5) in a milliseconds to seconds time-scale, as the direct computation of the clearance time can be cumbersome and time consuming.

To ensure that the equilibrium point $\delta_i^*, \dot{\delta}_i^* \forall i \in \mathcal{V}_l$ satisfying (5.3) is locally asymptotically stable, most of the approaches aggregate groups of generators in sets of *coherent generators* having similar dynamic behavior. These generators are grouped based on the fact that some of them "Swing together" after a disturbance, and thus will synchronize to a common frequency when isolated from the rest of the network. In order to determine the coherent generators sets, modal decomposition-based methods, like the slow coherency aggregation method [40, 179, 181] are applied on a linearization of the swing equation

model (3.22). Given a desired number of islands n_μ and after applying modal decomposition, the slow coherency aggregation selects the eigenvalues describing the first n_μ slowest modes of the network and the coherent generators within each island are aggregated based on the similarity between the rows of the associated left eigenvector subspace matrix. Keeping coherent generators within the same islands allows the fulfillment of the specification (5.3).

Independently from the chosen formulation, the problem of partitioning a grid into a set of microgrids or islands is usually modelled as a combinatorial problem, see for example [14, 80, 81, 116] and sometimes is recast as a graph optimization problem [1, 70, 155]. Often, solving these problems numerically is cumbersome or inefficient so that heuristic strategies are frequently used to seek a suboptimal solution, while meeting the required computational times that allow the network to stabilize after a contingency [69, 100, 105, 168].

In the following, we focus on proposing a distributed solution for the islanding problem. Our distributed solution allows the nodes of the power network to self-organize so as to enhance the suboptimal solution found by the islanding problem formulation in (5.5).

5.5 Towards a distributed solution for the islanding problem

Although the average absolute power imbalance in (5.4), defined for simplicity as

$$\mathcal{J} := \frac{1}{n_\mu} \sum_{l=1}^{n_\mu} |\bar{P}_l|, \quad (5.8)$$

is a good adequacy indicator, we must first define a procedure to minimize it in a distributed manner, that is, without the need that each node knows the topology and the power imbalance of the power network. In doing so, note that as $\sum_{l=1}^{n_\mu} |\bar{P}_l| \geq |\sum_{l=1}^{n_\mu} \bar{P}_l| = |P_{\text{tot}}|$, then the average absolute power imbalance will reach a minimum at \mathcal{J}^* , defined as

$$\mathcal{J}^* := \left| \frac{P_{\text{tot}}}{n_\mu} \right|. \quad (5.9)$$

This implies that if we deploy a method that finds a partition Π such that its islands \mathcal{M}_l have a power imbalance \bar{P}_l equal to $\frac{P_{\text{tot}}}{n_\mu}$, we can then minimize \mathcal{J} . As the nodal power values P_i in (5.1) are fixed, it is possible to have power imbalances \bar{P}_l close, but not equal, to $\frac{P_{\text{tot}}}{n_\mu}$.

To accomplish this, given an initial partition of the power grids into n_μ islands, say $\Pi(0)$, we propose a heuristic distributed approach based on two fundamental ingredients:

1. a *distributed dynamic estimator* based on average consensus dynamics that nodes can use to estimate the power imbalance in their own island and of their neighbors;

2. a *migration criterion* according to which a boundary node can decide whether to migrate from its island to a neighboring one.

As each migration changes the node set of two islands, and thus the network partition, we will denote by $\Pi(k)$ the partition after k migrations, with $\mathcal{M}_l(k) = (\mathcal{V}_l(k), \mathcal{E}_l(k))$, $l = 1, \dots, n_\mu$, being the corresponding islands, $\bar{P}_l(k)$, $l = 1, \dots, n_\mu$, their power imbalances, and $\mathcal{J}(k)$ the corresponding value of the cost function in (5.8).

Our migration procedure requires that each boundary node is able to correctly estimate the power imbalance of its neighboring islands and of the island it belongs to. Hence, before formalizing our migration procedure, we will introduce a consensus based estimation strategy that nodes can use to evaluate the power imbalances of the islands in a distributed fashion.

5.6 Distributed power imbalance estimation

Each node, say i , can obtain an estimate of the power imbalance $\bar{P}_l(k)$ of an island, say $\mathcal{M}_l(k) = (\mathcal{V}_l(k), \mathcal{E}_l(k))$ at a migration step k , by running a consensus based estimation strategy. To explain such strategy let us define the auxiliary graph $\widehat{\mathcal{M}}_l(k) := (\widehat{\mathcal{V}}_l(k), \widehat{\mathcal{E}}_l(k))$ with

$$\widehat{\mathcal{V}}_l(k) := \begin{cases} \mathcal{V}_l(k) \setminus i, & \text{if } i \in \mathcal{V}_l(k) \\ \mathcal{V}_l(k) \cup i, & \text{if } i \notin \mathcal{V}_l(k) \end{cases}, \quad (5.10)$$

and $\widehat{\mathcal{E}}_l(k) := (\widehat{\mathcal{V}}_l(k) \times \widehat{\mathcal{V}}_l(k)) \cap \mathcal{E}$. To perform the estimation, node i must start the distributed solution of the *virtual* consensus dynamics given by:

$$\dot{x}_h = P_h + \sum_{j \in \mathcal{V}_l(k)} (x_j - x_h), \quad \forall h \in \mathcal{V}_l(k) \quad (5.11a)$$

$$\dot{\hat{x}}_h^i = P_h + \sum_{j \in \widehat{\mathcal{V}}_l(k)} (\hat{x}_j^i - \hat{x}_h^i), \quad \forall h \in \widehat{\mathcal{V}}_l(k) \quad (5.11b)$$

starting from null initial conditions. Here, x_h and \hat{x}_h^i are the virtual states associated with each node $h \in \mathcal{V}_l(k)$ and $h \in \widehat{\mathcal{V}}_l(k)$, respectively. The superscript i denotes that the virtual dynamics was triggered by node i .

Remark 5.2. To run the consensus dynamics (5.11) in a distributed manner, the virtual states x_h and \hat{x}_h^i are broadcast to all neighboring nodes $\mathcal{N}_h \subseteq \mathcal{V}_l(k)$ and $\widehat{\mathcal{N}}_h \subseteq \widehat{\mathcal{V}}_l(k)$ respectively.

Now, dynamics (5.11a) can be recast in matrix form as

$$\dot{\mathbf{x}} = \mathbf{P} - \mathbf{L}\mathbf{x}, \quad (5.12)$$

where \mathbf{x} is the stack vector of the virtual states x_h and \mathbf{P} is the stack vector of the power values P_h . To obtain the asymptotic behaviour, we premultiply (5.12) by the eigenvectors

of L , thus diagonalizing (5.12). Recall that, as L is the Laplacian matrix associated with a connected undirected graph, it is symmetric and all its eigenvalues are positive, except for one, which is zero, with $\mathbf{1}$ as an eigenvector. From this, it is immediate to obtain that, for all time t , $\mathbf{1}^\top \dot{\mathbf{x}}(t) = \mathbf{1}^\top \mathbf{P}$, and that $\lim_{t \rightarrow \infty} \dot{\mathbf{x}}(t) \in \text{span}(\mathbf{1})$. Hence, $\lim_{t \rightarrow \infty} \dot{\mathbf{x}}(t) = \mathbf{1}\omega_l$, where

$$\omega_l = \frac{\bar{P}_l(k)}{|\mathcal{V}_l(k)|}, \quad (5.13)$$

with $\bar{P}_l(k) = \sum_{j \in \mathcal{V}_l(k)} P_j$. Applying the same rationale to (5.11b), we obtain that $\lim_{t \rightarrow \infty} \hat{\mathbf{x}}(t) = \mathbf{1}\hat{\omega}_l$, with

$$\hat{\omega}_l = \frac{1}{|\hat{\mathcal{V}}_l(k)|} \sum_{j \in \hat{\mathcal{V}}_l(k)} P_j. \quad (5.14)$$

From (5.10), (5.14) can be recast as

$$\hat{\omega}_l = \begin{cases} \frac{1}{|\mathcal{V}_l(k)|-1} (\bar{P}_l(k) - P_i), & \text{if } i \in \mathcal{V}_l(k) \\ \frac{1}{|\mathcal{V}_l(k)|+1} (\bar{P}_l(k) + P_i), & \text{if } i \notin \mathcal{V}_l(k) \end{cases}. \quad (5.15)$$

Then (5.13) and (5.15) can be solved for the unknowns $\bar{P}_l(k)$ and $|\mathcal{V}_l(k)|$ obtaining

$$\bar{P}_l(k) = a_l \omega_l \frac{P_i - \hat{\omega}_l}{\hat{\omega}_l - \omega_i}, \quad (5.16a)$$

$$|\mathcal{V}_l(k)| = a_l \frac{P_i - \hat{\omega}_l}{\hat{\omega}_l - \omega_i}, \quad (5.16b)$$

with

$$a_l = \begin{cases} -1, & \text{if } i \in \mathcal{V}_l(k) \\ 1 & \text{if } i \notin \mathcal{V}_l(k) \end{cases}, \quad (5.17)$$

From (5.16a), to estimate $\bar{P}_l(k)$, node i needs to compute ω_l and $\hat{\omega}_l$. To do so in a distributed fashion, node i starts the distributed computation of the consensus dynamics (5.11a) and (5.11b) by broadcasting its virtual states x_i and \hat{x}_i^i to the nodes in $\mathcal{N}_i \cap \mathcal{V}_l(k)$. In turn, each node $j \in \mathcal{N}_i \subseteq \mathcal{V}_l(k)$ starts sharing its virtual states x_j and \hat{x}_j^i with a subset of its neighbors, that is $\mathcal{N}_j \cap \mathcal{V}_l(k)$. This is repeated until all nodes in $\mathcal{V}_l(k)$ join the distributed simulation. Note that the aforementioned procedure can be conducted through one-hop communication if each network node h has knowledge of the island index $l \in \{1, \dots, n_\mu\}$ to which it belongs and of its consumed or generated power p_h . If so, $\bar{P}_l(k)$ can be computed locally and thus the proposed power imbalance estimator is distributed.¹ In what follows, we will show how the network nodes can exploit this estimation process to self-organize into a partition of the power network whose power imbalance approximates the minimum of (5.8).

¹Note that in a practical implementation the grid nodes should be equipped with sufficient computational and communication power to run the virtual consensus dynamics on a timescale that is compatible with the grid requirements.

Remark 5.3. Note that our estimation strategy can reveal if the migration of a node out of an island would make it disconnected. Indeed, if there is a node $i \in \mathcal{V}_l(k)$ such that $\mathcal{M}_l(k) \setminus i$ is not connected, the virtual state derivatives \hat{x}_h of its neighbors in $\widehat{\mathcal{M}}_l$ will in general converge to different values \hat{x}_h^* .

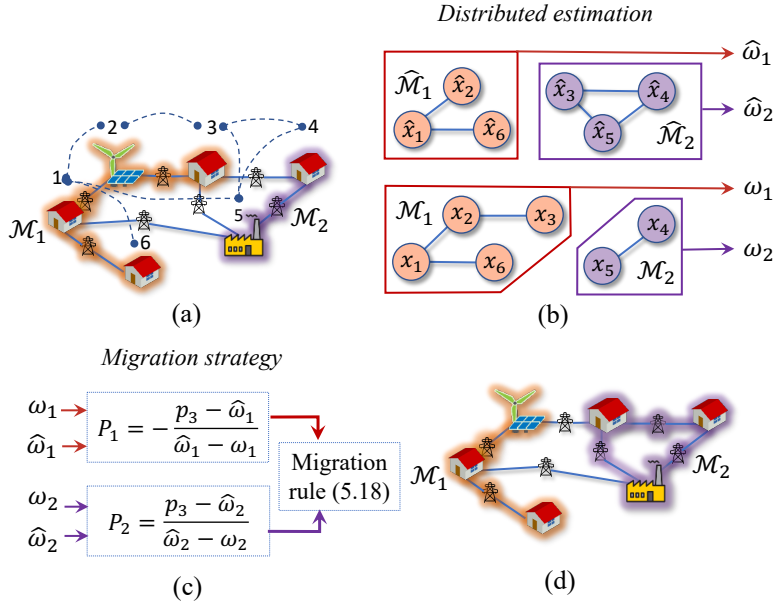


Figure 5.1: (a) Initial partition of the power network, with dashed lines representing the communication links among nodes, whose topology is equal to that of the power network itself (b) The boundary node 3 triggers the distributed simulation of the virtual consensus dynamics in (5.11) for both islands \mathcal{M}_1 and \mathcal{M}_2 and computes the steady state values $\omega_1, \omega_2, \widehat{\omega}_1, \widehat{\omega}_2$. Given these values, (c) the boundary node 3 computes an estimate of the power imbalances \bar{P}_1 of \mathcal{M}_1 and \bar{P}_2 of \mathcal{M}_2 using (5.16a) and determines the possibility of migration from island \mathcal{M}_1 to \mathcal{M}_2 by using (5.18). (d) Power network partition after the migration step

In the following, we introduce an algorithm based on node migration, that allow us to accomplish this.

5.7 A distributed migration strategy

Exploiting our consensus based estimation strategy, a boundary node in island $\mathcal{M}_m(k)$, say i , can decide whether to migrate to a neighboring island $\mathcal{M}_l(k)$ (see Figure 5.1) by computing the power imbalances $\bar{P}_l(k)$ and $\bar{P}_m(k)$. Specifically, node i will migrate from $\mathcal{M}_m(k)$ to $\mathcal{M}_l(k)$ if and only if both the conditions hold that

$$\min(\bar{P}_l(k), \bar{P}_m(k)) < \min(\bar{P}_l(k+1), \bar{P}_m(k+1)), \quad (5.18a)$$

$$\mathcal{M}_m(k+1) \text{ is connected.} \quad (5.18b)$$

where

$$\bar{P}_l(k+1) = \bar{P}_l(k) + P_i, \quad (5.19a)$$

$$\bar{P}_m(k+1) = \bar{P}_m(k) - P_i, \quad (5.19b)$$

$$\mathcal{V}_l(k+1) = \mathcal{V}_l(k) \cup i, \quad (5.19c)$$

$$\mathcal{V}_m(k+1) = \mathcal{V}_m(k) \setminus i. \quad (5.19d)$$

Here, we assume that only one boundary node can migrate at a time and that we consider each migration step by the index $k \in 1, \dots, K$, with K being the last migration step. With this, we can define power imbalances $\bar{P}_l(k)$ and $\bar{P}_m(k)$, and islands $\mathcal{M}_m(k)$ to $\mathcal{M}_l(k)$ for each k .

5.8 Proof of Convergence

In the following, we will show that, under some assumption on the network structure, the migration process governed by rule (5.18) generates a finite sequence of $K \in \mathbb{N}$ partitions $\Pi(k)$ such that $\mathcal{J}(K)$ remains within a certain bound from \mathcal{J}^* computed in (5.8). To this aim, let us define the stack vector of the power imbalances of the n_μ islands, i.e., $\bar{\mathbf{P}}(k) := [\bar{P}_1(k), \dots, \bar{P}_{n_\mu}(k)]^\top$ and the vector $\bar{\mathbf{P}}^* := p^* \mathbf{1}^\top$, with $p^* := P_{\text{tot}}/n_\mu$ and give the following Lemma.

Lemma 5.4. *Under the migration rule (5.18), if*

$$|\bar{P}_l(k) - \bar{P}_m(k)| \leq p^{\max} \quad \forall l, m : \mathcal{N}(\mathcal{V}_m(k)) \cap \mathcal{V}_l(k) \neq \emptyset, \quad (5.20)$$

where $p^{\max} := \max_{i \in \mathcal{V}} |P_i|$, then

$$\mathcal{J}(k) - \mathcal{J}^* \leq \frac{2}{n_\mu} \left(\sum_{l=l^*+1}^{n_\mu} p^* + p^{\max} \left(l - \frac{n_\mu + 1}{2} \right) \right) - (p^* + |p^*|). \quad (5.21)$$

with

$$l^* = \left\lceil -\frac{p^*}{\bar{p}} + \frac{n_\mu + 1}{2} \right\rceil. \quad (5.22)$$

Proof. Note that, from (5.8), we have that

$$\mathcal{J}(k) = \frac{1}{n_\mu} \left(\sum_{l: \bar{P}_l(k) > 0} \bar{P}_l(k) - \sum_{l: \bar{P}_l(k) \leq 0} \bar{P}_l(k) \right). \quad (5.23)$$

Moreover, as

$$\sum_{l: \bar{P}_l(k) > 0} \bar{P}_l(k) + \sum_{l: \bar{P}_l(k) \leq 0} \bar{P}_l(k) = P_{\text{tot}} = n_\mu p^*,$$

we can recast (5.23) as

$$\mathcal{J}(k) = \frac{1}{n_\mu} \left(2 \sum_{l: \bar{P}_l(k) > 0} \bar{P}_l(k) - n_\mu p^* \right). \quad (5.24)$$

Hence, as $\mathcal{J}^* = |p^*|$ we obtain

$$\mathcal{J}(k) - \mathcal{J}^* = \frac{2}{n_\mu} \sum_{l: \bar{P}_l(k) > 0} \bar{P}_l(k) - (p^* + |p^*|). \quad (5.25)$$

Without loss of generality, let us relabel the islands so that $\bar{P}_1(k) \leq \bar{P}_2(k) \leq \dots \leq \bar{P}_{n_\mu}(k)$. Then, as the graph \mathcal{G} is connected and so are all the islands for all k , then also the graph $\mathcal{G}^{\text{II}(k)}$ will be connected and thus (5.20) implies that

$$\bar{P}_{l+1}(k) \leq \bar{P}_l(k) + p^{\max}, \quad \forall l \in \{1, \dots, n_\mu - 1\}. \quad (5.26)$$

Recalling (5.2), we have $\sum_{l=1}^{n_\mu} \bar{P}_l(k) = P_{\text{tot}} = n_\mu p^*$, which leads us to write (5.26) as

$$\bar{P}_l(k) \leq p^* + p^{\max} \left(l - \frac{n_\mu + 1}{2} \right), \quad \forall l \in \{1, \dots, n_\mu\}, \quad (5.27)$$

Note that, from (5.25), $\mathcal{J}(k) - \mathcal{J}^*$ is maximized when (5.27) is an equality. In such case, to compute $\mathcal{J}(k) - \mathcal{J}^*$ by leveraging (5.25), we must first find

$$l^* : \bar{P}_l(k) \geq 0, \quad \forall l \in \{l^*, \dots, n_\mu\} \quad (5.28)$$

Hence, to find l^* we must find the smallest integer l such that

$$p^* + p^{\max} \left(l - \frac{n_\mu + 1}{2} \right) \geq 0. \quad (5.29)$$

yielding (5.22). Then, from (5.28), (5.27), and (5.25), we obtain (5.21). \square

Now, let us show that the migration rule (5.18) triggers a finite sequence of K migrations such that (5.20)—and thus (5.21)—holds for $k = K$.

Theorem 5.5. Assume that at each step k - there exist a node i and islands $\mathcal{M}_l(k)$ and $\mathcal{M}_m(k)$ (that is a triplet (l, m, i)) such that

$$\begin{cases} i \in \{\mathcal{V}_m(k) \cap \mathcal{N}(\mathcal{V}_l(k))\} \\ \wedge \\ \mathcal{M}_m(k) \setminus i \text{ is connected} \end{cases} \quad (5.30a)$$

and

$$\begin{cases} \bar{P}_l(k) > \bar{P}_m(k) \wedge P_i < 0 \\ \vee \\ \bar{P}_l(k) < \bar{P}_m(k) \wedge P_i > 0. \end{cases} \quad (5.30b)$$

Then, the sequence $\Pi(k)$ obtained under the migration rule (5.18) is finite and converges to a partition $\Pi(K)$ such that $\mathcal{J}(K)$ fulfills (5.21).

Proof. Let us start by showing that, given a triplet (l, m, i) fulfilling (5.30), a migration will occur, i.e., that (5.18) holds if and only if (l, m, i) also fulfills

$$|\bar{P}_m(k) - \bar{P}_l(k)| > |P_i|. \quad (5.31)$$

To prove sufficiency, note that when (5.18) holds and $\bar{P}_l(k) > \bar{P}_m(k)$, we have

$$\begin{cases} \bar{P}_m(k) < \bar{P}_l(k+1) = \bar{P}_l(k) + P_i \\ \wedge \\ \bar{P}_m(k) < \bar{P}_m(k+1) = \bar{P}_m(k) - P_i \end{cases} \quad (5.32)$$

with $P_i < 0$. If instead $\bar{P}_m(k) > \bar{P}_l(k)$, we have

$$\begin{cases} \bar{P}_l(k) < \bar{P}_l(k+1) = \bar{P}_l(k) + P_i \\ \wedge \\ \bar{P}_l(k) < \bar{P}_m(k+1) = \bar{P}_m(k) - P_i \end{cases} \quad (5.33)$$

with $P_i > 0$. From (5.32) and (5.33) we can say that if (5.18) and (5.30a) hold

$$\begin{cases} \bar{P}_m(k) - \bar{P}_l(k) < P_i < 0 \\ \vee \\ \bar{P}_m(k) - \bar{P}_l(k) > P_i > 0. \end{cases} \quad (5.34)$$

Note that both cases in (5.34) satisfy (5.31) and thus we have proved that (5.18) implies (5.31)

Now, let us prove that (5.31) and (5.30) imply (5.18). To do so, note that (5.31) is satisfied if there exists (l, m, i) such that

$$\begin{cases} \bar{P}_l(k) > \bar{P}_m(k) + |P_i| \\ \vee \\ \bar{P}_m(k) > \bar{P}_l(k) + |P_i|. \end{cases} \quad (5.35)$$

Moreover, from (5.30), (5.35) can be recast as

$$\begin{cases} \bar{P}_l(k) > \bar{P}_m(k) - P_i = \bar{P}_m(k+1) \\ \vee \\ \bar{P}_m(k) > \bar{P}_l(k) + P_i = \bar{P}_l(k+1). \end{cases} \quad (5.36)$$

As both cases in (5.36) satisfy the migration rule we have proved that (5.31) and (5.30) imply (5.18).

As (5.18) is equivalent to (5.31) and (5.30), then if at some step, say K , no triplet (l, m, i) existed fulfilling (5.31), the migration process would stop and as the network \mathcal{G} is connected and so is the graph $\mathcal{G}^{\Pi(K)}$ at that step we would have

$$|\bar{P}_l(K) - \bar{P}_m(K)| \leq \max_{i \in \mathcal{V}} |P_i| \quad \forall l, m : \mathcal{V}_m(K) \cap \mathcal{N}(\mathcal{V}_l(K)) \neq \emptyset. \quad (5.37)$$

As from Lemma 5.4, (5.37) implies that the bound (5.21) holds, to prove our thesis we are left with showing that K exists. Firstly, note that such a step K exists if (5.18) fulfills

$$\|\bar{\mathbf{P}}(k+1) - \bar{\mathbf{P}}^*\|_2 \leq \alpha \|\bar{\mathbf{P}}(k) - \bar{\mathbf{P}}^*\|_2 \quad k \in \{0, \dots, K-1\} \quad (5.38)$$

for some positive scalar $\alpha < 1$ as if (5.38) were satisfied, then our migration rule would be a contraction mapping. In such case, from the Banach-Caccioppoli theorem [94], there would be no limit cycles in the sequence $\{\bar{\mathbf{P}}(k)\}$ and thus also in $\{\Pi(k)\}$. Hence, as the number of possible partitions is finite, so would be the sequence $\{\bar{\mathbf{P}}(k)\}$ and thus, to complete our proof, we need to show that (5.18) implies (5.38). As we have enforced that only one migration occurs at each step k , then $\bar{\mathbf{P}}(k+1)$ only differs from $\bar{\mathbf{P}}(k)$ for the l -th and m -th entries. Hence, proving (5.38), only requires showing that

$$\begin{aligned} (\bar{P}_l(k+1) - p^*)^2 + (\bar{P}_m(k+1) - p^*)^2 \\ < (\bar{P}_l(k) - p^*)^2 + (\bar{P}_m(k) - p^*)^2 \end{aligned} \quad (5.39)$$

for $\forall k \in \{0, \dots, K-1\}$. From (5.18) and (5.19), condition (5.39) reduces to

$$P_i(\bar{P}_l(k) - \bar{P}_m(k) + P_i) < 0 \quad k \in \{0, \dots, K-1\}, \quad (5.40)$$

which is trivially fulfilled by any triplet (l, m, i) fulfilling (5.30) and (5.31), yielding that (5.30) and (5.31) imply (5.38). In turn, as (5.30) and (5.31) implies (5.18), the existence of K and thus our thesis remain proved. \square

5.9 Migration Algorithm

Having introduced the distributed power imbalance estimator and the migration rule, we can now illustrate how the nodes can combine these tools and exploit one-hop communication with their neighbors so to reduce the overall grid's power imbalance defined in (5.2) in a distributed fashion. We will do so by taking the perspective of the generic node

$h \in \mathcal{V}_m(k)$. For simplicity of notation, we will assume that all boundary nodes can be neighbors to only one island, i.e., for all islands \mathcal{M}_m , for all nodes $h \in \mathcal{M}_m$, there exist at most one other island \mathcal{M}_l such that $\mathcal{N}_h \cap \mathcal{V}_l \neq \emptyset$.

Note that as all boundary nodes trigger a different distributed simulation of virtual consensus dynamics such as that in (5.11b), then each node can be part of a number of these distributed simulations and in general be endowed of several virtual states. We will denote by \mathcal{X}_h the set encompassing all the virtual states of node h (each one relating to a different distributed simulation), by \mathcal{A}_h the set of states that node h is asked to add to \mathcal{X}_h , and by \mathcal{R}_h the set of states that node h is asked to remove from \mathcal{X}_h .

As our strategy starts from an initial partition $\Pi(0)$ of the grid, our Migration Algorithm is initialized based on this initial partition. Then, to allow all boundary nodes of its island to estimate $\bar{P}_m(0)$ node h must participate to the distributed simulation of (5.11a). To do so, it must create the virtual state variable x_h . Note that as all boundary nodes of $\mathcal{M}_m(0)$ can exploit the same distributed simulation of (5.11a) there will be only one virtual dynamics (5.11a) for each island. Moreover, if h were a boundary node (i.e., if there exists l such that $\mathcal{N}_h \cap \mathcal{V}_l(0) \neq \emptyset$), then node h must trigger two distributed simulations of (5.11b), so as to estimate $P_m(0)$ and $P_l(0)$. As $h \notin \widehat{\mathcal{V}}_m(0)$ while $h \in \widehat{\mathcal{V}}_l(0)$, this implies that node h must (i) create \widehat{x}_h^h and (ii) ask each of its neighbors to create the virtual state variable \widehat{x}_j^h . Our initialization procedure is outlined in Algorithm 1.

After this initialization, node h will continuously update the sets \mathcal{A}_h and \mathcal{R}_h so to fulfill the requests it receives from its neighbors of adding or removing virtual states from \mathcal{X}_h . Then, it will update the set \mathcal{X}_h consistently with the current sets \mathcal{A}_h and \mathcal{R}_h and it will compute the current value of its virtual states sharing them with its neighbors. If node h is a boundary node of island $\mathcal{M}_m(k)$, whenever a steady state in the simulations of (5.11) is achieved it will update its estimates of $\bar{P}_l(k)$ and $\bar{P}_m(k)$ and, if necessary, it will migrate to a neighboring island $\mathcal{M}_l(k+1)$. Whenever this is the case, any neighbor $j \in \mathcal{V}_l(k+1)$ of node h that ceases being a boundary node because of the migration will add \widehat{x}_j^j to the set of states \mathcal{R}_j it must remove. The pseudocode for our strategy is given in Algorithm 2 in which, for notation purposes, we have omitted the dependence of the quantities from the migration step k whenever the context allowed us to do so.

Algorithm 1: Initialization Algorithm

- 1 $\mathcal{X}_h = \{x_h\}$;
 - 2 $\mathcal{X}_{hj} = x_h, \forall j \in (\mathcal{N}_h \cap \mathcal{V}_m(0))$;
 - 3 $\mathcal{A}_h = \emptyset$;
 - 4 $\mathcal{R}_h = \emptyset$;
 - 5 **if** $\mathcal{N}_h \setminus \mathcal{V}_m(0) \neq \emptyset$ **then**
 - 6 $\mathcal{X}_h \leftarrow \mathcal{X}_h \cup \widehat{x}_h^h$;
 - 7 $\mathcal{A}_j = \widehat{x}_j^h, \forall j \in \mathcal{N}_h$;
-

Algorithm 2: Migration Algorithm

```

1 for  $j \in \mathcal{N}_h \cap \mathcal{V}_m$  do
2    $\mathcal{A}_h \leftarrow \mathcal{A}_h \cup \{\hat{x}_h^i \forall i, j : j \in \mathcal{N}_h \cap \mathcal{V}_m, \hat{x}_j^i \in \mathcal{A}_j\};$ 
3    $\mathcal{R}_h \leftarrow \mathcal{R}_h \cup \{\hat{x}_h^i \forall i, j : j \in \mathcal{N}_h \cap \mathcal{V}_m, \hat{x}_j^i \in \mathcal{R}_j\};$ 
4  $\mathcal{A}_h \leftarrow \mathcal{A}_h \setminus \mathcal{X}_h;$ 
5  $\mathcal{R}_h \leftarrow \mathcal{R}_h \cap \mathcal{X}_h;$ 
6  $\mathcal{X}_h \leftarrow \mathcal{X}_h \cup \mathcal{A}_h;$ 
7  $\mathcal{X}_h \leftarrow \mathcal{X}_h \setminus \mathcal{R}_h;$ 
8 solve
9    $\hat{x}_h = p_h + \sum_{j \in \mathcal{N}_h \cap \mathcal{V}_m} (x_j - x_h)$ 
10   $\hat{x}_h^i = p_h + \sum_{j \in \mathcal{N}_h \cap \mathcal{V}_m} (\hat{x}_j^i - \hat{x}_h^i), \forall i \neq h \mid \hat{x}_h^i \in \widehat{\mathcal{X}}_h;$ 
11 if  $\exists l \neq m : \mathcal{N}_h \cap \mathcal{V}_l(k) \neq \emptyset$  then
12   solve  $\hat{x}_h^l = p_h + \sum_{j \in \mathcal{N}_h \setminus \mathcal{V}_m} (\hat{x}_j^l - \hat{x}_h^l), \forall i \neq h \mid \hat{x}_h^l \in \mathcal{X}_h;$ 
13   if possible, update the estimates  $P_l^h$  and  $P_m^h$  of  $P_l$  and  $P_m$ 
14   if  $(\exists l : \mathcal{N}_h \cap \mathcal{V}_l \neq \emptyset) \wedge \{p_h, P_l^h, P_m^h, \mathcal{M}_m, \mathcal{M}_l\}$  fulfill (5.18) then
15      $\mathcal{V}_m(k+1) \leftarrow \mathcal{V}_m(k) \setminus h;$ 
16      $\mathcal{V}_l(k+1) \leftarrow \mathcal{V}_l(k) \cup h;$ 
17     for  $j \in \mathcal{V}_l \cap \mathcal{N}_h : (\hat{x}_j^j \in \mathcal{X}_j) \wedge (\mathcal{N}_j \cap \mathcal{V}_m) = \emptyset$  do
18        $\mathcal{R}_j = \hat{x}_j^j$ 

```

5.10 Numerical Validation

To demonstrate the effectiveness of our algorithm, we apply it to the IEEE 118 and 300 test cases [126] for which we compute the nodal power values p_i by solving an Optimal Power Flow (OPF) problem leveraging MATPOWER 6.0 [184].

As the test cases include nodes with null nodal power $P_i = 0$, we allow for these nodes to migrate from their island, say $\mathcal{M}_m(k)$, to a neighboring island, say $\mathcal{M}_l(k)$, as long as (i) their migration does not disconnect $\mathcal{M}_m(k)$ and (ii) $\bar{P}_l(k) \neq \bar{P}_l(h), \forall h < k : i \in \mathcal{V}_l(h)$. Note that condition (ii) allows also null nodal power nodes to migrate without generating limit cycles in the sequence $\Pi(k)$.

We applied algorithm 1-2 to different initial partitions. First, we obtained an initial partition for both the IEEE 118 and 300 test cases by using the Search Space Reduction Procedure described in [100] which generates a spanning tree connecting groups of coherent generators. Then the remaining nodes of the network are aggregated to the tree using the Breadth-First Search algorithm [46]. We call this approach for generating $\Pi(0)$ as SSRP+BFS. For both test cases, we consider the coherent generators reported in [100]. We also considered selected partitions from [24, 69, 100] as initial conditions for our algorithm. Our algorithm was also able to reduce the difference among the power

imbalances of the islands for all initial conditions and in all cases. (See Table 5.1)

Remark 5.6. *Throughout our numerical analyses, whenever a node, say i , can choose to migrate to more than one island, it will select the one maximizing the difference*

$$\Delta \bar{P}_l = \min(\bar{P}_l(k) + P_i, \bar{P}_m(k) - P_i) - \min(\bar{P}_l(k), \bar{P}_m(k)).$$

This choice ensures that the average absolute power imbalance is improved the most after the migration.

5.10.1 IEEE 118 test system

We consider the problem of partitioning the IEEE 118 test system in $n_\mu = 2$ and $n_\mu = 3$ islands. We consider only a set of $n_g = 19$ generators, namely, we do not consider the reactive compensators.

Moreover, we assume that the migration process is triggered by a three phase solid ground fault at bus 15 forcing line 14-15 to disconnect. We start the proposed algorithm 1-2 from two different initial partitions generated by the SSRP+BFS approach for the $n_\mu = 2$ and $n_\mu = 3$ cases and we also consider as initial partition the final partitions reported in [69] for $n_\mu = 2$ and in [100] for $n_\mu = 3$. The initial power imbalances $\bar{P}_l(0)$, the initial value of the cost function $\mathcal{J}(0)$ and the cut-set representing $\Pi(0)$ are reported in Table 5.1 for all cases.

Next, we run algorithm 1-2. The cut-set representing the resultant partition $\Pi(K)$, its final power imbalances $\bar{P}_l(K)$ and the final value of the cost function $\mathcal{J}(K)$ are reported also in Table 5.1. The proposed algorithm is able to find partitions that minimize \mathcal{J} in a small number of migration steps.

We depict in Figure 5.2 the scenario in which the IEEE 118 test system is partitioned in $n_\mu = 2$ islands and the initial partition is generated with the SSRP+BFS approach. After running Algorithms 1-2, we obtained a sequence of $K = 10$ migrations yielding an average absolute power imbalance $\mathcal{J}(10) = 58.25$ MW with $\bar{P}_1(10) = 53.74$ MW and $\bar{P}_2(10) = 62.75$ MW. The islands defining $\Pi(10)$ are depicted in Figure 5.2b and the power imbalances of both islands at each migration step k is depicted in 5.2a. As from the OPF results we have that $\max_i |P_i| = 542.78$ MW and $\mathcal{J}^* = 58.25$ MW which implies that the bound (5.21) is satisfied as $|\mathcal{J}(10) - \mathcal{J}^*| = 0$ (See Table 5.1).

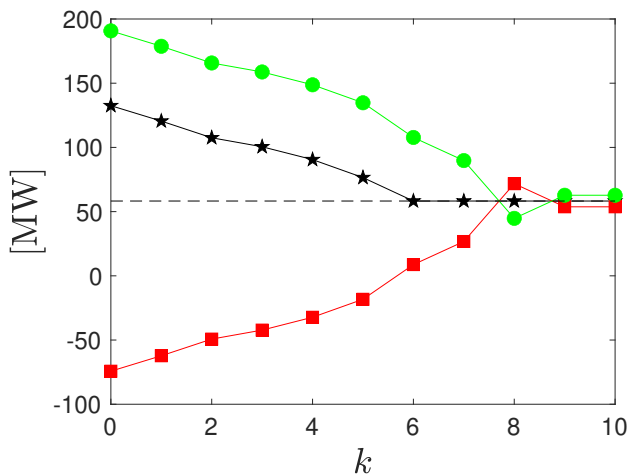
5.10.2 IEEE 300 test system

Next, we use algorithms 1-2 to partition the IEEE 300 test system in $n_\mu = 3$ and $n_\mu = 4$ islands assuming a failure affects line 194-195. Again, we use different initial partitions $\Pi(0)$ obtained by using the SSRP+BFS approach. We also consider the reported partition in [100] for $n_\mu = 4$ and an arbitrary partition whose cut-set is reported in Table 5.1. Note that the IEEE 300 test system is already defined as the interconnection of three independent subsystems, each of them representing an island itself. The coherent generators in [100] are grouped accordingly.

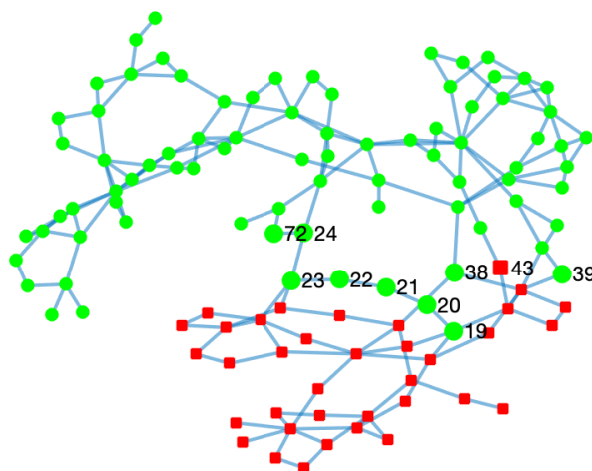
The initial partitions computed with the SSRP+BFS approach and the partition in [100] are already optimal but our algorithm is able to further decrease the power imbalances differences between islands (See Table 5.1).

We depict in Figure 5.3 the scenario in which the IEEE 300 test case is partitioned in $n_\mu = 3$ islands defined by an arbitrary initial partition $\Pi(0)$ whose cut-set is given in the 6th row of Table 5.1. As shown in Figure 5.3a, the initial average absolute power imbalance is $\mathcal{J}(0) = 529.49$ MW (black stars) and our migration algorithm allows $\mathcal{J}(k)$ to converge to its optimal value $\mathcal{J}^* = 102.92$ MW in $K = 12$ steps. The sequence of the power imbalances $\mathcal{J}(k)$ is depicted in Figure 5.3a while the final partition $\Pi(12)$ is depicted in Figure 5.3b. Interestingly, across all our numerical experiments, not only does our algorithm ensure fulfillment of the bound in (5.21), but it also always ensures $\mathcal{J}(K) = \mathcal{J}^*$.

Note that, As shown in Table 5.1, there are multiple optimal solutions that have the same minimum value of the average absolute power imbalance, for a given test case and a desired number of islands n_μ . This opens the possibility of developing a multi-objective partitioning strategy.



(a)



(b)

Figure 5.2: The algorithms 1-2 are applied to the IEEE 118 test system to partition it into $n_\mu = 2$ islands. (a) Sequence of the island power imbalances (red squares for $\bar{P}_1(k)$ and green circles for $\bar{P}_2(k)$) and average absolute power imbalance (black star). The average absolute power imbalance reaches its optimal value $\mathcal{J}^* = 58.25$ MW (black segmented line). (b) Final network partition $\Pi(10)$. Red squares represent the nodes of \mathcal{M}_1 , green circles those of \mathcal{M}_2 . Nodes 72, 24, 23, 22, 21, 39, 20, 19, 38 migrated from \mathcal{M}_1 to \mathcal{M}_2 in the given order, while node 43 migrated from \mathcal{M}_2 to \mathcal{M}_1 at $k = 9$. Note that the last migration does not change the power imbalances as it involves node 38 with nodal power is zero.

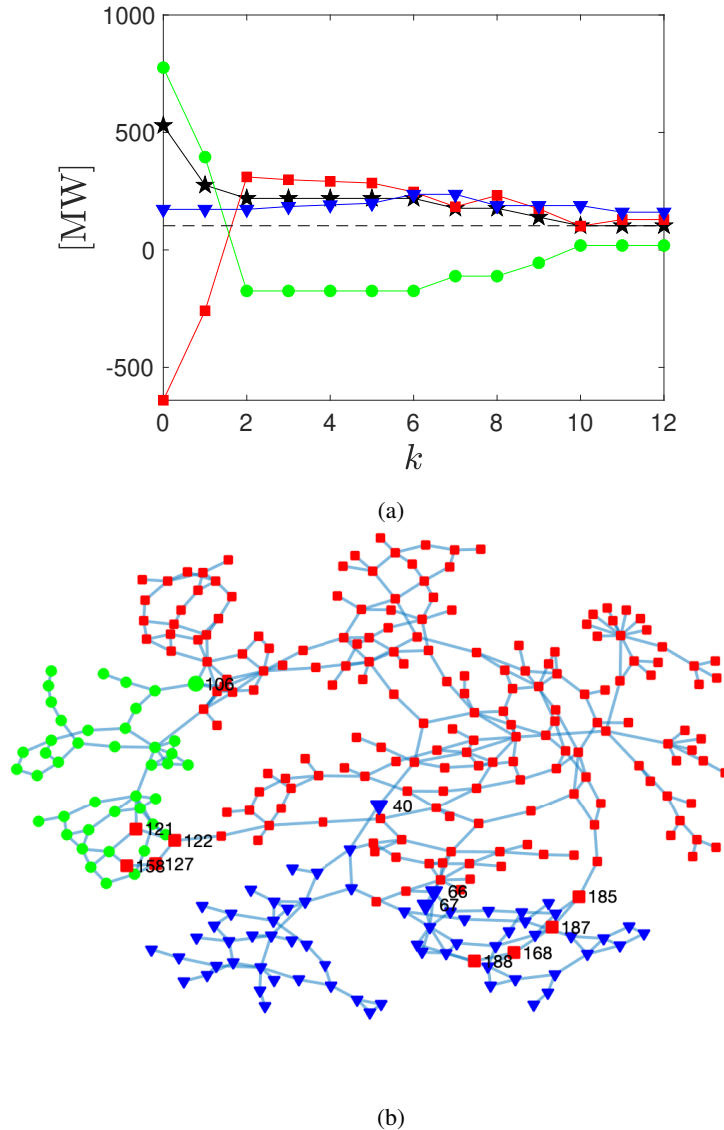


Figure 5.3: The algorithms 1-2 applied to the IEEE 300 test system to partition it into $N_\mu = 3$ islands. (a) Island power imbalances (red squares for $P_1(k)$ and green circles for $P_2(k)$ and blue triangles for $P_3(k)$) and average absolute power imbalance (black star) at each node migration. The average absolute power imbalance reaches its optimal value $\mathcal{J}^* = 102.92$ MW (black segmented line) in $K = 12$ iterations. (b) The Final network partition after $K = 12$ iterations with red squares representing nodes of \mathcal{M}_1 , green circles nodes of \mathcal{M}_2 and blue triangles nodes of \mathcal{M}_3 . The nodes' migration order is 106, 122, 185, 187, 168, 188, 127, 66, 121, 158, 67 and 40.

Case	n_r, K	Cut-set at $\Pi(0)$	Source of $\Pi(0)$	Cut-set at $\Pi(K)$	$\mathcal{J}(0)$ [MW]	$\mathcal{J}(K)$ [MW]	\mathcal{J}^* [MW]	$P(0)$ [MW]	$P(K)$ [MW]	Bound (5.2) [MW]
IEEE 118	2 10	{24 - 70, 34 - 43, 37 - 40, 38 - 65, 39 - 40, 71 - 72}	SSRP + BFS	{15 - 19, 18 - 19, 19 - 34, 23 - 25, 23 - 32, 30 - 38, 37 - 38, 37 - 39, 37 - 40, 43 - 44}	120.5	58.25	58.25	{-74.26, 190.75}	{53.74, 62.75}	213.14
	118 2 9	{1 - 2, 3 - 12, 5 - 8, 6 - 7, 11 - 12, 15 - 17, 15 - 19, 24 - 70, 30 - 38, 34 - 36, 44 - 45, 70 - 71}	[69]	{4 - 5, 5 - 11, 11 - 12, 15 - 17, 15 - 19, 30 - 38, 34 - 37, 35 - 37, 43 - 44, 69 - 70, 70 - 75, 74 - 75}	205.5	58.25	58.25	{-258.25, 374.74}	{65.75, 50.74}	213.14
IEEE 118	3 7	{24 - 70, 34 - 43, 37 - 40, 38 - 65, 39 - 40, 68 - 81, 69 - 77, 71 - 72, 75 - 77, 76 - 118}	SSRP + BFS	{19 - 34, 21 - 22, 23 - 25, 23 - 32, 30 - 38, 34 - 36, 34 - 37, 37 - 38, 37 - 39, 37 - 40, 68 - 81, 69 - 77, 75 - 77, 76 - 118}	80.34	38.83	38.83	{-74.26, 188.77}	{53.74, 1.98, 60.77}	335.97
	118 3 8	{24 - 70, 24 - 72, 38 - 65, 40 - 42, 41 - 42, 44 - 45, 69 - 77, 75 - 77, 81 - 80, 118 - 76}	[100]	{24 - 70, 42 - 49, 44 - 45, 61 - 64, 63 - 64, 65 - 66, 65 - 68, 69 - 77, 71 - 72, 75 - 77, 76 - 118, 80 - 81}	147	38.83	38.83	{-199.26, 313.77, 1.98}	{83.66, 30.86, 1.98}	335.97
IEEE 300	3 3	{3 - 129, 7 - 110, 40 - 68, 54 - 123, 57 - 66, 64 - 67, 66 - 190, 67 - 190, 68 - 73, 185 - 186}	SSRP + BFS	{3 - 129, 40 - 68, 54 - 123, 57 - 66, 64 - 67, 66 - 190, 68 - 73, 109 - 110, 184 - 185, 185 - 187}	102.92	102.92	102.92	{6.11, 129.98, 172.65}	{6.11, 129.98, 145.98, 156.65}	1254.95
	300 3 12	{40 - 68, 57 - 66, 66 - 190, 67 - 190, 68 - 73, 106 - 113, 112 - 116, 122 - 123, 185 - 186}	Arbitrary	{36 - 40, 39 - 40, 61 - 66, 64 - 67, 65 - 66, 68 - 73, 105 - 106, 106 - 107, 106 - 147, 112 - 116, 119 - 121, 121 - 154, 122 - 124, 122 - 128, 127 - 157, 154 - 158, 157 - 158, 168 - 180, 172 - 187, 177 - 188, 184 - 185}	529.49	102.92	102.92	{-639.87, 775.96, 172.65}	{129.21, 18.89, 160.65}	1254.95
IEEE 300	4 5	{3 - 129, 7 - 110, 40 - 68, 54 - 123, 61 - 66, 64 - 67, 65 - 66, 68 - 73, 68 - 173, 174 - 198, 185 - 186}	SSRP + BFS	{3 - 129, 7 - 110, 40 - 68, 54 - 123, 57 - 180, 57 - 190, 66 - 190, 67 - 190, 68 - 73, 68 - 173, 174 - 198, 185 - 186}	77.187	77.187	77.187	{19.76, 6.11, 205.98, 76.9}	{114.76, 6.11, 110.98, 76.9}	1908.2
	300 4 3	{68 - 173, 109 - 110, 109 - 129, 122 - 123, 174 - 191, 174 - 198, 184 - 185, 185 - 187}	[100]	{7 - 110, 57 - 66, 66 - 190, 67 - 190, 68 - 173, 109 - 129, 122 - 123, 168 - 187, 172 - 187, 174 - 191, 174 - 198, 184 - 185}	77.187	77.187	77.187	{145.98, 79.76, 6.11, 76.9}	{110.98, 114.76, 6.11, 76.9}	1908.2

Table 5.1: Results after applying the algorithms 1-2 to the IEEE test cases 118 and 300, considering different initial partitions $\Pi(0)$

5.11 Summary

This Chapter discussed the power network islanding as an approach to operate the power network in case of emergency due to major failures. First, we introduced the power network islanding problem and provided the specifications that an ICI strategy must fulfill. As the islanding problem itself is difficult to solve, we provided simpler versions of the original islanding problem. We then gave a brief review of the current literature on ICI strategies. Afterwards, we explained the rationale behind the distributed solution of the islanding problem that we proposed and explain the distributed power balance estimator and the distributed migration strategy, which define the key elements of our approach. Our strategy allows the network nodes to self-organize so as to minimize the average absolute power imbalance among islands. We demonstrated analytically that our algorithm converges in finite time to a partition whose average absolute power imbalance is in a given neighborhood of the optimal one. We tested the strategy on two benchmark power networks, the IEEE 118 and 300 bus systems, after the disconnection of one of their transmission lines. We found that our migration algorithm always converges to optimal partitions.

6 Conclusions

The power network is a critical infrastructure of high relevance for our welfare and development. In this Thesis, the power network has been studied with a combination of different modelling and control tools.

Specifically, After introducing the Thesis motivation, the key research questions and challenges in Chapter 1, a literature review of the main models of the power network components was given in Chapter 2 explaining the physics behind each of them and deriving their models from first principles. Then, by analysing the energy flow inside of the generators models through proper Hamiltonian functions, we unveiled the underlying mechanism governing the power balance inside each of the devices and highlighted their similarities. We also provided an electrical network model of the power grid, highlighting the network characteristics of transmission lines through graph theoretical tools and providing the mechanisms for generators and loads to interact with this network. Based on this model, we introduced the main control specifications for each bus of the network and, based on the generators models, we mapped them into specific control specifications for each generator's type.

In Chapter 3. we focused on introducing the swing equation as a simpler model of the power network at a macro-scale and on the power flow equations as a steady state model of the power network. We then provided a framework that maps each element of the primary layer into a set of parameters for the swing equation itself. Given this mapping, we then explained in Chapter 4 the role of each of the control layers of the power network in the frequency control task and their respective time-scales. We found that the coupling between control layers is provided by the power and voltage set-points given to the primary layer, as they can be written as a function of the secondary and tertiary control signals. We also found that the main requirement for the secondary and tertiary layers to work properly is that the primary controllers are able to stabilize the power network after a disturbance, as these layers provide additional adjustment to correct any steady state error on the frequency and proper steady state power flow.

Based on the swing equation, we then gave the frequency control specifications of the secondary layer and stated the secondary frequency control problem as an optimization problem. We provided an overview of the different secondary control strategies classifying them depending on the number of integrator used and the type of communication network

among them. We also gave proper relevance to the AGC as the industry standard for secondary frequency control.

After this, the tertiary control specifications were shown and the set-point computation task of the tertiary layer was stated as an optimization problem. Finally, we provided an overview of the tertiary control problem literature and the strategies that have been proposed to solve it.

In Chapter 5 we analyzed the power network when the hierarchical control architecture shown in the previous chapters is not able to provide proper compensation after major disturbances. We showed that migrating nodes among the islands proposed by an initial partition computed offline can provide a distributed solution of the *Average absolute power-imbalance minimization problem* and, as a consequence, a distributed ICI strategy. The main ingredients of the proposed ICI strategy are a *Distributed power imbalance estimator* based on consensus dynamics and a *distributed migration strategy* that each boundary node of the network uses to determine if its migration can be beneficial, such that the power imbalance difference among the islands decreases. Given the main building blocks of our method, we proved analytically that our method finds, under some assumptions on the network structure and in a finite number of migration steps, a partition of the power network such that the average absolute power imbalance remains within a certain bound from the total power imbalance of the power network and we give an analytical expression for this bound. After this, we provided an algorithm for the distributed deployment of our ICI strategy, by classifying the different tasks that a node must compute when it is a boundary node or not such that the migration decision-making is self-organized and the minimization of the average absolute power-imbalance an emergent behavior of the migration algorithm. Finally, we validated the migration algorithm for the IEEE- 118 and 300 test cases after the disconnection of one of their transmission lines and for different initial partitions and showed that in all the cases we were able to find a partition on finite migration steps and that respected the given bound on the Average absolute power-imbalance.

Finally, in Appendix A we briefly describe the work done related with the modelling of the COVID-19 epidemic in Italy and the proposal of intermittent regional strategies to alleviate its spread.

A A network model of Italy shows that intermittent regional strategies can alleviate the COVID-19 epidemic

This chapter briefly describes the work done for a completely different topic, but one that is of great relevance in these present-day times. The COVID-19 pandemic has considerably changed our lifestyle and behavior since it began and has also posed a new challenge for humankind. Although this is not the first pandemic we have faced, it has indeed been the one that has generated one of the worst global crises of the modern era, forcing entire countries to impose nationwide lockdown measures in order to mitigate its expansion, resulting in worldwide economic and social decline. Understanding the underlying dynamics of the COVID-19 outbreak is crucial for adequate decision making in terms of when, where and for how long to impose lockdowns in the future, and can provide strategies for the management of similar crises we may have yet to face. For these reasons, I decided to participate in a joint modelling and control effort whose main product was the study in [52].

Among the countries that faced the first wave of COVID-19 cases right after China's first outbreak, Italy was hit particularly badly, and consequently suffered a saturated national health service and high death toll. This forced the authorities to impose strict national lockdown measures for mitigating the spread of the disease, despite the pseudo-federal nature of the Italian constitution that allows each administrative region to independently manage their own share of the national health service, so that they can decide to strengthen or even weaken any disease spread mitigation strategy at regional level.

By the time our study was published, the absence of regional heterogeneity was common in previous studies related with COVID-19 epidemic containment strategies in Italy, where a classical aggregated SIR modelling approach was used. However, this approach dismisses the spatial dynamics of the epidemic that we consider fundamental for the proper decision making. Another essential missing element was the effect of regional heterogeneity on the efficacy of the measures taken so far and the possibility of adopting

differentiated and localized intervention strategies.

To fill these gaps, we propose in [52] a network model of the COVID-19 dynamics, where each node represents the dynamics of the epidemic spread inside one of the 20 regions of Italy and the links represent fluxes of people among these regions, so that we were able to account for new infections in a region originating from the flux of infected commutes (See Figure A.1). The model was then parametrized based on real data provided by Italy’s national health service, publicly available mobility data and on an ad-hoc algorithm. All of this, with the purpose to (i) provide evidence of the effectiveness of the nationwide lockdown at regional level, (ii) show that controlling the inter-regional fluxes is key to avoid new epidemic waves and (iii) demonstrate that controlling social distancing and the inflow/outflow of people in each region depending on the saturation of the local hospital capacity, can be a more cost efficient solution for disease spread mitigation, compared to a nationwide lockdown.

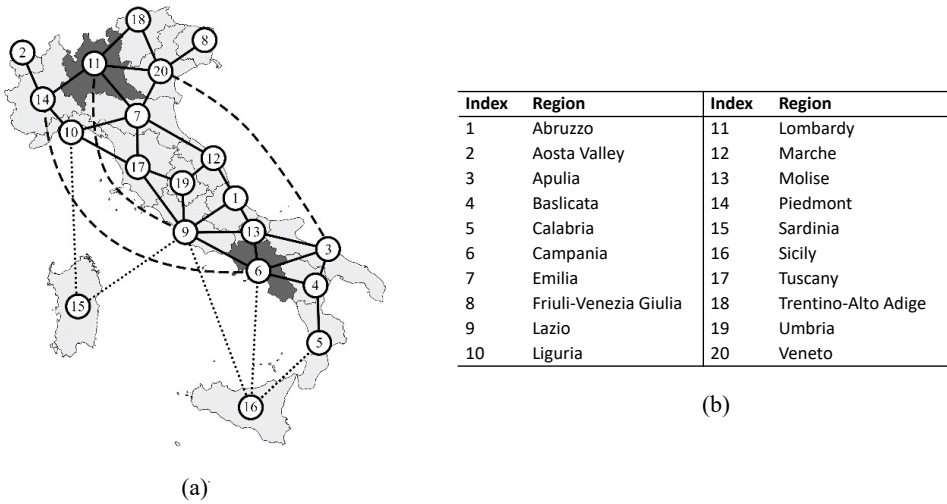


Figure A.1: (a) Schematic diagram of the network model structure proposed in [52]. Solid lines represent proximity links, dashed lines long distance transportation routes (air, train, road), dotted lines show major ferry routes between insular regions and the Italian mainland. (b) Table of the Italian region names and their positions in the graph.

Specifically, the COVID-19 epidemic spread dynamics was modelled, in each of the 20 regions, by a compartmental model describing the dynamics of the amount of susceptible, infected, quarantined, hospitalized, recovered and deceased people in an specific region. The structure of the links among the compartments was constructed by

testing how different configurations affected the model ability to capture the available data. Then, we extended the modelling approach in [150] in order to interconnect all the regional compartmental models using links modelling commuter flows and major transportation routes among regions. The parameters of this model were then identified with an ad-hoc algorithm designed to automatically detect the time instants where notable parameter changes occur, This was done with the purpose of accounting for the effects of changes to the national lockdown measures. (see the manuscript [52] and Supplementary Information for additional details).

Based on this model, we then formulated intermittent regional strategies to contain the impact of the COVID-19 epidemic in Italy, ranging from regional lockdown measures to inflow and outflow modulation, all of them as function of the ICU occupancy rate in each region.

The results confirm the efficacy of national containment measures at a regional level and our modelling approach unveils the regional effects of the national lockdown measures put in place by the Italian government during the time span of the data. They also suggest that intermittent regional strategies are as effective as a national lockdown in avoiding future waves of the epidemic, while guaranteeing that no region exceeds its own ICU occupancy rate, at substantially lower economic cost for the country. In fact, similar containment strategies have been adopted by the Italian government during the subsequent waves of COVID cases.

Bibliography

- [1] MM Adibi, RJ Kafka, Sandeep Maram, and Lamine M Mili. On power system controlled separation. *IEEE Transactions on Power Systems*, 21(4):1894–1902, 2006.
- [2] International Energy Agency. Electricity market report, january 2022. <https://www.iea.org/reports/electricity-market-report-january-2022>. Accessed: 2021-01-24.
- [3] International Energy Agency. Global electricity demand is growing faster than renewables, driving strong increase in generation from fossil fuels. <https://www.iea.org/news/global-electricity-demand-is-growing-faster-than-renewables-driving-strong-increase-in-generation-from-fossil-fuels>, 2021. Accessed: 2021-01-24.
- [4] TP Imthias Ahamed, PS Nagendra Rao, and PS Sastry. A reinforcement learning approach to automatic generation control. *Electric power systems research*, 63(1):9–26, 2002.
- [5] H Akagi and A Nabae. The p-q theory in three-phase systems under non-sinusoidal conditions. *European Transactions on Electrical Power*, 3(1):27–31, 1993.
- [6] Sultan Alghamdi, Johannes Schiffer, and Emilia Fridman. Distributed secondary frequency control design for microgrids: Trading off l 2-gain performance and communication efforts under time-varying delays. In *2018 European Control Conference (ECC)*, pages 758–763. IEEE, 2018.
- [7] O Alsac and Brian Stott. Optimal load flow with steady-state security. *IEEE transactions on power apparatus and systems*, PAS-93(3):745–751, 1974.
- [8] Martin Andreasson, Dimos V Dimarogonas, Karl H Johansson, and Henrik Sandberg. Distributed vs. centralized power systems frequency control. In *2013 European Control Conference (ECC)*, pages 3524–3529. IEEE, 2013.
- [9] Martin Andreasson, Dimos V Dimarogonas, Henrik Sandberg, and Karl H Johansson. Distributed pi-control with applications to power systems frequency control. In *2014 American Control Conference*, pages 3183–3188. IEEE, 2014.

-
- [10] Martin Andreasson, Dimos V Dimarogonas, Henrik Sandberg, and Karl Henrik Johansson. Distributed control of networked dynamical systems: Static feedback, integral action and consensus. *IEEE Transactions on Automatic Control*, 59(7):1750–1764, 2014.
- [11] Martin Andreasson, Emma Tegling, Henrik Sandberg, and Karl H Johansson. Coherence in synchronizing power networks with distributed integral control. In *2017 IEEE 56th Annual Conference on Decision and Control (CDC)*, pages 6327–6333. IEEE, 2017.
- [12] Dimitra Apostolopoulou, Peter W Sauer, and Alejandro D Domínguez-Garcia. Automatic generation control and its implementation in real time. In *2014 47th Hawaii International Conference on System Sciences*, pages 2444–2452. IEEE, 2014.
- [13] Seyed Ali Arefifar and Yasser Abdel-Rady I Mohamed. Dg mix, reactive sources and energy storage units for optimizing microgrid reliability and supply security. *IEEE Transactions on Smart Grid*, 5(4):1835–1844, 2014.
- [14] Seyed Ali Arefifar, A-RI Mohamed Yasser, and Tarek HM El-Fouly. Optimum microgrid design for enhancing reliability and supply-security. *IEEE Transactions on Smart Grid*, 4(3):1567–1575, 2013.
- [15] Catalin Arghir, Dominic Groß, and Florian Dörfler. On the steady-state behavior of a nonlinear power network model. *IFAC-PapersOnLine*, 49(22):61–66, 2016.
- [16] Catalin Arghir, Taouba Jouini, and Florian Dörfler. Grid-forming control for power converters based on matching of synchronous machines. *Automatica*, 95:273–282, 2018.
- [17] Anmar Arif, Zhaoyu Wang, Jianhui Wang, Barry Mather, Hugo Bashualdo, and Dongbo Zhao. Load modeling—a review. *IEEE Transactions on Smart Grid*, 9(6):5986–5999, 2017.
- [18] Pathom Attaviriyapap, Hiroyuki Kita, Eiichi Tanaka, and Jun Hasegawa. New bidding strategy formulation for day-ahead energy and reserve markets based on evolutionary programming. *International Journal of Electrical Power & Energy Systems*, 27(3):157–167, 2005.
- [19] Chiara Balestra, Franz Kaiser, Debsankha Manik, and Dirk Witthaut. Multistability in lossy power grids and oscillator networks. *Chaos: An Interdisciplinary Journal of Nonlinear Science*, 29(12):123119, 2019.
- [20] Yazdan Batmani and Hêmin Golpîra. Automatic voltage regulator design using a modified adaptive optimal approach. *International Journal of Electrical Power & Energy Systems*, 104:349–357, 2019.
-

- [21] Arthur R Bergen and David J Hill. A structure preserving model for power system stability analysis. *IEEE Transactions on Power Apparatus and Systems*, PAS-100(1):25–35, 1981.
- [22] Hassan Bevrani, Arindam Ghosh, and Gerard Ledwich. Renewable energy sources and frequency regulation: survey and new perspectives. *IET Renewable Power Generation*, 4(5):438–457, 2010.
- [23] Hassan Bevrani, Takashi Hiyama, and Yasunori Mitani. Power system dynamic stability and voltage regulation enhancement using an optimal gain vector. *Control Engineering Practice*, 16(9):1109–1119, 2008.
- [24] Janusz W Bialek and Vahid Vahidinasab. Tree-partitioning as an emergency measure to contain cascading line failures. *IEEE Transactions on Power Systems*, 37(1):467–475, 2021.
- [25] Ali Bidram and Ali Davoudi. Hierarchical structure of microgrids control system. *IEEE Transactions on Smart Grid*, 3(4):1963–1976, 2012.
- [26] Vladimir Blasko and Vikram Kaura. A new mathematical model and control of a three-phase ac-dc voltage source converter. *IEEE transactions on Power Electronics*, 12(1):116–123, 1997.
- [27] Maude-Josée Blondin, Javier Sanchis, Pierre Sicard, and JM Herrero. New optimal controller tuning method for an avr system using a simplified ant colony optimization with a new constrained nelder–mead algorithm. *Applied soft computing*, 62:216–229, 2018.
- [28] Hedi Bouattour, John W Simpson-Porco, Florian Dörfler, and Francesco Bullo. Further results on distributed secondary control in microgrids. In *52nd IEEE Conference on Decision and Control*, pages 1514–1519. IEEE, 2013.
- [29] Stephen Boyd, Neal Parikh, Eric Chu, Borja Peleato, and Jonathan Eckstein. Distributed optimization and statistical learning via the alternating direction method of multipliers. *Foundations and Trends® in Machine learning*, 3(1):1–122, 2011.
- [30] Sina Y Caliskan and Paulo Tabuada. Uses and abuses of the swing equation model. In *2015 54th IEEE Conference on Decision and Control (CDC)*, pages 6662–6667, Osaka, Japan, 2015. IEEE.
- [31] Sina Yamac Caliskan and Paulo Tabuada. Compositional transient stability analysis of multimachine power networks. *IEEE Transactions on Control of Network systems*, 1(1):4–14, 2014.
- [32] Florin Capitanescu and Louis Wehenkel. Sensitivity-based approaches for handling discrete variables in optimal power flow computations. *IEEE Transactions on Power Systems*, 25(4):1780–1789, 2010.

-
- [33] J Carpentier. Contribution a l'étude du dispatching économique. *Bulletin de la Société Française des Electriciens*, 3(1):431–447, 1962.
- [34] Sambuddha Chakrabarti, Matt Kraning, Eric Chu, Ross Baldick, and Stephen Boyd. Security constrained optimal power flow via proximal message passing. In *2014 Clemson University Power Systems Conference*, pages 1–8. IEEE, 2014.
- [35] Gan-Ping Chen, OP Malik, GS Hope, Yi-Hong Qin, and Guo-Yu Xu. An adaptive power system stabilizer based on the self-optimizing pole shifting control strategy. *IEEE transactions on Energy Conversion*, 8(4):639–645, 1993.
- [36] Lin Chen, Jin Zhong, and Deqiang Gan. Optimal automatic generation control (agc) dispatching and its control performance analysis for the distribution systems with dgs. In *2007 IEEE Power Engineering Society General Meeting*, pages 1–6. IEEE, 2007.
- [37] Hsiao-Dong Chiang. *Direct methods for stability analysis of electric power systems: theoretical foundation, BCU methodologies, and applications*. John Wiley & Sons, 2011.
- [38] Gianfranco Chicco and Pierluigi Mancarella. Distributed multi-generation: A comprehensive view. *Renewable and sustainable energy reviews*, 13(3):535–551, 2009.
- [39] JH Chow, JR Winkelman, MA Pai, and PW Sauer. Singular perturbation analysis of large-scale power systems. *International Journal of Electrical Power & Energy Systems*, 12(2):117–126, 1990.
- [40] Joe H. Chow. *Time-Scale Modeling of Dynamic Networks with Applications to Power Systems*. Springer-Verlag Berlin Heidelberg, 1982.
- [41] Se-Kyo Chung. A phase tracking system for three phase utility interface inverters. *IEEE Transactions on Power electronics*, 15(3):431–438, 2000.
- [42] TS Chung and YZ Li. A hybrid ga approach for opf with consideration of facts devices. *IEEE Power Engineering Review*, 20(8):54–57, 2000.
- [43] Guy Cohen. Auxiliary problem principle and decomposition of optimization problems. *Journal of optimization Theory and Applications*, 32(3):277–305, 1980.
- [44] Pascal Combes, François Malrait, Philippe Martin, Pierre Rouchon, et al. Energy-based modeling of electric motors. In *53rd IEEE Conference on Decision and Control*, pages 6009–6016, Los Angeles, CA, USA, 2014. IEEE.
- [45] Antonio J Conejo, Francisco J Nogales, and Francisco J Prieto. A decomposition procedure based on approximate newton directions. *Mathematical programming*, 93(3):495–515, 2002.
- [46] Thomas H. Cormen, editor. *Introduction to algorithms*. MIT Press, 3rd edition, 2009.
-

- [47] North American Electric Reliability Corporation. Reliability guideline: Power plant model verification and testing for synchronous machines. <https://www.nerc.com>, 2018.
- [48] North American Electric Reliability Corporation. Reliability guideline primary frequency control. <https://www.nerc.com>, 2019.
- [49] North American Electric Reliability Corporation. Reliability guideline bps-connected inverter-based resource performance. <https://www.nerc.com>, 2020.
- [50] Karel De Brabandere, Bruno Bolsens, Jeroen Van den Keybus, Achim Woyte, Johan Driesen, and Ronnie Belmans. A voltage and frequency droop control method for parallel inverters. *IEEE Transactions on power electronics*, 22(4):1107–1115, 2007.
- [51] Claudio De Persis, Nima Monshizadeh, JF Schiffer, and Florian Dörfler. A lyapunov approach to control of microgrids with a network-preserved differential-algebraic model. In *Proceedings of IEEE Conference on Decision and Control*. IEEE, 2016.
- [52] Fabio Della Rossa, Davide Salzano, Anna Di Meglio, Francesco De Lellis, Marco Coraggio, Carmela Calabrese, Agostino Guarino, Ricardo Cardona-Rivera, Pietro De Lellis, Davide Liuzza, Francesco Lo Iudice, Giovanni Russo, and Mario di Bernardo. A network model of Italy shows that intermittent regional strategies can alleviate the COVID-19 epidemic. *Nature Communications*, 11(1):5106, December 2020.
- [53] Eoin Devane, Andreas Kasis, Marina Antoniou, and Ioannis Lestas. Primary frequency regulation with load-side participation—part ii: Beyond passivity approaches. *IEEE Transactions on Power Systems*, 32(5):3519–3528, 2016.
- [54] Alexandros G Dimakis, Soumya Kar, José MF Moura, Michael G Rabbat, and Anna Scaglione. Gossip algorithms for distributed signal processing. *Proceedings of the IEEE*, 98(11):1847–1864, 2010.
- [55] Hermann W Dommel and William F Tinney. Optimal power flow solutions. *IEEE Transactions on power apparatus and systems*, PAS-87(10):1866–1876, 1968.
- [56] Florian Dörfler, Saverio Bolognani, John W Simpson-Porco, and Sergio Grammatico. Distributed control and optimization for autonomous power grids. In *2019 18th European Control Conference (ECC)*, pages 2436–2453. IEEE, 2019.
- [57] Florian Dorfler and Francesco Bullo. Kron reduction of graphs with applications to electrical networks. *IEEE Transactions on Circuits and Systems I: Regular Papers*, 60(1):150–163, 2012.
- [58] Florian Dorfler and Francesco Bullo. Synchronization and transient stability in power networks and nonuniform kuramoto oscillators. *SIAM Journal on Control and Optimization*, 50(3):1616–1642, 2012.

-
- [59] Florian Dörfler and Francesco Bullo. Synchronization in complex networks of phase oscillators: A survey. *Automatica*, 50(6):1539–1564, 2014.
- [60] Florian Dörfler, Michael Chertkov, and Francesco Bullo. Synchronization in complex oscillator networks and smart grids. *Proceedings of the National Academy of Sciences*, 110(6):2005–2010, 2013.
- [61] Florian Dörfler and Sergio Grammatico. Gather-and-broadcast frequency control in power systems. *Automatica*, 79:296–305, 2017.
- [62] Florian Dörfler, John W Simpson-Porco, and Francesco Bullo. Breaking the hierarchy: Distributed control and economic optimality in microgrids. *IEEE Transactions on Control of Network Systems*, 3(3):241–253, 2015.
- [63] Florian Dörfler, John W Simpson-Porco, and Francesco Bullo. Electrical networks and algebraic graph theory: Models, properties, and applications. *Proceedings of the IEEE*, 106(5):977–1005, 2018.
- [64] WC Duesterhoeft, Max W Schulz, and Edith Clarke. Determination of instantaneous currents and voltages by means of alpha, beta, and zero components. *Transactions of the American Institute of Electrical Engineers*, 70(2):1248–1255, 1951.
- [65] Salvatore D’Arco, Jon Are Suul, and Olav B Fosso. A virtual synchronous machine implementation for distributed control of power converters in smartgrids. *Electric Power Systems Research*, 122:180–197, 2015.
- [66] Thomas W Eberly and Richard C Schaefer. Voltage versus var/power-factor regulation on synchronous generators. *IEEE transactions on industry applications*, 38(6):1682–1687, 2002.
- [67] Armin Eichmann, Alessandro Kohler, OP Malik, and Jose Taborda. A prototype self-tuning adaptive power system stabilizer for damping of active power swings. In *2000 Power Engineering Society Summer Meeting (Cat. No. 00CH37134)*, volume 1, pages 122–126. IEEE, 2000.
- [68] Tomaso Erseghe. Distributed optimal power flow using admm. *IEEE transactions on power systems*, 29(5):2370–2380, 2014.
- [69] Xinkai Fan, Emanuele Crisostomi, Dimitri Thomopoulos, Baohui Zhang, and Songhao Yang. Controlled islanding algorithm for ac/dc hybrid power systems utilising dc modulation. *IET Generation, Transmission & Distribution*, 14(26):6440–6449, 2020.
- [70] Pablo Fernández-Porras, Mathaios Panteli, and Jairo Quirós-Tortós. Intentional controlled islanding: when to island for power system blackout prevention. *IET Generation, Transmission & Distribution*, 12(14):3542–3549, 2018.
- [71] Arthur Eugene Fitzgerald, Charles Kingsley, Stephen D Umans, and B James. *Electric machinery*, volume 5. McGraw-Hill New York, 2003.
-

- [72] Hendrik Flamme, Emma Tegling, and Henrik Sandberg. Performance limitations of distributed integral control in power networks under noisy measurements. In *2018 Annual American Control Conference (ACC)*, pages 5380–5386. IEEE, 2018.
- [73] Roberto A. Flores-Mendez. Towards a standardization of multi-agent system framework. *XRDS: Crossroads, The ACM Magazine for Students*, 5(4):18–24, June 1999.
- [74] Stephen Frank, Ingrida Steponavice, and Steffen Rebennack. Optimal power flow: a bibliographic survey i. *Energy Systems*, 3(3):221–258, 2012.
- [75] Stephen Frank, Ingrida Steponavice, and Steffen Rebennack. Optimal power flow: a bibliographic survey ii. *Energy Systems*, 3(3):259–289, 2012.
- [76] Paolo Frasca, Hideaki Ishii, Chiara Ravazzi, and Roberto Tempo. Distributed randomized algorithms for opinion formation, centrality computation and power systems estimation: A tutorial overview. *European journal of control*, 24:2–13, 2015.
- [77] A Ghosh, G Ledwich, OP Malik, and GS Hope. Power system stabilizer based on adaptive control techniques. *IEEE transactions on power apparatus and systems*, PAS-103(8):1983–1989, 1984.
- [78] Mevludin Glavic. (deep) reinforcement learning for electric power system control and related problems: A short review and perspectives. *Annual Reviews in Control*, 48:22–35, 2019.
- [79] N Grudin. Reactive power optimization using successive quadratic programming method. *IEEE Transactions on Power Systems*, 13(4):1219–1225, 1998.
- [80] Hossein Haddadian and Reza Noroozian. Multi-microgrids approach for design and operation of future distribution networks based on novel technical indices. *Applied energy*, 185:650–663, 2017.
- [81] Saeed Hasanvand, Majid Nayeripour, Eberhard Waffenschmidt, and Hossein Fallahzadeh-Abarghouei. A new approach to transform an existing distribution network into a set of micro-grids for enhancing reliability and sustainability. *Applied Soft Computing*, 52:120–134, 2017.
- [82] Cody A Hill, Matthew Clayton Such, Dongmei Chen, Juan Gonzalez, and W Mack Grady. Battery energy storage for enabling integration of distributed solar power generation. *IEEE Transactions on smart grid*, 3(2):850–857, 2012.
- [83] David J Hill. Nonlinear dynamic load models with recovery for voltage stability studies. *IEEE transactions on power systems*, 8(1):166–176, 1993.
- [84] AS Ibrahim, BW Hogg, and MM Sharaf. Self-tuning automatic voltage regulators for a synchronous generator. In *IEE Proceedings D-Control Theory and Applications*, volume 136, pages 252–260. IET, 1989.

-
- [85] Ali Ipakchi and Farrokh Albuyeh. Grid of the future. *IEEE power and energy magazine*, 7(2):52–62, 2009.
- [86] Rabih A Jabr. Optimal power flow using an extended conic quadratic formulation. *IEEE transactions on power systems*, 23(3):1000–1008, 2008.
- [87] Nasser Jaleeli, Louis S VanSlyck, Donald N Ewart, Lester H Fink, and Arthur G Hoffmann. Understanding automatic generation control. *IEEE transactions on power systems*, 7(3):1106–1122, 1992.
- [88] JQ James, David J Hill, Albert YS Lam, Jiatao Gu, and Victor OK Li. Intelligent time-adaptive transient stability assessment system. *IEEE Transactions on Power Systems*, 33(1):1049–1058, 2017.
- [89] Amin Kargarian, Javad Mohammadi, Junyao Guo, Sambuddha Chakrabarti, Masoud Barati, Gabriela Hug, Soumya Kar, and Ross Baldick. Toward distributed/decentralized dc optimal power flow implementation in future electric power systems. *IEEE Transactions on Smart Grid*, 9(4):2574–2594, 2016.
- [90] Daniel Karlsson and David J Hill. Modelling and identification of nonlinear dynamic loads in power systems. *IEEE Transactions on Power Systems*, 9(1):157–166, 1994.
- [91] Andreas Kasis, Eoin Devane, Chrysovalantis Spanias, and Ioannis Lestas. Primary frequency regulation with load-side participation—part i: Stability and optimality. *IEEE Transactions on Power Systems*, 32(5):3505–3518, 2016.
- [92] Subodh Kharel and Bahman Shabani. Hydrogen as a long-term large-scale energy storage solution to support renewables. *Energies*, 11(10):2825, 2018.
- [93] Yousef Khayat, Qobad Shafiee, Rasool Heydari, Mobin Naderi, Tomislav Dragičević, John W Simpson-Porco, Florian Dörfler, Mohammad Fathi, Frede Blaabjerg, Josep M Guerrero, et al. On the secondary control architectures of ac microgrids: An overview. *IEEE Transactions on Power Electronics*, 35(6):6482–6500, 2019.
- [94] William A Kirk and Brailey Sims. *Handbook of metric fixed point theory*. Springer, 2002.
- [95] Petar V Kokotovic and Peter W Sauer. Integral manifold as a tool for reduced-order modeling of nonlinear systems: A synchronous machine case study. *IEEE Transactions on Circuits and Systems*, 36(3):403–410, 1989.
- [96] Matt Kraning, Eric Chu, Javad Lavaei, Stephen Boyd, et al. Dynamic network energy management via proximal message passing. *Foundations and Trends® in Optimization*, 1(2):73–126, 2014.
- [97] Prabhat Kumar, Dwarka P Kothari, et al. Recent philosophies of automatic generation control strategies in power systems. *IEEE transactions on power systems*, 20(1):346–357, 2005.
-

- [98] Prabha Kundur, Neal J Balu, and Mark G Lauby. *Power system stability and control*. McGraw-hill New York, 1994.
- [99] Prabha Kundur, John Paserba, Venkat Ajjarapu, Göran Andersson, Anjan Bose, Claudio Canizares, Nikos Hatziargyriou, David Hill, Alex Stankovic, Carson Taylor, et al. Definition and classification of power system stability ieeecigre joint task force on stability terms and definitions. *IEEE transactions on Power Systems*, 19(3):1387–1401, 2004.
- [100] Alexis Kyriacou, Panayiotis Demetriou, Christos Panayiotou, and Elias Kyriakides. Controlled islanding solution for large-scale power systems. *IEEE Transactions on Power Systems*, 33(2):1591–1602, 2017.
- [101] Gillian Lalor, Alan Mullane, and Mark O’Malley. Frequency control and wind turbine technologies. *IEEE Transactions on power systems*, 20(4):1905–1913, 2005.
- [102] Javad Lavaei and Steven H Low. Zero duality gap in optimal power flow problem. *IEEE Transactions on Power Systems*, 27(1):92–107, 2011.
- [103] Na Li, Changhong Zhao, and Lijun Chen. Connecting automatic generation control and economic dispatch from an optimization view. *IEEE Transactions on Control of Network Systems*, 3(3):254–264, 2015.
- [104] Hao Liang, Bong Jun Choi, Weihua Zhuang, and Xuemin Shen. Stability enhancement of decentralized inverter control through wireless communications in microgrids. *IEEE Transactions on Smart Grid*, 4(1):321–331, 2013.
- [105] Zhipeng Liu, Andrew Clark, Linda Bushnell, Daniel S Kirschen, and Radha Poovendran. Controlled islanding via weak submodularity. *IEEE Transactions on Power Systems*, 34(3):1858–1868, 2019.
- [106] Jacqueline Llanos, Daniel E Olivares, John W Simpson-Porco, Mehrdad Kazerani, and Doris Sáez. A novel distributed control strategy for optimal dispatch of isolated microgrids considering congestion. *IEEE Transactions on Smart Grid*, 10(6):6595–6606, 2019.
- [107] E Lobato, L Rouco, MI Navarrete, R Casanova, and G Lopez. An lp-based optimal power flow for transmission losses and generator reactive margins minimization. In *2001 IEEE Porto Power Tech Proceedings (Cat. No. 01EX502)*, volume 3, pages 5–pp, Porto, Portugal, 2001. IEEE.
- [108] Daniel Alberto Burbano Lombana and Mario Di Bernardo. Distributed pid control for consensus of homogeneous and heterogeneous networks. *IEEE Transactions on Control of Network Systems*, 2(2):154–163, 2014.
- [109] Daniel Alberto Burbano Lombana and Mario Di Bernardo. Multiplex pi control for consensus in networks of heterogeneous linear agents. *Automatica*, 67:310–320, 2016.

-
- [110] Jan Machowski, Janusz W Bialek, and James R Bumby. *Power System Dynamics and Control*. Wiley, 2007.
- [111] Enrique Mallada, Changhong Zhao, and Steven Low. Optimal load-side control for frequency regulation in smart grids. *IEEE Transactions on Automatic Control*, 62(12):6294–6309, 2017.
- [112] Uros Markovic, Ognjen Stanojev, Petros Aristidou, Evangelos Vrettos, Duncan S Callaway, and Gabriela Hug. Understanding small-signal stability of low-inertia systems. *IEEE Transactions on Power Systems*, 36(2):3997 – 4017, 2021.
- [113] Amin Kargarian Marvasti, Yong Fu, Saber DorMohammadi, and Masoud Rais-Rohani. Optimal operation of active distribution grids: A system of systems framework. *IEEE Transactions on Smart Grid*, 5(3):1228–1237, 2014.
- [114] Yang Mi, Yang Fu, Dongdong Li, Chengshan Wang, Poh Chiang Loh, and Peng Wang. The sliding mode load frequency control for hybrid power system based on disturbance observer. *International Journal of Electrical Power & Energy Systems*, 74:446–452, 2016.
- [115] Federico Milano, Florian Dörfler, Gabriela Hug, David J Hill, and Gregor Verbič. Foundations and challenges of low-inertia systems. In *2018 Power Systems Computation Conference (PSCC)*, pages 1–25. IEEE, 2018.
- [116] Sirius Mohammadi, Soodabeh Soleymani, and Babak Mozafari. Scenario-based stochastic operation management of microgrid including wind, photovoltaic, micro-turbine, fuel cell and energy storage devices. *International Journal of Electrical Power & Energy Systems*, 54:525–535, 2014.
- [117] Daniel K Molzahn, Florian Dörfler, Henrik Sandberg, Steven H Low, Sambuddha Chakrabarti, Ross Baldick, and Javad Lavaei. A survey of distributed optimization and control algorithms for electric power systems. *IEEE Transactions on Smart Grid*, 8(6):2941–2962, 2017.
- [118] Nima Monshizadeh, Claudio De Persis, and John W Simpson-Porco. The cost of dishonesty on optimal distributed frequency control of power networks. In *2016 IEEE 55th Conference on Decision and Control (CDC)*, pages 873–878. IEEE, 2016.
- [119] Pooya Monshizadeh, Claudio De Persis, Nima Monshizadeh, and Arjan J van der Schaft. Nonlinear analysis of an improved swing equation. In *2016 IEEE 55th Conference on Decision and Control (CDC)*, pages 4116–4121, Las Vegas, NV, USA, 2016. IEEE.
- [120] A Monticelli, MVF Pereira, and S Granville. Security-constrained optimal power flow with post-contingency corrective rescheduling. *IEEE Transactions on Power Systems*, 2(1):175–180, 1987.
-

- [121] Thomas Morstyn, Branislav Hredzak, and Vassilios G Agelidis. Control strategies for microgrids with distributed energy storage systems: An overview. *IEEE Transactions on Smart Grid*, 9(4):3652–3666, 2018.
- [122] Adilson E Motter, Seth A Myers, Marian Anghel, and Takashi Nishikawa. Spontaneous synchrony in power-grid networks. *Nature Physics*, 9(3):191–197, 2013.
- [123] Hamdy AM Moussa and Yao-nan Yu. Optimal power system stabilization through excitation and/or governor control. *IEEE Transactions on Power Apparatus and Systems*, PAS-91(3):1166–1174, 1972.
- [124] Takashi Nishikawa, Ferenc Molnar, and Adilson E Motter. Stability landscape of power-grid synchronization. *IFAC-PapersOnLine*, 48(18):1–6, 2015.
- [125] Takashi Nishikawa and Adilson E Motter. Comparative analysis of existing models for power-grid synchronization. *New Journal of Physics*, 17(1):015012, 2015.
- [126] University of Washington College of Engineering. Power systems test case archive. <http://labs.ece.uw.edu/pstca/>. Accessed: 2021-01-17.
- [127] Reza Olfati-Saber, J Alex Fax, and Richard M Murray. Consensus and cooperation in networked multi-agent systems. *Proceedings of the IEEE*, 95(1):215–233, 2007.
- [128] Romeo Ortega, Martha Galaz, Alessandro Astolfi, Yuanzhang Sun, and Tielong Shen. Transient stabilization of multimachine power systems with nontrivial transfer conductances. *IEEE Transactions on Automatic Control*, 50(1):60–75, 2005.
- [129] Romeo Ortega, Arjan J Van Der Schaft, Iven Mareels, and Bernhard Maschke. Putting energy back in control. *IEEE Control Systems Magazine*, 21(2):18–33, 2001.
- [130] Sakshi Pahwa, M Youssef, P Schumm, C Scoglio, and N Schulz. Optimal intentional islanding to enhance the robustness of power grid networks. *Physica A: Statistical Mechanics and its Applications*, 392(17):3741–3754, 2013.
- [131] Mathaios Panteli and Pierluigi Mancarella. Influence of extreme weather and climate change on the resilience of power systems: Impacts and possible mitigation strategies. *Electric Power Systems Research*, 127:259–270, 2015.
- [132] Mania Pavella, Damien Ernst, and Daniel Ruiz-Vega. *Transient stability of power systems: a unified approach to assessment and control*, volume 581. Springer Science & Business Media, 2000.
- [133] Fang Zheng Peng and Jih-Sheng Lai. Generalized instantaneous reactive power theory for three-phase power systems. *IEEE transactions on instrumentation and measurement*, 45(1):293–297, 1996.

-
- [134] Pouyan Pourbeik, Prabha S Kundur, and Carson W Taylor. The anatomy of a power grid blackout—root causes and dynamics of recent major blackouts. *IEEE Power and Energy Magazine*, 4(5):22–29, 2006.
- [135] Task Force on Turbine-Governor Modeling Power System Dynamic Performance Committee, Power System Stability Subcommittee. Dynamic models for turbine-governors in power system studies, report pes-tr1. <https://resourcecenter.ieee-pes.org/publications/technical-reports/PESTR1.html>, 2013. Accessed: 2021-01-24.
- [136] W W Price, C W Taylor, and G J Rogers. Standard load models for power flow and dynamic performance simulation. *IEEE Transactions on Power Systems*, 10(3), 1995.
- [137] Zhifeng Qiu, Geert Deconinck, and Ronnie Belmans. A literature survey of optimal power flow problems in the electricity market context. In *2009 IEEE/PES Power Systems Conference and Exposition*, pages 1–6, Seattle, WA, USA, 2009. IEEE.
- [138] H Quinot, H Bourles, and T Margotin. Robust coordinated avr+ pss for damping large scale power systems. *IEEE Transactions on Power Systems*, 14(4):1446–1451, 1999.
- [139] IEEE Committee Report. Dynamic models for steam and hydro turbines in power system studies. *IEEE transactions on power apparatus and systems*, PAS-92(6):1904–1915, 1973.
- [140] Joan Rocabert, Alvaro Luna, Frede Blaabjerg, and Pedro Rodriguez. Control of power converters in ac microgrids. *IEEE transactions on power electronics*, 27(11):4734–4749, 2012.
- [141] M Saïdy. A unified approach to voltage regulator and power system stabiliser design based on predictive control in analogue form. *International Journal of Electrical Power & Energy Systems*, 19(2):103–109, 1997.
- [142] Peter W Sauer, Mangalore A Pai, and Joe H Chow. *Power system dynamics and stability: with synchrophasor measurement and power system toolbox*. John Wiley & Sons, 2017.
- [143] Peter W Sauer and Mangalore Anantha Pai. *Power system dynamics and stability*. Prentice hall Upper Saddle River, NJ, 1998.
- [144] Johannes Schiffer, Thomas Seel, Jörg Raisch, and Tevfik Sezi. Voltage stability and reactive power sharing in inverter-based microgrids with consensus-based distributed voltage control. *IEEE Transactions on Control Systems Technology*, 24(1):96–109, 2015.
- [145] Johannes Schiffer, Daniele Zonetti, Romeo Ortega, Aleksandar M Stanković, Tevfik Sezi, and Jörg Raisch. A survey on modeling of microgrids—from fundamental physics to phasors and voltage sources. *Automatica*, 74:135–150, 2016.
-

- [146] Gab-Su Seo, Marcello Colombino, Irina Subotic, Brian Johnson, Dominic Groß, and Florian Dörfler. Dispatchable virtual oscillator control for decentralized inverter-dominated power systems: Analysis and experiments. In *2019 IEEE Applied Power Electronics Conference and Exposition (APEC)*, pages 561–566. IEEE, 2019.
- [147] Qobad Shafiee, Josep M Guerrero, and Juan C Vasquez. Distributed secondary control for islanded microgrids—a novel approach. *IEEE Transactions on power electronics*, 29(2):1018–1031, 2013.
- [148] John W Simpson-Porco, Florian Dörfler, and Francesco Bullo. Synchronization and power sharing for droop-controlled inverters in islanded microgrids. *Automatica*, 49(9):2603–2611, 2013.
- [149] John W Simpson-Porco, Qobad Shafiee, Florian Dörfler, Juan C Vasquez, Josep M Guerrero, and Francesco Bullo. Secondary frequency and voltage control of islanded microgrids via distributed averaging. *IEEE Transactions on Industrial Electronics*, 62(11):7025–7038, 2015.
- [150] Lucas M. Stolerman, Daniel Coombs, and Stefanella Boatto. SIR-Network Model and Its Application to Dengue Fever. *SIAM Journal on Applied Mathematics*, 75(6):2581–2609, January 2015.
- [151] B Stott, JL Marinho, and O Alsac. Review of linear programming applied to power system rescheduling. In *IEEE Conference Proceedings Power Industry Computer Applications Conference, 1979. PICA-79.*, pages 142–154. IEEE, 1979.
- [152] Brian Stott, Jorge Jardim, and Ongun Alsaç. Dc power flow revisited. *IEEE Transactions on Power Systems*, 24(3):1290–1300, 2009.
- [153] Irina Subotic, Dominic Groß, Marcello Colombino, and Florian Dorfler. A lyapunov framework for nested dynamical systems on multiple time scales with application to converter-based power systems. *IEEE Transactions on Automatic Control*, 66(12):5909–5924, 2020.
- [154] Andy X Sun, Dzung T Phan, and Soumyadip Ghosh. Fully decentralized ac optimal power flow algorithms. In *2013 IEEE Power & Energy Society General Meeting*, pages 1–5. IEEE, 2013.
- [155] Kai Sun, Da-Zhong Zheng, and Qiang Lu. Splitting strategies for islanding operation of large-scale power systems using obdd-based methods. *IEEE transactions on Power Systems*, 18(2):912–923, 2003.
- [156] N Mahdavi Tabatabaei, A Jafari Aghbolaghi, Nicu Bizon, and Frede Blaabjerg. Reactive power control in ac power systems. *Switzerland: Springer*, 2017.
- [157] Ali Tayyebi, Florian Dörfler, Friederich Kupzog, Zoran Miletic, and Wolfgang Hribernik. Grid forming converters—inevitability, control strategies and challenges in future grids application. In *CIREN 2018 Ljubljana Workshop on Microgrids and Local Energy Communities*. CIREN, AIM, 2018.

-
- [158] Ali Tayyebi, Dominic Groß, Adolfo Anta, Friederich Kupzog, and Florian Dörfler. Frequency stability of synchronous machines and grid-forming power converters. *IEEE Journal of Emerging and Selected Topics in Power Electronics*, 8(2):1004–1018, 2020.
- [159] Emma Tegling, Martin Andreasson, John W Simpson-Porco, and Henrik Sandberg. Improving performance of droop-controlled microgrids through distributed pi-control. In *2016 American Control Conference (ACC)*, pages 2321–2327. IEEE, 2016.
- [160] Remus Teodorescu, Marco Liserre, and Pedro Rodriguez. *Grid converters for photovoltaic and wind power systems*. John Wiley & Sons, 2011.
- [161] S Tosserams, LFP Etman, PY Papalambros, and JE Rooda. An augmented lagrangian relaxation for analytical target cascading using the alternating direction method of multipliers. *Structural and multidisciplinary optimization*, 31(3):176–189, 2006.
- [162] Sebastian Trip, Mathias Bürger, and Claudio De Persis. An internal model approach to (optimal) frequency regulation in power grids with time-varying voltages. *Automatica*, 64:240–253, 2016.
- [163] Sebastian Trip, Michele Cucuzzella, Claudio De Persis, Antonella Ferrara, and Jacquelin MA Scherpen. Robust load frequency control of nonlinear power networks. *International Journal of Control*, 93(2):346–359, 2020.
- [164] Sebastian Trip, Michele Cucuzzella, Claudio De Persis, Arjan van der Schaft, and Antonella Ferrara. Passivity-based design of sliding modes for optimal load frequency control. *IEEE Transactions on control systems technology*, 27(5):1893–1906, 2018.
- [165] Andreas Ulbig, Theodor S Borsche, and Göran Andersson. Impact of low rotational inertia on power system stability and operation. *IFAC Proceedings Volumes*, 47(3):7290–7297, 2014.
- [166] Arjan van der Schaft and Tjerk Stegink. Perspectives in modeling for control of power networks. *Annual Reviews in Control*, 41:119–132, 2016.
- [167] Krešimir Vrdoljak, Nedjeljko Perić, and Ivan Petrović. Sliding mode based load-frequency control in power systems. *Electric Power Systems Research*, 80(5):514–527, 2010.
- [168] CG Wang, BH Zhang, ZG Hao, J Shu, P Li, and ZQ Bo. A novel real-time searching method for power system splitting boundary. *IEEE Transactions on Power Systems*, 25(4):1902–1909, 2010.
- [169] Youyi Wang, David J Hill, Rick H Middleton, and Long Gao. Transient stabilization of power systems with an adaptive control law. *Automatica*, 30(9):1409–1413, 1994.
-

- [170] Zhaojian Wang, Feng Liu, Steven H Low, Changhong Zhao, and Shengwei Mei. Distributed frequency control with operational constraints, part i: Per-node power balance. *IEEE Transactions on Smart Grid*, 10(1):40–52, 2017.
- [171] Zhaojian Wang, Feng Liu, Steven H Low, Changhong Zhao, and Shengwei Mei. Distributed frequency control with operational constraints, part ii: Network power balance. *IEEE Transactions on Smart Grid*, 10(1):53–64, 2017.
- [172] Zhaoyu Wang, Bokan Chen, Jianhui Wang, Miroslav M Begovic, and Chen Chen. Coordinated energy management of networked microgrids in distribution systems. *IEEE Transactions on Smart Grid*, 6(1):45–53, 2014.
- [173] Eric W. Weisstein. Harmonic addition theorem. *MathWorld*, <https://mathworld.wolfram.com/HarmonicAdditionTheorem.html>. Accessed: 2021-01-21.
- [174] Erik Weitenberg, Yan Jiang, Changhong Zhao, Enrique Mallada, Claudio De Persis, and Florian Dörfler. Robust decentralized secondary frequency control in power systems: Merits and tradeoffs. *IEEE Transactions on Automatic Control*, 64(10):3967–3982, 2018.
- [175] DW Wells. Method for economic secure loading of a power system. In *Proceedings of the Institution of Electrical Engineers*, pages 1190–1194. IET, 1968.
- [176] Xiaofan Wu, Florian Dörfler, and Mihailo R Jovanović. Input-output analysis and decentralized optimal control of inter-area oscillations in power systems. *IEEE Transactions on Power Systems*, 31(3):2434–2444, 2015.
- [177] Xiaofan Wu, Florian Dörfler, and Mihailo R Jovanović. Topology identification and design of distributed integral action in power networks. In *2016 American Control Conference (ACC)*, pages 5921–5926. IEEE, 2016.
- [178] Amirnaser Yazdani and Reza Iravani. *Voltage-sourced converters in power systems*, volume 34. Wiley Online Library, 2010.
- [179] Haibo You, Vijay Vittal, and Xiaoming Wang. Slow coherency-based islanding. *IEEE Transactions on power systems*, 19(1):483–491, 2004.
- [180] Hui Yu, MA Awal, Hao Tu, Iqbal Husain, and Srdjan Lukic. Comparative transient stability assessment of droop and dispatchable virtual oscillator controlled grid-connected inverters. *IEEE Transactions on Power Electronics*, 36(2):2119–2130, 2020.
- [181] SB Yusof, GJ Rogers, and RTH Alden. Slow coherency based network partitioning including load buses. *IEEE Transactions on Power Systems*, 8(3):1375–1382, 1993.
- [182] Changhong Zhao, Enrique Mallada, and Florian Dörfler. Distributed frequency control for stability and economic dispatch in power networks. In *2015 American Control Conference (ACC)*, pages 2359–2364. IEEE, 2015.

- [183] Qing-Chang Zhong and George Weiss. Synchronverters: Inverters that mimic synchronous generators. *IEEE transactions on industrial electronics*, 58(4):1259–1267, 2010.
- [184] Ray Daniel Zimmerman, Carlos Edmundo Murillo-Sánchez, and Robert John Thomas. Matpower: Steady-state operations, planning, and analysis tools for power systems research and education. *IEEE Transactions on power systems*, 26(1):12–19, 2010.